LATERAL LOADING OF SHEAR WALL MODELS

LATERAL LOADING OF SHEAR WALL MODELS

By

MOHAMMAD AFSAR, B.E.

A Thesis

Submitted to the Faculty of Graduate Studies

in Partial Fulfilment of the Requirements

for the Degree

Master of Engineering

McMaster University

August 1967

MASTER OF ENGINEERING (1967)
(Civil Engineering)

McMASTER UNIVERSITY
Hamilton, Ontario

TITLE: Lateral Loading of Shear Wall Models

AUTHOR: Mohammad Afsar, B.E.(Peshawar University)

SUPERVISOR: Dr. A. C. Heidebrecht

NUMBER OF PAGES: xi, 111

SCOPE AND CONTENTS:

This thesis describes the development of a technique to build small-scale shear wall building models using a suitable concrete mortar. Tests were conducted to study the behaviour of such models under lateral load. The analysis of the problem was done by treating the model as a thin-walled cantilever beam based on Vlasov's thin-walled beam theory. The test and analytical results are compared to investigate the validity of this approach.

ACKNOWLEDGEMENTS

I wish to express my sincere gratitude to Dr. A. C. Heidebrecht and Dr. W. K. Tso for their invaluable guidance and encouragement during the entire course of this work.

My thanks are also due to Mr. J. L. Myers and Mr. J. Speirs for their cooperation and help in the modelling and testing of the present work.

This investigation was made possible through the financial assistance of the Canada Emergency Measures Organization, to whom I extend my sincere thanks.

CONTENTS

Contents (continued) Page

NOTATION

δ	wall thickness
A	cross-sectional area
o	centroid of the section
S	shear centre
a_x, a_y	coordinates of shear centre
E	modulus of elasticity
G	modulus of elasticity in shear
ν	Poisson's ratio
U	longitudinal displacement in z-direction
V	transverse displacement, directed along the tangent of the profile line of the cross section
W	transverse normal displacement
ε	longitudinal strain
ℓ	length of the model
ω	principal sectorial area
I_x, I_y	moments of inertia of plane area with respect to x and y axes
ξ, η	displacements of shear centre in the X and Y directions, respectively
θ	rotation of the section about shear centre
Q	resultant lateral load

e	eccentricity with respect to shear centre
I_ω	sectorial moment of inertia $I_\omega = \int_A \omega^2 dA$
M	applied torsional moment
B	bimoment
H	resisting torsional moment
I_d	torsional rigidity
γ	shearing strain

LIST OF FIGURES

Figure		Page
17	Loading Cap	68
18	Support for Hydraulic Jack	69
19	Photograph Showing Hydraulic Jack Assembly and the Supporting Column	70
20	Dimensional Sketch of Load-Cell	71
21	Photograph Showing the Model, the Loading Arrangement and Instrumentation	72
22a	Location of Deflection-Gages	73
22b	Location of Strain-Gages	74
23a-c	Crack Location Model No. 2	75-76
24	Crack Location Model No. 3	77
25	Crack Location Model No. 4	78
26	Crack Location Model No. 5	79
27	Comparison of Strain Distribution, z = 2" (Model No. 2)	80
28	Comparison of Strain Distribution, z = 45" (Model No. 2)	81
29-30	Comparison of Deflections (Model No. 2)	82-83
31	Deflected Shape of the Sections, Q = 40 lbs. (Model No. 5)	84
32	Deflected Shape of the Sections, Q = 100 lbs. (Model No. 5)	85
33	Deflected Shape of the Sections, Q = 180 lbs. (Model No. 5)	86
34	Displacement of Section Under Flexural-Torsional Loading	87
35	Profile Line and Axis of the Model	88
36a	Displacements in the Longitudinal Plane	89
36b	Sectorial Area ω	89

LIST OF TABLES

CHAPTER I

INTRODUCTION

1.1 Description of Typical Shear Wall Construction

Shear walls are the important structural components of the modern high-rise apartment and other tall buildings. Their function is two-fold.

1) To support the vertical loading.

2) To resist lateral forces such as those due to wind, earthquakes and blast effects etc.

Dictated by functional requirements, these walls normally contain openings for doors, windows and corridors. A wall may have a single band of openings (Fig. 1a), two symmetric bands of openings (Fig. 1b) or the openings may be assymetric with respect to the centre line of the wall (Fig. 1c). In some cases the openings may be staggered as shown in Figure 1d.

In actual building lay-outs shear walls may be found in two types of structures. The first type are buildings in which the shear walls are laid parallel to each other and are interconnected by floor slabs at each storey level. Figure 2 illustrates such a disposition for a six storey building. In the second type of construction, known as box-core type, the shear walls may not be plane-rectangular in cross section but may have a channel or other shape. Channel section shear walls with interconnecting slabs (Fig. 3) represent a typical box-core construction type. In this type of construction the shear walls are built with their webs parallel. The flanges are connected by beams at each floor level and the floors are then added. The shear walls may have openings of the one of the band types as described earlier. In addition, horizontal floor slabs may be attached to each web at all floor levels; their outer corners being supported by four columns or in some other fashion to form the outer bays.

1.2 Methods of Analysis of Shear Walls

The problem of shear walls with openings has been approached, up to date, using a number of analytical methods. In reviewing the research literature, it is found that much work has been published in which shear walls with row openings have been idealized as an interaction of columns (or walls) and beams. In what has been called the equivalent frame method[1*], the shear wall is treated as a rigid frame in which the lengths of the beams are taken to be the distances between the centroidal axes of the adjacent columns (Fig. 4a). The approach is unrealistic when the widths of the columns are not negligible compared with their centre to centre distances. This approach will

---

*Numbers refer to the Bibliography listing.

generally over-estimate deflections for shear walls with holes and therefore has limited applicability.

A more general approach is to consider the beam length as being the clear distance between the columns. Account is taken in the analysis, of the finite deflection at the ends of the beams due to the rotation of the columns. This idealization might be considered as a frame with rigid members as shown in Figure 4b and is termed the wide column frame analogy.

A simplified analysis has been produced by assuming that the discrete system of connections, formed by lintel beams in between the consecutive openings, may be replaced by an equivalent continuous medium (Fig. 4c). The method, apparently originally suggested by Pippard[2] in connection with the analysis of spoked wheels, was first used by Chitty[3] in the analysis of a cantilever composed of a number of parallel beams interconnected by cross-bars. This approach is called the shear-connection method of analysis. Using this form of approach, and treating the row of beams as a continuous medium in pure shear, Rosman[4] produced an elegant solution by establishing a single second order differential equation in terms of the specific shear in the connecting medium and solving it for particular load cases. The main assumptions made in this formulation are that the axial deformations of the beams are negligible and that there is a point of contraflexure at the centre of the beams. The upper end beam has one-half the cross section and one-half the moment of inertia of an interior connecting beam.

Rosman treated the cases of a single band of openings and two bands of openings for walls whose piers are fixed to the foundation in various manners. This solution appears to give good results for a variety of practical cases. In the experimental investigation conducted by Barnard and Schwaighofer[5] in which they used epoxy sheet models, Rosman's theory was found to be in good agreement with experimental results.

A more recent approach to the solution of shear wall structures is the lattice anology and finite element methods. McHenry[6a] and Hrennikoff[6b] are several of the original researchers who described the lattice analogy method as adopted to the numerical solution of a number of types of two dimensional stress problems involving elastic materials.

Figure 5 illustrates the idealization technique involved in solving two dimensional problems of elasticity by the frame-work method. The elastic continuous medium of length "ℓ" and thickness "t" is substituted by a pin-jointed frame-work consisting of vertical, horizontal and diagonal members. The frame-work so formed is given the same external outline and the same boundary restraints. The elements of the equivalent structure are endowed with suitable elastic properties so as to represent the wall continuum; and the frame-work is subjected to the same loads as the solid body. The uniformly distributed load (Fig. 5a) is replaced by a statically equivalent system of concentrated forces acting at the joints of the articulated structure (Fig. 5b). The problem then is to solve for the displacements in this lattice, and the stresses and strains are then computed from the displacements.

The resulting structure is highly indeterminate, and by the conventional methods applied to indeterminate structures, as many equations would be required as the number of members. (In the present example, because of the symmetry, only half the lattice structure is to be solved.) It is apparent that the direct solution is very laborious.

Before the advent of digital computers, Southwell's method of relaxation was the only indirect method for the numerical solution of such problems. The accuracy of results would depend on the number of lattices of the equivalent frame-work (Fig. 5b). When "m_ℓ" is decreased the accuracy of approximation is improved and in the limiting case when "m_ℓ" approaches zero the solution converges to the exact solution. Therefore, the accuracy of the results is controlled primarily by the labor expended. This great labor of computation, which is the main disadvantage of the frame-work method, has been overcome by the use of digital computers in conjunction with the use of matrix methods. This approach, therefore, is gaining popularity in solving a great variety of problems including shear walls.

In his shear wall investigation, MacLeod[7] employed McCormick[8] lattice of the type shown in Figure 5b to compare the results with those from the other methods and those obtained from the experiment. Grinter's[9] grid analogy has been applied to shear walls with openings by Kazimi[10].

A more recent development is the finite element method. Triangular and rectangular element stiffness matrices have been formulated for plane-stress analysis. Using the rectangular element stiffness matrix given by Argyris[11], MacLeod has used the finite element method to solve the shear wall problem.

1.3 Experimental Investigation by Model Testing

With regard to experimental investigation by way of model testing, the first major research into pure shear wall structures appears to be a series of tests carried out in the United States, to provide data for the design of blast-resistant structures. The full report was presented by Whitney, Anderson and Cohen[12] in a comprehensive paper dealing with the behaviour of structures designed to resist blast loads. In their report, approximate methods based on simple "strength of materials" theories were proposed to predict the stiffness and ultimate load of simple shear wall structures subjected to lateral loading. Benjamin and Williams[13-16] carried out a large number of tests on models of single-storey brick and reinforced concrete shear walls with and without openings, and on reinforced concrete shear wall assemblies consisting of one and two-storey parallel shear walls connected by diaphragms. Of particular interest in these investigations was the concern of the investigators with the scale effects of modelling. This is the first problem facing any study using models. In their investigations full-scale was assumed to be an 8 ft. high, 12 ft. long wall with 8 inches thick panel. A series of reinforced concrete walls ranging from 1/8th to 3/8ths scale were tested, all walls being proportioned on a purely geometrical basis. It was concluded from test results that no scale-effect was present. This leads to the conclusion that in model study of shear walls the choice of scale could be made on the basis of testing facilities available and other factors involved in making of such models and yet the models would yield results applicable to the prototype. Various investigators used small-scale metallic models in their experimental investigations to draw a comparison between the experimental results and theoretical estimations from one or more approaches as mentioned earlier. MacLeod employed 1/16" thick aluminum sheets for his model study, a cantilever of aspect ratio 3:1 with one band of openings along the centre. The purpose of this study was to compare the experimental results with theoretical calculations based on finite element analogy and lattice analogy and the results given by basic strength of materials theory.

For the purpose of establishing the width of the "slab strip" which is acting as the connecting media between the shear walls and to determine the accuracy of Rosman's theory and his own simplified theory, Barnard used models cut from 1/4" thick epoxy sheets. He used a scale of model to prototype as 1:64. Jenkins and Harrison[17] constructed models of both the parallel shear wall and box-core types using 1/4" thick sheet perspex. From the experimental investigations cited it is apparent that no definite rule has been followed by these researchers in the choice of the scale factor.

However, in all these approaches the problem essentially is a plane-stress problem.

1.4 Purpose of the Present Study

In the present study a different approach is taken in the sense that not just a shear wall but a shear wall building is taken as an object of study. The reason which prompted the necessity of such a study is that a shear wall would seldom exist as an independent structure. Although single-panel shear wall analysis is desirable from the point of view of detailed analysis of deflections and local stress distributions, the walls in practice do not act as independent cantilevers owing to the coupling action of slabs and other walls. The simplest approach would be to calculate the loads in the walls assuming that all interconnected walls deflect equally and no torsion occurs due to the high in-plane stiffness of the floor slabs. A design which does not effectively incorporate the interaction effect due to connected shear walls as well as floor slabs, would be highly uneconomical since the shear walls do derive strength from the connecting floors. By definition, a shear wall building is a three dimensional entity composed of interconnected shear walls and floor slabs in which the whole strength of the building is derived from the interaction of these structural members.

One theoretical approach is to study each shear wall independently and derive their interaction by matching the boundary conditions. This approach is lengthy and is justified if detailed force and stress distribution is desired.

Another approach which is the approach taken in this study is to use thin-walled beam theory. The theory of thin-walled beams is well laid down by Vlasov[18] and is known to give good results when the beam is long, i.e., in this case a tall shear wall building. If only gross behaviour of the building is required, it seems that this will be a fruitful approach. In order to establish the validity of this theory, an experimental programme is undertaken as described below.

The present experimental programme forms the first phase of a more general experimental programme and consists of casting shear wall building models without floors or wall openings and testing them under some form of lateral load. It was decided to build a model 8 ft. in height and having a cross section as shown in Figure 6. It was decided, also, to use concrete mortar as the modelling material.

The choice of metal rather than mortar as a model material has the definite advantage of material homogenity and ease of building such models. On the other hand, considerable difficulty is involved in modelling if mortar is used because of the inherent properties of this material. Perhaps this might be one of the major reasons why many shear wall investigators avoided the use of concrete or concrete mortar as a model material. However, it is more realistic to use mortar as a model material because mortar is a brittle material with cracking and failure properties similar to full scale concrete. The use of mortar as model material, therefore, lends an opportunity for better appreciation of the problem as a whole and in making correlation of the behaviour of the model with that of the prototype. The other advantage is the cost of the models if an extended programme is to be undertaken. Once a form-work is manufactured it could be used repeatedly resulting in much smaller costs for an investigation programme as a whole.

The purpose of the present investigation is therefore two-fold:

1) To determine the most suitable mix design and to develop and perfect the modelling technique.

2) To study the behaviour of the model under some form of lateral load.

The loading and the loading arrangement are discussed in detail in a later chapter. However, the loading arrangement is such that with base fixed (Fig. 6), the model is essentially subjected to eccentric lateral loads at the top. This type of loading induces the combined bending and torsional effects. The lateral deflections and stress distribution across the cross sections as obtained experimentally are then compared with the corresponding values, as predicted on the basis of Vlasov's thin-walled beam theory.

CHAPTER II

CONSTRUCTION OF MODELS

2.1 Description of Models

For the experimental investigation, in the present work, it was proposed to build 8-ft. high models using a mortar mix most suitable for this purpose. Figure 6 illustrates the general appearance including the size and shape of the proposed model. The design criterion for the mix used in terms of its proportions and other details are discussed in section 3 of this chapter. The form-work is designed so that a 2" thick 48" x 24" concrete base is cast monolithic with the model proper using suitable connections so that the model is completely fixed to the base. A 1/2" thick 5' x 4' aluminum plate, rigidly held to the concrete base through studs embedded in concrete, completes the base of the model. The aluminum base-plate is then held to the floor, rigidly, through anchor bolts. The purpose of using extra large size aluminum plate is to have space available for erecting a steel frame-work all around the model for attaching deflection gages. This arrangement permits the deflections to be obtained relative to the fixed base.

2.2 General Description of Form-Work

In order to achieve maximum uniformity in the properties of the model throughout its height, it was decided to design a form-work to enable the casting of the models in a single pour. This is preferred to the method of pouring by lifts though the latter simulates the actual method of pouring prototype shear wall structures. Any discrepancies at joints of various lifts may affect the final results significantly. Although it was intended in the beginning to pour the models by method of lifts, this had to be abandoned due to the difficulties in obtaining proper bond between various lifts.

Laminated plywood (3/4" size) was used in constructing the form-work. The form-work consists of three pairs of 8 ft. long panels of plywood laid over a platform and resting on their long edges. The main platform is constructed by rigidly bolting two layers of 3/4" plywood base on a 10' x 5' wheeled tri-legged steel frame as shown in Figure 7. The plywood base has circular openings for access from underneath the steel frame. The vertical height of the outer panels is 16" whereas the inner panels are 14-3/4" in depth. Figures 8a through 8c show the sequential mounting of the panels. A spacing of 1/2" between each pair of panels is achieved by the help of cross-boards marked 1 to 8 in Figure 8a. The cross-boards, which are rigidly bolted to the platform, also prevent lateral buckling of the panels due to lateral pressure.

Figure 9 shows the aluminum plate which was used as a base-plate. This plate is attached at the end of the frame-work through 2" x 4" wooden spacers which provice for the 2" thick monolithic concrete base. The wire mesh (Fig. 9) is used to obtain a proper connection between the base and the model proper. Studs (Fig. 9) of 1/4" diameter and passing through the aluminum plate are used to act as shear connectors between aluminum and concrete surfaces when embedded in the concrete base. Figure 10 shows the cross section of the assembled form-work. The whole form-work was painted with two coats of liquid plastic (poly-urethane). This produced smooth and tough mould surfaces and effective water proofing against damage due to warping.

2.3 Design and Properties of Mix

The first problem in small-scale modelling of concrete structures is the determination of the best type of materials to be used as model substitutes for the actual concrete. For the particular model at hand, the mix design should meet the following requirements:

1) It should be highly workable.

2) Its initial setting time should permit adequate time for pouring and other manipulations required with the

available facilities in the laboratory.

3) It should have high early strength in order that the form-work could be removed earlier and in order to reasonably shorten the overall time from pouring to the testing of the model.

4) The model mix should simulate the behaviour of its prototype, i.e., the stress-strain curve of the mix should have the same general shape as that of structural concrete.

A programme of mix design was undertaken by one of senior undergraduate students in the summer of 1966. The test programme consisted of pouring 1/2" thick slabs 18" x 12", with various trial mixes and examining the final product as related to the initial workability of the mix. Aluminum sheets were used for the forms although this was later changed to plastic-coated plywood forms.

In the selection of the mix materials, White's[19] concrete model mix was used as a guide line. White's mix consists of the following mix proportions:

Ultracal 30 (a high-strength gypsum)	40%
Ottawa sand	20%
Crushed limestone (0.065" - 0.131")	40%
Water (percent by weight of ultracal 30)	33.4%

Tests in the cited reference show that this mix is an excellent substitute for structural concrete. In the design-mix for the present work, a combination of ultracal 30 and high early-strength cement was considered in order to accomplish high compressive strengths. The proportions of sand and limestone were varied keeping the ratio of cementing and filling materials constant (as in White's mix) while varying the quantity of water independently to gain higher workability.

The set of tests consisted of pouring several trial mixes into plastic-coated plywood moulds to obtain 1/2" thick 18" x 12" slabs. Since the actual form-work was to be plastic-coated plywood similar material was used for the form-work of small test slabs. After pouring the mix in small slab moulds, it was vibrated in the same manner as that to be used later for the actual model. The test slabs made from various trial mixes were examined for surface voids and uniformity of the final product. The following mix was recommended on the basis of high workability, setting time and high early strength.

Ultracal 30	2%
High early-strength cement	38%
Ottawa sand	25%
Dolomite limestone chips (1/8")	35%
Water (percent by weight of ultracal 30 and high early-strength cement)	53%

Grading curves for the dolomite limestone chips and for fine Ottawa sand are shown in Figure 11 and Figure 12 respectively. The following table represents the ultimate strength (compressive) of two-inch test cubes, made from the design mix, at different ages.

Age	Compressive Strength P.S.I.
24 hrs.	2,070
48 hrs.	3,200
7 days	5,580
1 month	10,000

A typical stress-strain curve for a standard 6" diameter cylindrical specimen is shown in Figure 13. Young's modulus is defined as the initial tangent modulus of the stress-strain curve. This value of Young's modulus is found from the experimental curve (Fig. 13) to be 3×10^6 P.S.I.

2.4 Method of Pouring and Erection

Mineral oil was liberally applied on the form-work surfaces before a pour was made. The required volume of mortar was mixed in a single batch and pouring was done with mould lying horizontally. The assembled form-work is such that when the mortar is set the model is resting horizontally on the long edges of the flanges. Pouring is done from one end only (base end), letting the mortar flow into the mould by itself and thereby minimizing the chance of entrapping air. The compaction of the mortar is achieved both by tapping and using a vibrator against the form-work. Since the concrete mixer and test-apparatus are located in different rooms, the model has to be transported immediately after the completion of the pouring process. This is considered to be an aid in compaction and elimination of voids. The top surface (which is at the back of the model) is then levelled with a straight edge and is then covered with a top panel. Figure 14a shows a freshly poured model with top panel in place and bolted to the rest of the frame-work. The model is allowed to set, in this position, for two days before it is erected on its final test postiion. Figure 14b shows the end to which the chain is hooked for lifting the model. The point of suspension is carefully located at the centroid of the total mass. Figure 15 shows the whole assembly after being erected on its desired location.

The form-work is then stripped off the model by first removing the main platform and the two outer most panels (Fig. 16a). The remaining form-work is then removed in parts as shown in Figures 16b and 16c.

2.5 Problems Encountered and Improvement in the Technique

A total of six models were poured and in the process various difficulties were encountered in obtaining a completely sound model. The first problem encountered was the sticking of form-work to concrete surfaces. Even though the coated surfaces of the form-work were liberally oiled, the inside panels badly stuck to the model and on application of force to remove these panels, the first model shattered into pieces. This problem was overcome in the latter models by carefully wrapping the plywood panels with 6 mil. plastic (polyethelene) sheets. In addition, the panels in contact with the inside of the web of the model were each sliced into three pieces, the middle piece in each panel forming a sort of wedge. This central wedge could be removed first (Fig. 16b) thereby enabling the other parts of the form-work to be removed easily. This technique of wrapping the form-work with wrinkle-free polyethelene sheets produced a smooth and satisfactory surface.

The second and the most serious problem encountered during modelling was the occurrence of shrinkage cracks. Both vertical and horizontal cracks appeared in almost all models. In some models these cracks were visible right after the stripping of the forms. In others, such cracks appeared after some time and became visible when the mounting of the measurement gages was in progress. In one model horizontal cracks appeared in the model section very near the base. These cracks were completely covered by pouring an extra 6" high, 5000 P.S.I. concrete pad around the base, thus reducing the test height to 90 inches. In other models, the cracks extended high enough above the base so that it was impossible to completely nullify their effect by pouring an extra base. However, to be consistent, the test heights in all later models were maintained at 90 inches.

Having noticed the persistent appearance of cracks near the base in the first two models, a careful consideration was then given to the possible factors contributing to such cracks and then finding ways and means to avoid them. The following major factors could contribute to the development of cracks:

a) Shrinkage.

b) Handling of the models, i.e., modelling technique.

c) Differential rate of setting.

It was difficult, at that stage, to assess the relative degree of contribution of these factors. High water contents, finer aggregates and the type of cement used in the mix all contribute towards a greater possibility of having shrinkage cracks. Because of the time factor involved, it was not possible at that stage to consider another test programme in order to find a more suitable mix. The other two factors were carefully examined and attempts made to make improvements.

In order to avoid any harmful stressing of the model due to lifting and handling, an attempt was made to lift the model when the model was still green and allow it to set in its final vertical position. This attempt proved unsuccessful because the material leaked from the bottom due to the damage to the seal at the bottom resulting from large deflections of the centre of the aluminum plate. Nevertheless, this attempt revealed the necessity of stiffening the base plate. Since the aluminum plate is fixed to the frame-work only along the shorter edges, any possible deflection (however small it may be) during hoisting of the model may cause undue stressing of the model and hence cause cracks. To guard against such a possibility, the aluminum plate was stiffened against bending.

In order that no differential setting should take place, the model was covered immediately after pouring, thus sealing the model completely. The mortar was allowed to set for an extended time (4 days) so that the model would gain more strength before being hoisted. After the removal of the form-work the model is wet cured for one week. As a precaution against any possible damage to the model due to the use of a vibrator for the compaction of an extra base, it was decided to use the same mix as for the model for the extra 6" base. No vibratory action was found to be necessary with the use of this mix. The extra base was also cured well for a period of one week. It was observed, however, that the cracks began to appear two days after the curing stopped.

With careful examination of the evidence, it can be stated that the cracks existed due to the inherent properties of the mix itself rather than due to any other factors including modelling technique. This is discussed further later in this thesis.

CHAPTER III

LOADING AND TESTING OF MODELS

3.1 Design and Description of Loading-Cap

The loading-cap which is used to transmit the horizontal force to the model consists of a 1/4" aluminum plate 44" long and 28" wide. Aluminum angles (2" size) are bolted to the underside of this plate such that when the cap is placed on top of the model, the "E" section of the model is enclosed within the angles protruding underneath the plate (Fig. 17). The aluminum angles are slotted, as shown, to accommodate any slight irregularity in the section. This arrangement not only transmits load over the entire section of the model but also restricts externally the top end section of the model to maintain its regular "E" shape during the loading process. It is assumed that the total pressure is equally distributed over the flanges at the top end section.

3.2 General Description of Loading System

The model is loaded through a hydraulic jack. The piston rod of this hydraulic jack is 3/4" in diameter the end of which is threaded. The base of the hydraulic jack is bolted to a 1/2" thick (24" x 18") steel plate through two 6" long parallel slots (Fig. 18). This arrangement permits about 2" travel of hydraulic jack in the horizontal plane. The steel plate is slotted along its vertical edges through which the plate-jack assembly is bolted to the steel column. The vertical slots permit a 4" travel of the assembly in vertical plane. The horizontal and vertical slots, together, permit accurate alignment of loading. Figure 19 shows the loading jack attached to the steel column and the pump by means of which the piston is actuated. The pump is operated manually and though it does not permit precise control during unloading, as small as 25 lbs. increaments can easily be obtained by this arrangement. To the end of the piston is attached a strain-gage bonded load-cell (Fig. 20). A 3/8" diameter flexible wire, whose two ends are fixed to two points along the edge of the loading-cap, forms a loop which in turn is connected to the load-cell through a turn-buckle thereby completing the connecting arrangement between the piston and the loading-cap. The general photograph (Fig. 21) shows the various elements in the connecting arrangement. The turn-buckle permits removal of any initial slack in the connections. The centreline of the piston, which is the line of action of the resultant force,passes through the centre of the flanges giving an eccentricity of 13.30 inches with respect to the shear centre.

3.3 Instrumentation and Measurements

It was intended to record the magnitudes of deflections at significant points across the cross section and at different levels of height, and to record the magnitude and pattern of strain distribution across the corss sections. A steel frame-work (Fig. 21) footed on the aluminum base plate supports the deflection gages whereas the strain gages are bonded to the model surface at significant points where the strain measurements are intended. Figure 22a shows the locations at which deflections were recorded for all models. Except for Model No. 2, the locations at which longitudinal strains were measured are shown in Figure 22b. For Model No. 2, the figure on page 97 shows the locations at which the longitudinal strain measurements were made.

CHAPTER IV

OBSERVATIONS AND RESULTS

4.1 Cracking Patterns at Failure

Figures 23 through 26 show the crack patterns at failure for various models. Initial cracks due to shrinkage if any are also shown. Almost all the models failed in a brittle manner with a loud sound indicating that as soon as a crack appeared in a tension zone it extended over the entire cross-section. Of particular interest is the crack pattern shown in Figure 23 for the model with no initial shrinkage cracks in the test height. The flattened "V" shaped crack in the flange farthest from the load apparatus clearly indicates the type of strain distribution. A similar pattern is observed in the rest of the models too but these were affected to some degree by the presence of initial shrinkage cracks.

4.2 Load-Strain Results

Figures 27 and 28 show the typical strain distribution pattern over the cross-section as predicted by Vlasov's theory. The experimental values of strains recorded (Model No.2) for points across the cross section are plotted on the same diagrams for the purpose of comparison.

It may be seen from these diagrams that experimental values agree qualitatively with theoretically predicted tension and compression zones across the cross sections. However, the actual experimental values do not agree well with those predicted by theory and in general the experimental values are lower than the corresponding theoretical values. The difference between experimental and theoretical values is larger for points 1, 6, 7 and 12 which are close to the free edges of the flanges. For the sections at heights of 2" and 45" above the fixed end for which the strain distribution is plotted, it may be noted that the difference between the theoretical and the experimental values is smaller for the larger height (45") as compared to the height of 2 inches.

4.3 Load-Deflection Results

Figures 29 and 30 show a typical comparison of experimentally obtained deflections with those predicted theoretically. The curves show the variation of deflections along the height of the model. The deflections are larger at the free edges of the flanges and increase with the height above the fixed base. Generally, all the flanges deflected equally and the order of magnitude for maximum deflections (near the free edges of the flanges) is 0.1".

Although the theoretical and experimental values for deflections differ vastly, two notable trends can be observed.

1) The percentage difference between the theoretical and experimental values is smaller for points located near the free edges of the flanges than for points on the flanges near the corners.

2) Along the test height of the model the percentage difference between the two values is smaller for greater heights for both locations either near the free edges or near the corners. From the measured deflections the deformed configuration of the sections for various heights and different values of loads can be drawn; typical configurations of the deformed sections are shown in Figures 31 through 33 for Model No. 5. In constructing the deflected shapes a different scale (as indicated on Figures 31-33) is used for deflections than the scale used for sectional dimensions. The two perpendicular components of delfections for the corners of the section enable one to determine the final positions of the cross sectional components relative to each other. From this construction, it follows that even for small values of loads the deflected shape is no longer a regular "E". It can then be concluded that the assumption of rigid sections is in gross error in the

present problem. The experimental results show that this assumption is violated at all measured heights but the distortion at higher heights is relatively smaller than the distortion at lower levels. This agrees with the trend observed earlier when comparing theoretical and experimental values of deflections and strains. The top end is restricted externally through the use of loading plate to maintain its shape. The restraining effect is reduced at lower levels so that a larger percentage difference between theoretical and experimental values would be expected at lower levels, as was observed. It is therefore concluded that the kinematical relations for the theoretical deflections, given by Vlasov's theory and which follow from the assumption of rigid section, are in gross error because the section deforms in its own plane and the basic assumption is not true.

4.4 Variation of strain over the thickness of the cross section

The variation of strain over the cross sectional thickness is also considered. This was done by mounting strain gages exactly opposite to each other at two locations on one of the flanges. The results showed that the experimental values for each pair of strain gages were in good agreement. The difference between recorded values of strain within each pair was always less than 2 microinches per inch. This shows that the stresses across the thickness of the cross section are uniform for all practical purposes.

CHAPTER V

ANALYSIS OF RESULTS

5.1 Method of Analysis

Mathematical analysis adopted for the present problem is based on Vlasov's well known theory of thin-walled beams. The difference between this theory and ordinary beam theory is that it recognizes the distinctive feature of thin-walled beams that they can undergo longitudinal extensions as a result of torsion. Because of the warping of the sections, in thin-walled beams, longitudinal normal stresses are created proportional to the corresponding strains due to such longitudinal extensions. These longitudinal normal stresses, which arise as a result of the relative warping of the section and which are not examined in the theory of pure torsion, can attain very large values in thin-walled beams with open (rigid or flexible) cross sections and also in beams with closed flexible cross sections. Vlasov called the longitudinal normal stresses due to warping as complementary longitudinal normal stresses.

Vlasov made two basic hypotheses in his theory of thin-walled beams of open sections. The first is that a

thin-walled beam of open section can be considered as a shell of rigid (undeformable) section. On the basis of this hypothesis the deformation, under load, of the section of a thin-walled beam in its own plane shall consist of rigid body translation and rotation.
Figure 34 shows the contour line of the middle surface of the section of the model. Point "O" is the centroid of the section and point "S" is the shear centre. OX and OY are the principal axes, the former being the axis of symmetry. The shear centre lies on the axis of symmetry and is distant a_x from the centroid. ξ and η are the displacements of the point S in the direction of the coordinate axes OX and OY respectively, and θ is the angle through which the section rotates as a rigid body about the shear centre. If V and W are the displacements of a point lying on the section in the direction of the coordinate axes OX and OY respectively, then based on the aforementioned purely geometrical hypothesis, the following relations are obtained

$$V(z,y) = \xi(z) - (y-a_y)\,\theta(z) \qquad \ldots.(1)$$

$$W(z,x) = \eta(z) + (x-a_x)\,\theta(z) \qquad \ldots.(2)$$

In these equations z is the coordinate of a section along the axis of the beam from some fixed plane of origin. In a thin-walled beam in which both coordiante axes OX and OY are not the axes of symmetry, the line of shear centres is taken as the axis of the beam. Figure 35 shows the contour line of the middle surface of the model and the coordinate z along the axis of the model. This longitudinal axis together with the coordinate axes OX and OY form an orthogonal coordinate system.

The second assumption made in Vlasov's theory is that the shearing deformations of the middle surface are negligibly small and can be assumed to vanish. By means of the second hypothesis concerning the absence of shearing strains in the middle surface, Vlasov found the longitudinal displacement u(z,s) directed across the plane of the cross-section due to the deformation of the middle surface, and obtained the following relationship.

$$u(z,s) = \zeta(z) - \xi'(z)\ x(s) - \eta'(z)\ y(s) - \theta'(z)\ \omega(s) \qquad \ldots.(3)$$

In this equation s(x,y) is coordinate along the contour line of the section with respect to some fixed point on the section. The choice of the origin of the coordinate s(x,y) is arbitrary and is conveniently chosen depending on the shape of the contour line. Figure 36a represents the physical meaning of the second assumption, in which are shown the tangential displacements u(z,s) and v(z,s) occuring in the appropriate tangent planes, of four vertices M, a, b and c of an elementary rectangle. The shearing strain at the point

M is by definition equal to the sum of angles α and β through which the sides Ma and Mb of the elementary rectangle rotate during deformation. Denoting the shearing strain by γ, we have by the second hypothesis;

$$\gamma = \frac{\partial u}{\partial s} + \frac{\partial v}{\partial z} = o,$$

from which upon integration equation (3) is obtained. In equation (3) $\zeta(z)$ is an arbitrary function depending on z, which describes the longitudinal displacement of the point on the section which serves as the origin of the coordinate s. ξ', η', θ' are the first derivatives of the respective quantities with respect to variable z, and $\omega(s)$ is defined as sectorial area equal to twice the area enclosed between the radius vector PM_1 and PM. Point M_1 is the origin of the sectorial areas which is arbitrarily chosen depending on the shape of the section whereas point M is the mobile point along the middle surface. Point P (Fig. 36) is called the pole of the sectorial areas and when the pole is the same as the shear centre $\omega(s)$ is the principal sectorial area. Therefore, for a given profile line and specified points for the pole and the origin of the mobile radius vector, the sectorial area $\omega(s)$ is a well defined function of s just as x(s) and y(s). The sectorial area will be considered positive if the mobile radius vector PM (Fig. 36b) moves clockwise when observed from the negative z direction.

In equation (3), the function $\zeta(z)$ determines the axial deformation when the cross section undergoes only a rectilinear displacement along the axis of the beam. The function $\xi(z)$ and $\eta(z)$ describe the flexure of the axis of the beam ($x = a_x$, $y = a_y$) in the longitudinal planes OXZ and OYZ and characterize the bending deformation. The fourth term of equation (3) determines the part of displacements that does not obey the law of plane sections and which arises as a result of torsion and is termed as sectorial warping of the section. Knowing the longitudinal displacements $u(z,s)$ of the points of the middle surface, the longitudinal strain "ε" could be determined by taking the derivative of $u(z,s)$ with respect to z

$$\varepsilon = \frac{\partial u}{\partial z} = \zeta'(z) - \xi''(z)\ x(s) - \eta''(z)\ y(s) - \theta''(z)\ \omega(s) \qquad \ldots.(4)$$

Equation (4) allows the determination of longitudinal strain at any point of the middle surface of a thin-walled beam when the four functions $\zeta(z)$, $\xi(z)$, $\eta(z)$ and $\theta(z)$ are known.

These functions are determined from the following linearly uncoupled differential equations derived from equilibrium considerations. These equations are simplified form of Vlasov's general equations due to the absence of longitudinal load and shear forces along the longitudinal edges of the present model. Also there are no distributed loads q_x, q_y in the direction of x and y respectively and there is no distributed moment since the model is loaded at the top by an eccentric transverse load only. The differential equations are:

$$EA\zeta'' \doteq o \qquad \text{....(5)}$$

$$EI_y\xi^{IV} = o \qquad \text{....(6)}$$

$$EI_x\eta^{IV} = o \qquad \text{....(7)}$$

$$EI_\omega\theta^{IV} - GI_d\theta'' = o \qquad \text{....(8)}$$

A is the cross-sectional area of the section, I_y and I_x are the moments of inertia of the section, respectively, about y and x axes. $I_\omega = \int_A \omega^2 dA$, has the dimensions L^6 and is defined as sectorial moment of inertia, characterized only by the shape of the cross section. E and G are moduli of elasticity and rigidity and I_d is another geometric property of the section termed as torsional rigidity of the section.

Boundary Conditions

The model is fixed at the base (z=o) and loaded at top such that the resultant line of loading has an eccentricity "e" with respect to the shear centre. The effect of this load with respect to the line of shear centres is a flexural load (pure bending) "Q" and an anti-clockwise torsional moment M = Qe.

In absence of any externally applied loads in x and z directions, functions ζ and ξ are both zero. It is assumed that the compressive stresses due to self weight are negligible. The functions η and θ are obtained by integration of equation (7) and equation (8). Equation (8) has four constants of integration which are determined by applying four boundary conditions, two at each end. The solution of these basic equations for the determination of the functions η and θ are given in Appendix C.

The resulting equations are,

$$\eta(z) = \frac{Q}{EI_x} \quad [3\ell z^2 - z^3] / 6 \qquad \text{....(9)}$$

$$\eta''(z) = \frac{Q}{EI_x} \quad [\ell - z] \qquad \text{...(10)}$$

$$\theta(z) = \frac{Qe}{GI_d} \quad [z - \ell/k \{\tanh k(1 - \cosh k/\ell\ z) + \sinh k/\ell\ z\}] \qquad \text{...(11)}$$

$$\theta''(z) = \frac{Qe}{GI_d}\ k/\ell\ [\tanh k \cosh k/\ell\ z - \sinh k/\ell\ z] \qquad \text{...(12)}$$

where $k/\ell = \sqrt{\dfrac{GI_d}{EI_\omega}}$, and ℓ = length of the model.

Knowing the values of η and θ and their derivatives, the theoretical values of deflections $V(z,s)$, $W(z,s)$ and longitudinal strains $\varepsilon(z,s)$ are computed from the following relationships.

$$V(z,y) = -y\theta(z) \qquad \text{....(13)}$$

$$W(z,x) = \eta(z) + (x - a_x)\theta(z) \qquad \text{....(14)}$$

$$\varepsilon(z,s) = -\eta''(z)\, y(s) - \theta''(z)\, \omega(s) \qquad \text{....(15)}$$

5.2 Comparison of Typical Results

(a) Comparison on the basis of recorded strains:

Comparison of experimental values for longitudinal strain $\varepsilon(z,s)$ and component deflections $W(z,s)$ with those computed theoretically (equations 15 and 14), is heavily based on particular model which had no cracks prior to testing. The distribution of strain, and therefore stress across the cross section is qualitatively in agreement with that predicted by theory. However, the magnitude of longitudinal strain at a particular point of the section, as predicted by theory, is higher than the corresponding experimental value. An important observation is made when comparing the corresponding values for different heights. The percentage difference between the experimental and predicted values is not constant for all heights but is smaller for higher heights. Figure 37 shows such a comparison between experimental and predicted values of strains for two heights (z = 2" and z = 45").

(b) Comparison of deflections:

The following table represents the experimental values of deflections $W(z,s)$, for two locations of the section and different heights of the model against corresponding values computed theoretically.

Location	Height in Inches z	Deflections in Inches	
		Theoretical	Experimental
(1) 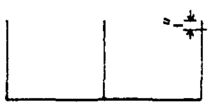	12" 48" 85"	0.00063 0.00870 0.02313	0.0037 0.015 0.028
(2) 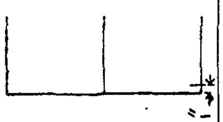	12" 48" 85"	0.00025 0.00328 0.00873	0.0029 0.010 0.016

No apparent correlation is seen to be present between theoretical and experimental values. Experimental values are much larger than what theory predicts. However, two significant trends seem to be obvious. It may be noted from the preceeding table that the percentage difference between theoretical and experimental values is smaller in case (1) for the point, on the section, located near the free edge as compared to case (2) where the point is located near the corner. In case (1), the percentage difference becomes smaller with increase in z, and for z = 85" the two values are quite comparable. A similar trend is observed in case (2), but to a lesser extent.

5.3 Discussion of Conditions Affecting Results

(a) Material properties:

Assuming that the basic assumptions made in the derivation of theoretical relationships (rigid sections and absence of shearing strains) are not violated, an investigation is made into the factors which could affect the theoretical results. The equations for θ (which is a measure of component deflection due to rotation about the shear centre) and θ'' (which is a measure of stresses and strains due to warping of the sections) are rewritten in the following form.

$$\theta(z) = \frac{2Qe(1+\nu)}{EI_d}\left[z - \sqrt{\left(\frac{2(1+\nu)I_\omega}{I_d}\right)}\left\{\tanh\sqrt{\left(\frac{I_d}{2I_\omega(1+\nu)}\right)}\,\ell(1-\cosh k/\ell\ z) + \sinh k/\ell\ z\right\}\right] \quad \text{....(16)}$$

$$\theta''(z) = \frac{Qe\sqrt{2(1+\nu)}}{E\sqrt{I_d I_\omega}}\left(\tanh k \cosh k/\ell\ z - \sinh k/\ell\ z\right) \quad \text{...(17)}$$

The above equations differ from equations (11) and (12) in that appropriate substitutions have been made. It could be seen from equations (16) and (17) that both θ and θ''

are inversely proportional to young's modulus E whereas poisson's ratio "ν" appears both in the numerator and denominator. The variation in the value of ν would also affect the values of the hyperbolic functions. It becomes apparent that both strains and deflections would decrease if the value of E is increased. The effect of variation in the value of ν is not obvious and could be ascertained only through computations for various values of ν. The value of E used in the analysis is that of the initial tangent modulus of the stress-strain curve found experimentally and is equal to 3.04×10^6 p.s.i. The value of poisson's ratio "ν" for concrete normally varies between 0.15 and 0.35 and a value of 0.15 is used for theoretical computations realizing the high compressive strength of the mix used. However, no appreciable difference is found in theoretical computations by varying the value of ν from 0.15 to 0.40 in increaments of 0.01.

The variation of E does not lead to any better agreement with the experimental behaviour since increase in the value of E would decrease the value of strains but also decrease deflections which are already much smaller than the experimental values.

(b) Load distribution:

Looking back into equations (16) and (17) it can be seen that both functions θ and θ'' are directly proportional to the rotational moment "M" and hence the eccentricity of loading. In the present arrangement of loading where the load is transmitted to the three cross-walls through the loading plate, it is assumed that the total load is equally distributed to the three cross-walls (Fig. 38). However, this could not be ascertained experimentally and it may be argued that the actual load distribution might be other than what has been assumed and the pressure distribution may not be equal for the three cross-walls. Any other type of distribution of load, different from the assumed one, may drastically change the stress distribution. The best way to know this important factor is to have a loading arrangement with clearly defined load points and line of load.

(c) Boundary conditions:

Boundary conditions are examined next. Since the aluminum plate is resting on top of the model it can be understood that the top end of the model, through friction between angles enclosing the section, is not free to warp; inducing that in the extreme case the top end section remains plane under load. With this assumption the boundary conditions are changed at the top end and the resulting relations for θ and θ'' are as follows:

$$\theta(z) = \frac{Qe}{GI_d}\,\ell/k\left[k/\ell z - \left\{\frac{\cosh k-1}{\sinh k}(1-\cosh k/\ell\, z) + \sinh k/\ell\, z\right\}\right] \quad \text{....(18)}$$

$$\theta''(z) = \frac{Qe}{GI_d} \; k/\ell \left[\frac{\cosh k-1}{\sinh k} \; \cosh k/\ell \; z - \sinh k/\ell \; z \right] \quad ....(19)$$

Comparing equations (18) and (19) with equations (11) and (12) it can be seen that these sets of equations differ only in the multiplying factors for the expressions $(1 - \cosh k/\ell \; z)$ in the equation for θ and for $\cosh k/\ell \; z$ in the relationship for θ''.

The multiplying factor for the set of equations (11) and (12) is tanh k and for the set of equations (18) and (19) is $\frac{\cosh k-1}{\sinh k}$. The numerical values for these are

$$\tanh k = 0.227$$

$$\frac{\cosh k-1}{\sinh k} = 0.115$$

On using equations (18) and (19) it is found that although the values of deflections were still much smaller, the values of strains are quite comparable with experimental values for the height z = 2". On carrying the computations for a higher value of z (z = 68.25") it is found, however, that the signs for strains are reversed for points located at higher heights along the same longitudinal line. This is contrary to the experimental observations and cannot be justified.

For the boundary condition at top end, however, it is more logical to assume the top end neither completely free nor remaining plane under load. The end condition may be thought to be in between these two extremes. This effect may be studied by introducing a coefficient "C" for the multiplying factor (tanh k) and computing theoretical values for the variation of "C" between values of 0.5 and 1.0. It is found that for values of "C: less than 0.9, the signs of theoretically computed strains at heights (z = 68.25") are reversed; again this is contrary to the experimental observations.

CHAPTER VI

CONCLUSIONS AND RECOMMENDATIONS

6.1 Applicability of Method of Analysis

From the deformed shapes of the cross sections constructed from experimental results, it is concluded that sections are not rigid in their own planes as assumed in the mathematical analysis. Looking at the geometrical dimensions of the model (depth of web $d = 40''$, flange width $d_1 = 16''$ and length of model $\ell = 90''$) it is seen that the ratio $d/\ell = 0.44$ as compared to the corresponding ratio of, equal to or less than 0.1, defining a thin-walled beam in Vlasov's theory. The rotational effect under eccentric load is much more pronounced than the pure bending effect because of the small value of torsional rigidity I_d for the section. The large measured values of deflections are due to the fact that the corners do not remain at right angles under load and also the final deflected points on the web lie on a curve instead of on a straight line as shown in an exaggerated manner in the Figure 39. Therefore, the deflections due to the rotational effect cannot be considered as those due to the rigid body rotation of the whole section about the shear centre.

When the section is deformable in its own plate, any bending within the web resulting into a curved contour line of the web would result in much higher deflections at the flange-tips than would occur due to rigid body rotation. The effect would be even more significant if the corners do not remain at right angles.

Therefore, it is concluded that the disagreement in the results, quantitatively, is due to the fact that the very basic assumption of rigid sections in Vlasov's theory of thin-walled beams is not valid in the present problem. Nevertheless, this theory serves a useful purpose for the model study because it indicates the nature of stress distribution across the section and regions of maximum tensile and compressive stresses. Of particular significance is the favourable trend near the top end which is externally restrained to maintain its shape and therefore is nearer the situation assumed in Vlasov's theory.

It may be recalled that a shear wall building is a three dimensional entity consisting of walls and interconnecting floors. The present model is a simplified form of the prototype in the sense that it contains no interconnecting floors. This simplification of the model was necessitated in order to develop a modelling technique. Once a satisfactory modelling technique is developed for the present model shape the floors can be added without much modification of the form-work. When the floors are added at various levels they would, essentially, help maintain the shape of the cross sections and therefore would ensure the validity of the assumption of rigid sections. Based on these arguments, it is concluded that Vlasov's theory of thin-walled beams may prove a satisfactory approach for the investigation of the models with floors and therefore a method of approach for the prediction of gross behaviour of the prototype on the basis of which improvements in design and construction could be suggested.

6.2 Implications for Design

The results of the present model study have clearly indicated the general behaviour and stress-distribution pattern in three dimensional shear wall buildings under the type of lateral loading used in this investigation. These results at the present stage, though having no direct bearing on the design of such a structure, are nevertheless useful in providing an understanding of the general behaviour of such structures. The mathematical approach is basic and simple in its application yet it so well defines the qualitative behaviour of such structures in terms of the nature of stresses and points of maximum stress. The maximum stresses due to the rotational effect are twice as much as those due to pure bending and therefore any design based on treating each wall separately as a plane stress problem will be in gross error. The indicated areas of maximum stresses can be properly reinforced to improve the design as a whole.

6.3 Recommendations for Construction Procedures

The main problem encountered in the whole modelling procedure was the occurance of cracks. These cracks, essentially, appeared near the base and therefore necessitated the pouring of extra 6" concrete base to cover them. In the very first model which was tested, the extra base completely covered the cracks but in other models these cracks extended high enough to be unable to cover them completely. However, to be consistent, the 6" extra base was poured around the structure in all models.

These cracks are attributed to the shrinkage effects which are inherent properties of concrete and mortars. The finer size materials, type of cement and the high percentage of water used in the present mix all contribute towards increasing the shrinkage effects and hence the shrinkage cracks. The small thickness of the section of the model and large surface area act to increase the significance of these factors. One of the reasons which led to the use of high early strength cement is the reduction of the curing time in order that the model be ready for test in a reasonably short time. However, the advantage of high early-strength is offset by the amount of time required to put the deflection gages in place and the mounting of strain gages. These operations required about three weeks, on the average, for each model. In view of this it is recommended that ordinary portland cement be used instead.

Greater percentage of finer material in a mix increases the chances of having shrinkage cracks. In the present mix even the largest aggregate size (1/8") is fine in terms of the general definition of coarse aggregate. The percentage of limestone aggregate should be increased with decreased percentage of silica sand.

The remaining important factor in the mix related to shrinkage effects concern the percentage of water used. High water-cement ratio increases the chances of shrinkage cracks. The high water-cement ratio (0.53) in the present mix is called for in order to have a high workability. Since the model section is only 1/2" thick and the form-work is such that the mortar has to be pushed through this small space of the mould to make a 16" deep vertical section, the mix has to be extremely workable in order to avoid any voids. Any such voids could seriously effect the results. It is therefore desirable to investigate, further, the possibility of reducing the water-cement ratio without seriously impairing the workability of the mix.

The 2" thick monolithic base involves a large volume of mortar at one end of the model as compared to the sectional area of the model proper and therefore restricts the changes in the volume of the model at that end during setting process. This is probably the reason for the shrinkage cracks persistently occuring near the base. The volume changes in the extra 6" concrete pad which is poured after the model is hoisted in place may have similar effects. It is therefore recommended that such large volumes of concrete at one end may be avoided in future modelling and other means should be considered to achieve fixed end conditions at the base.

Careful consideration should be given in attaining favourable humidity conditions. With a heated laboratory during the winter, quick surface drying of the model can take place and is therefore another factor which could cause surface cracks. Therefore, it is recommended that future testing be done in a laboratory with humidity control.

6.4 Other Recommendations

Loading device:

Vlasov's theory of thin-walled beams is essentially the rejection of the law of plane sections as assumed in the ordinary beam theory. The applicability of Saint Venant's principle is also doubtful in the case of thin-walled beams. At present, little information is available regarding the validity of this principle and the extent of possible deviations for problems such as in the present investigation. Under such circumstances, it is important to establish a clearly defined line of load. Therefore, it is suggested that loading cap should be improved in order to achieve this purpose and some method should be devised, also, to indicate the pressure distribution along the cross walls.

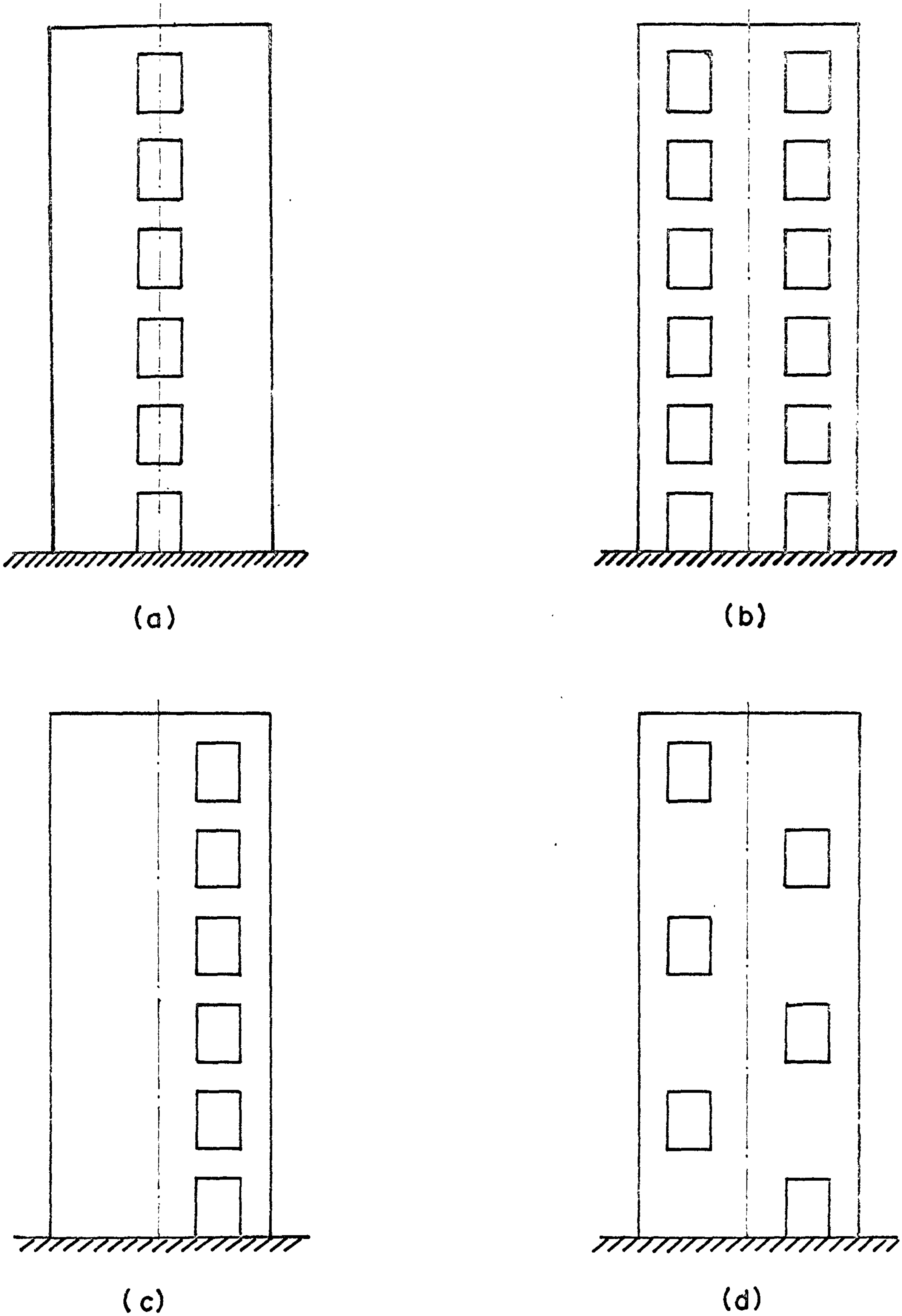

FIG. 1_TYPES OF OPENINGS IN SHEAR WALLS.

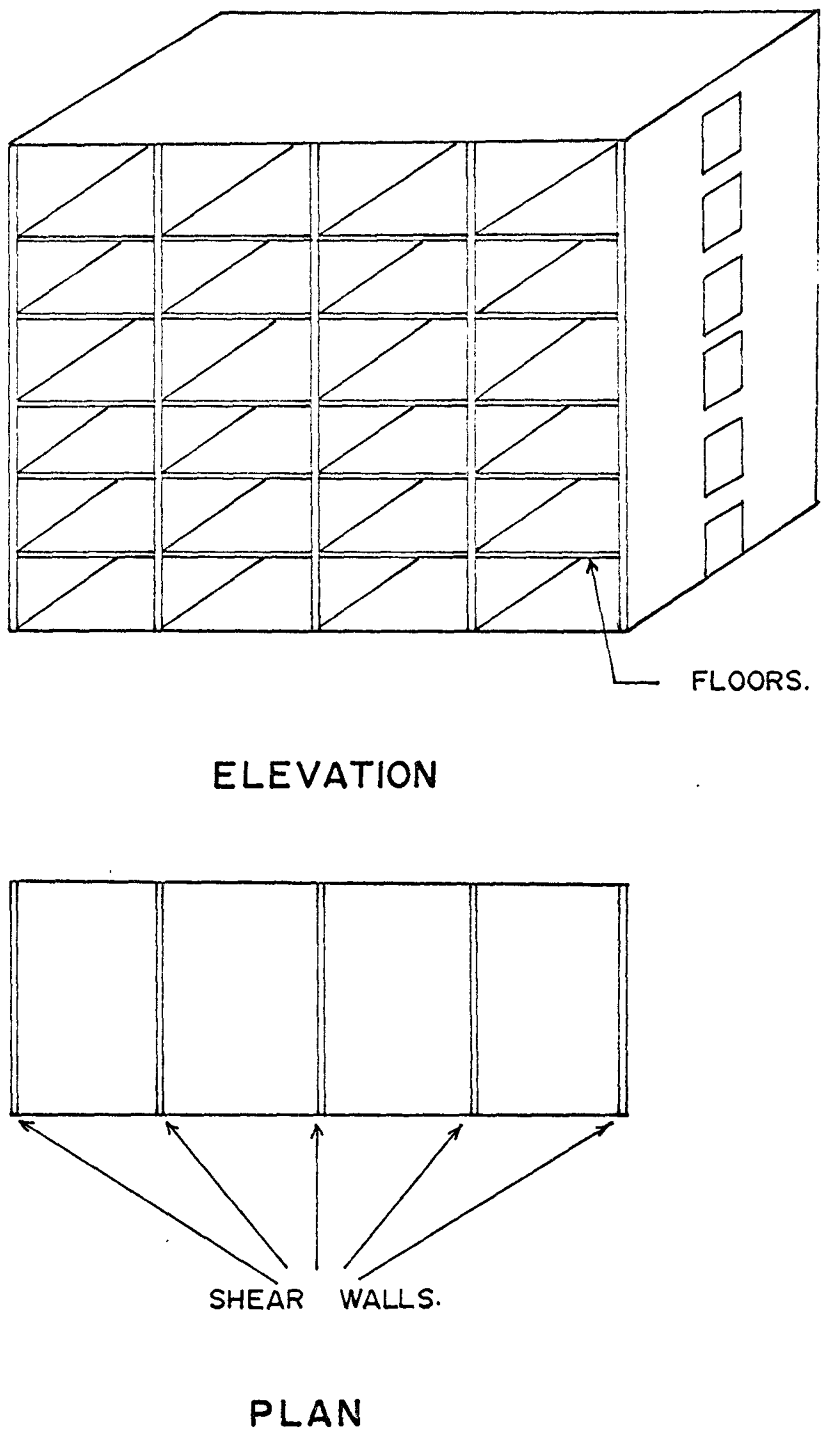

FIG.2 _ CONSTRUCTION USING RECTANGULAR-SECTION SHEAR WALLS IN A SIX-STOREY BUILDING.

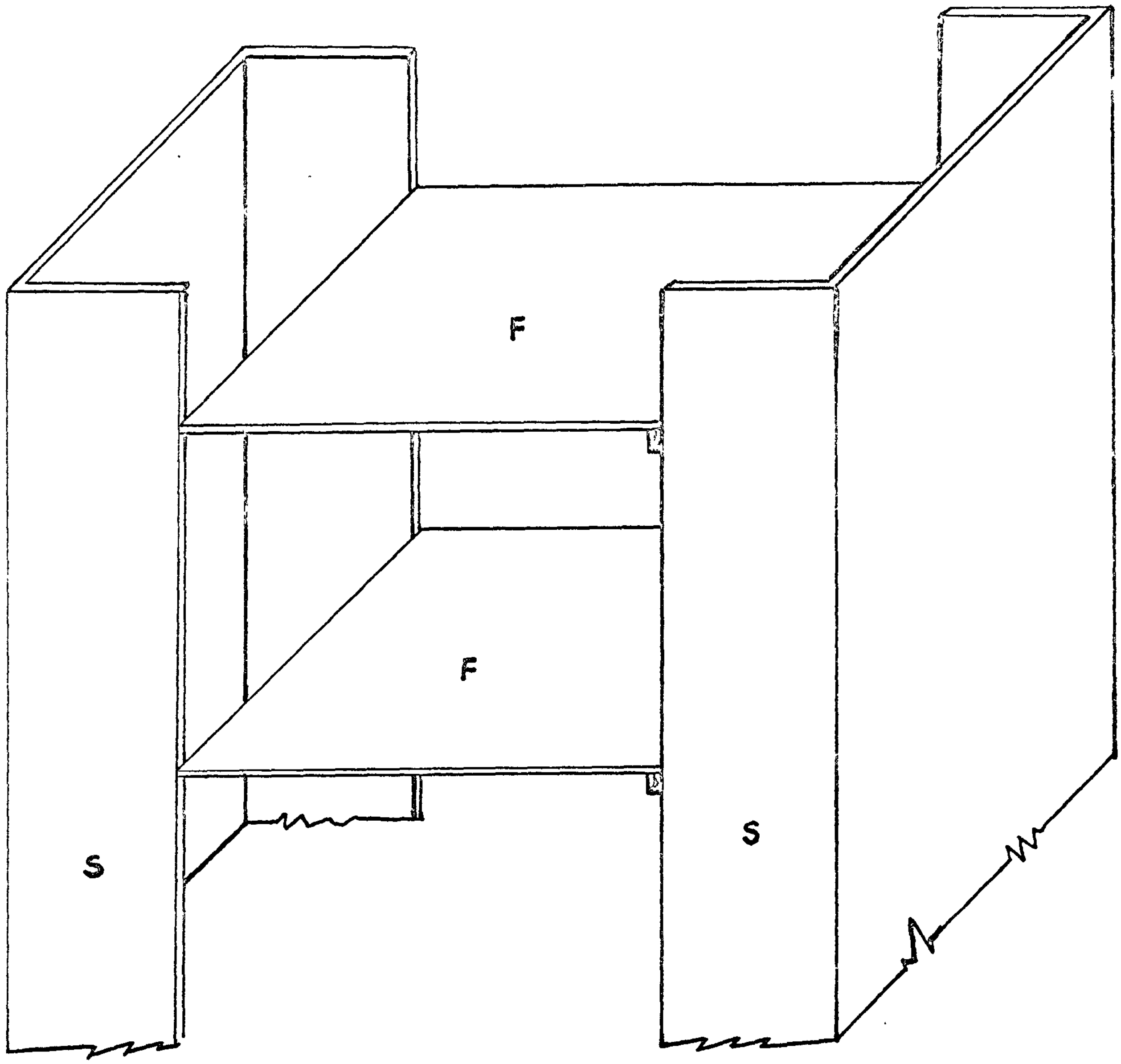

S — SHEAR WALLS

F — FLOORS

FIG.3 — CONSTRUCTION USING CHANNEL-SECTION SHEAR WALLS.

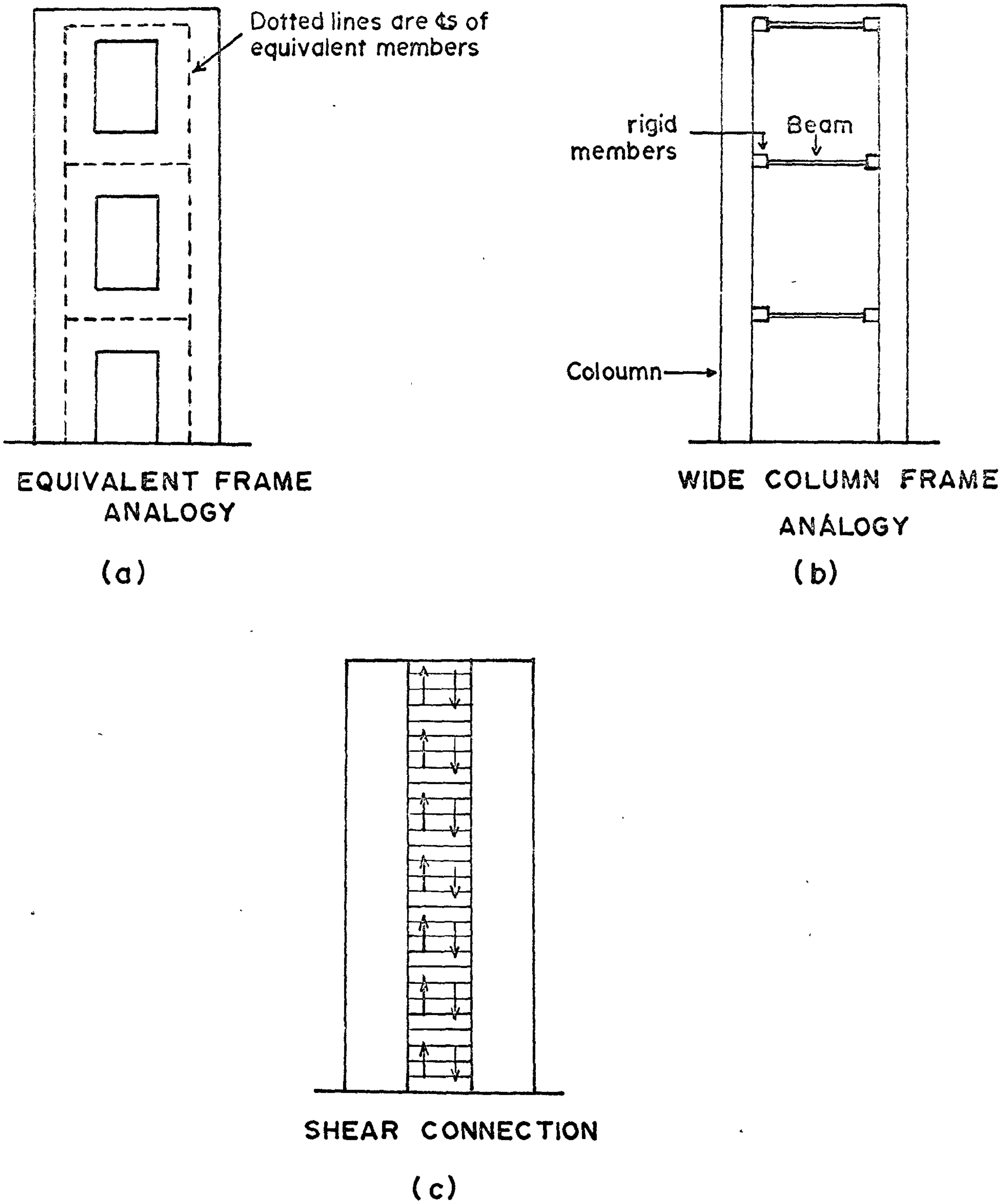

FIG.4_FRAME ANALOGIES & SHEAR CONNECTION METHOD OF ANALYSIS.

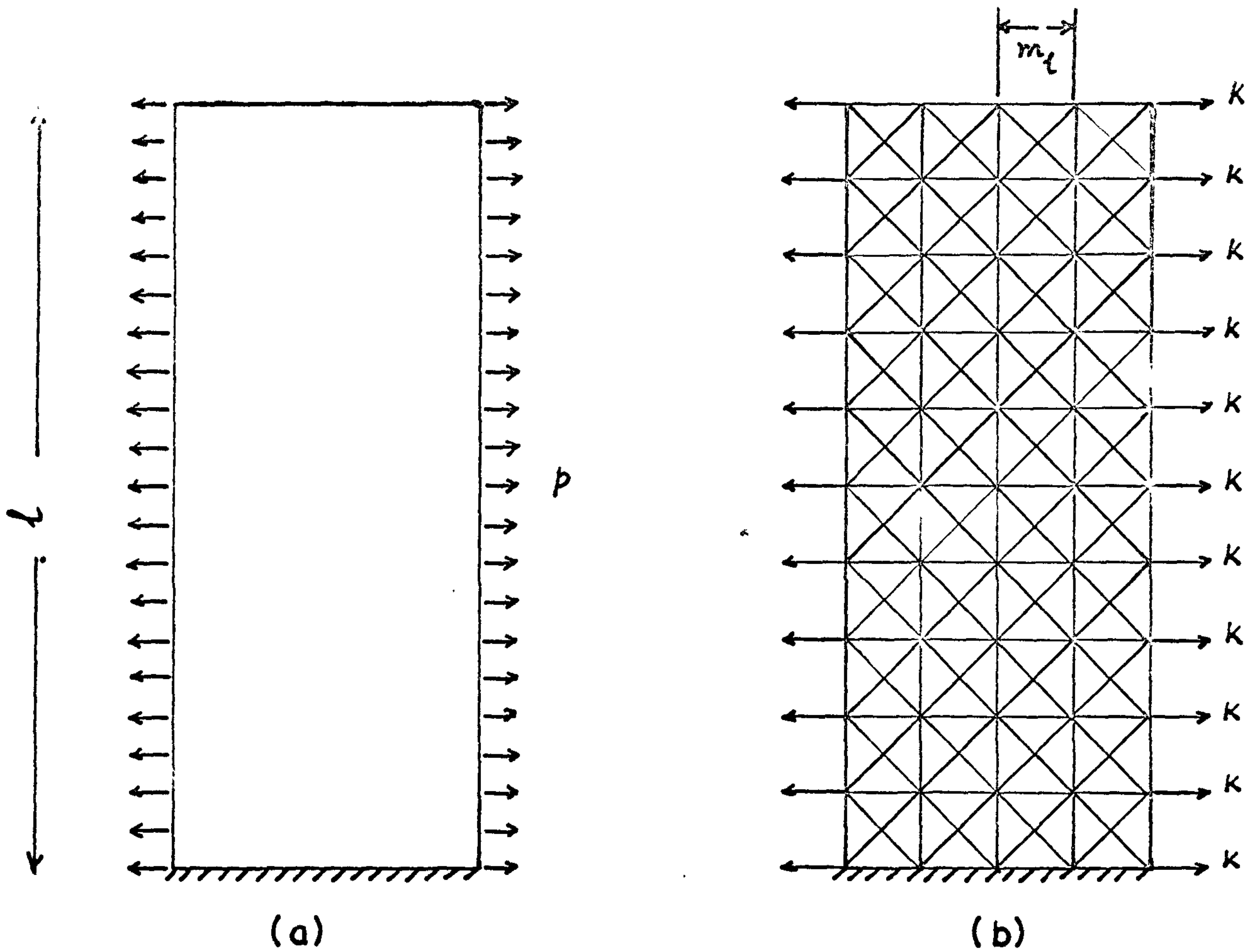

P = pl

K = P/n

n = Number of joints at the long boundary

FIG.5_LATTICE ANALOGY FOR TWO-DIMENSION STRESS PROBLEM.

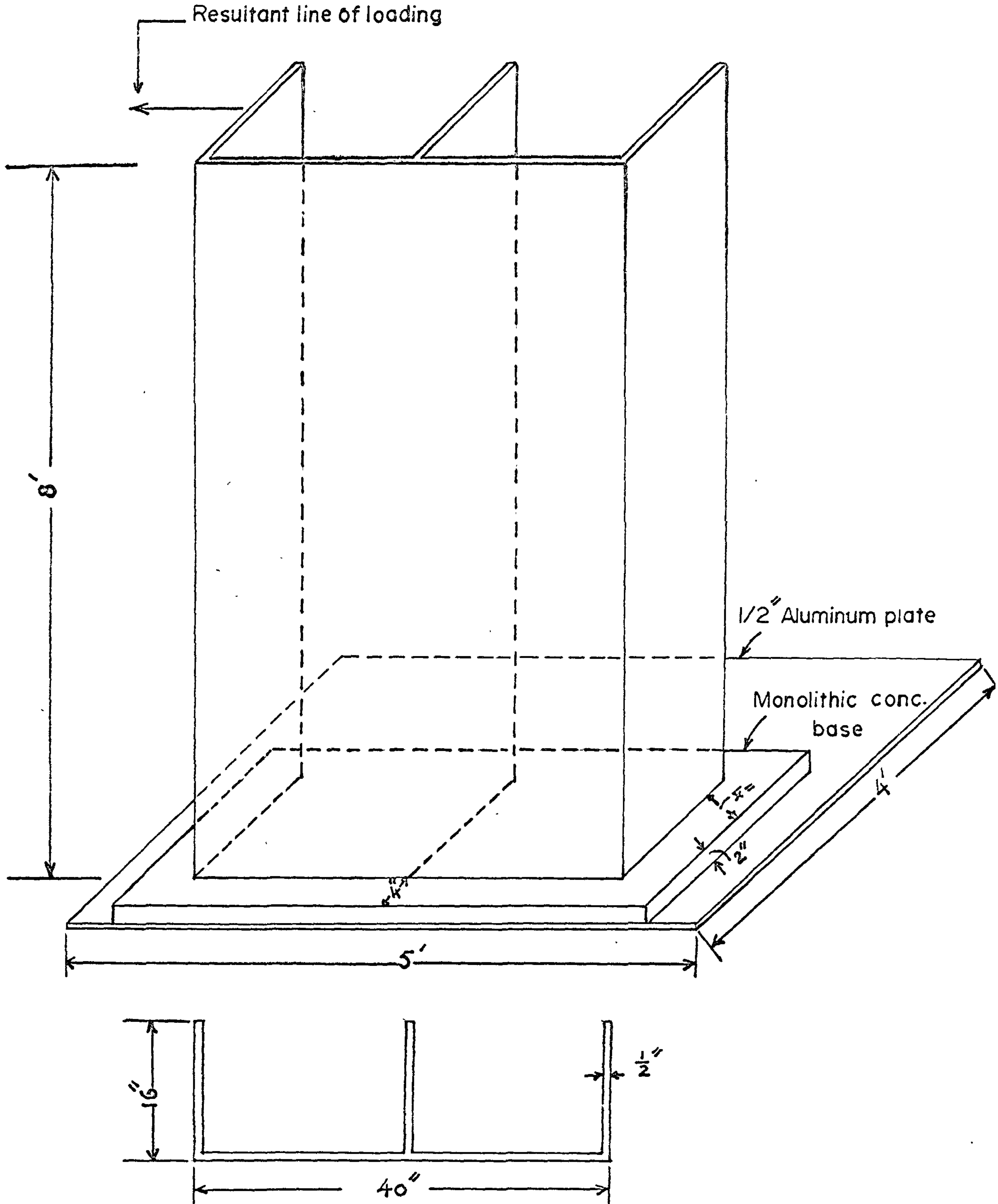

FIG. 6 _ DIMENSIONAL SKETCH OF THE PROPOSED MODEL.

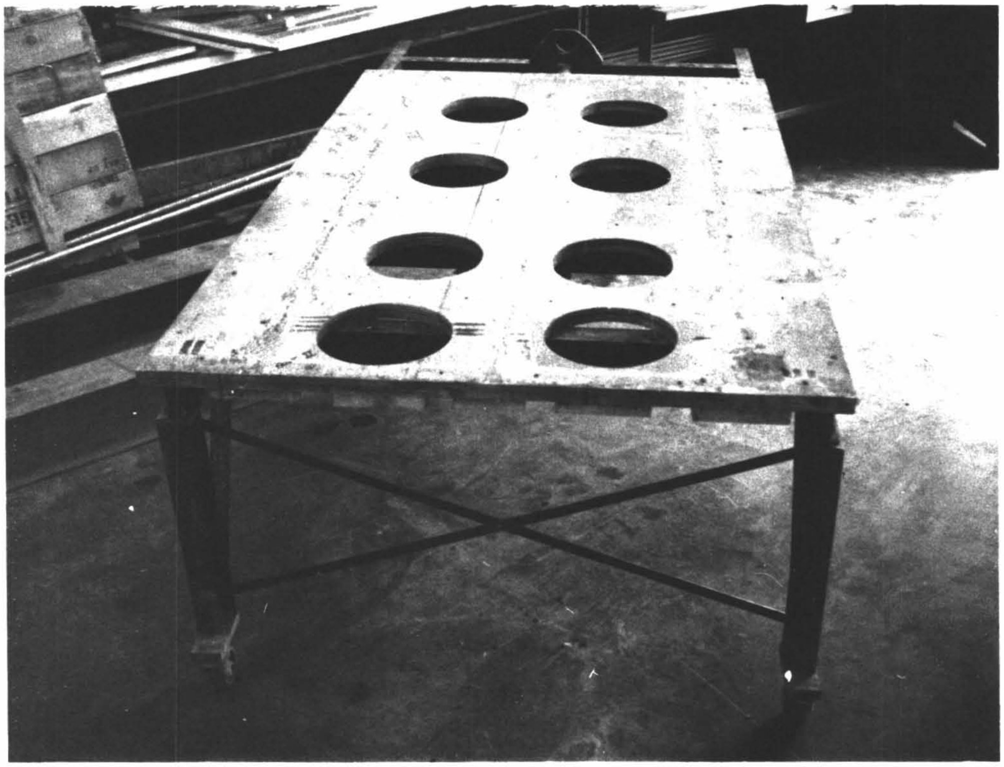

Fig. 7. Photograph showing the main platform on the tri-legged steel frame.

Fig. 8a. Assembling the form-work; outer panels and cross-boards in place.

Fig. 8b. Assembling the form-work; inside panels added.

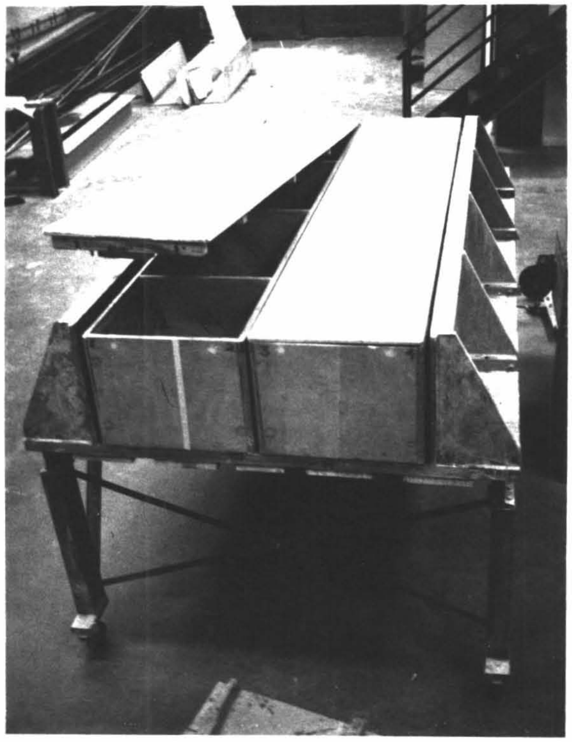

Fig. 8c. Assembling the form-work; panels B-B added.

Fig. 9. Photograph showing the base plate.

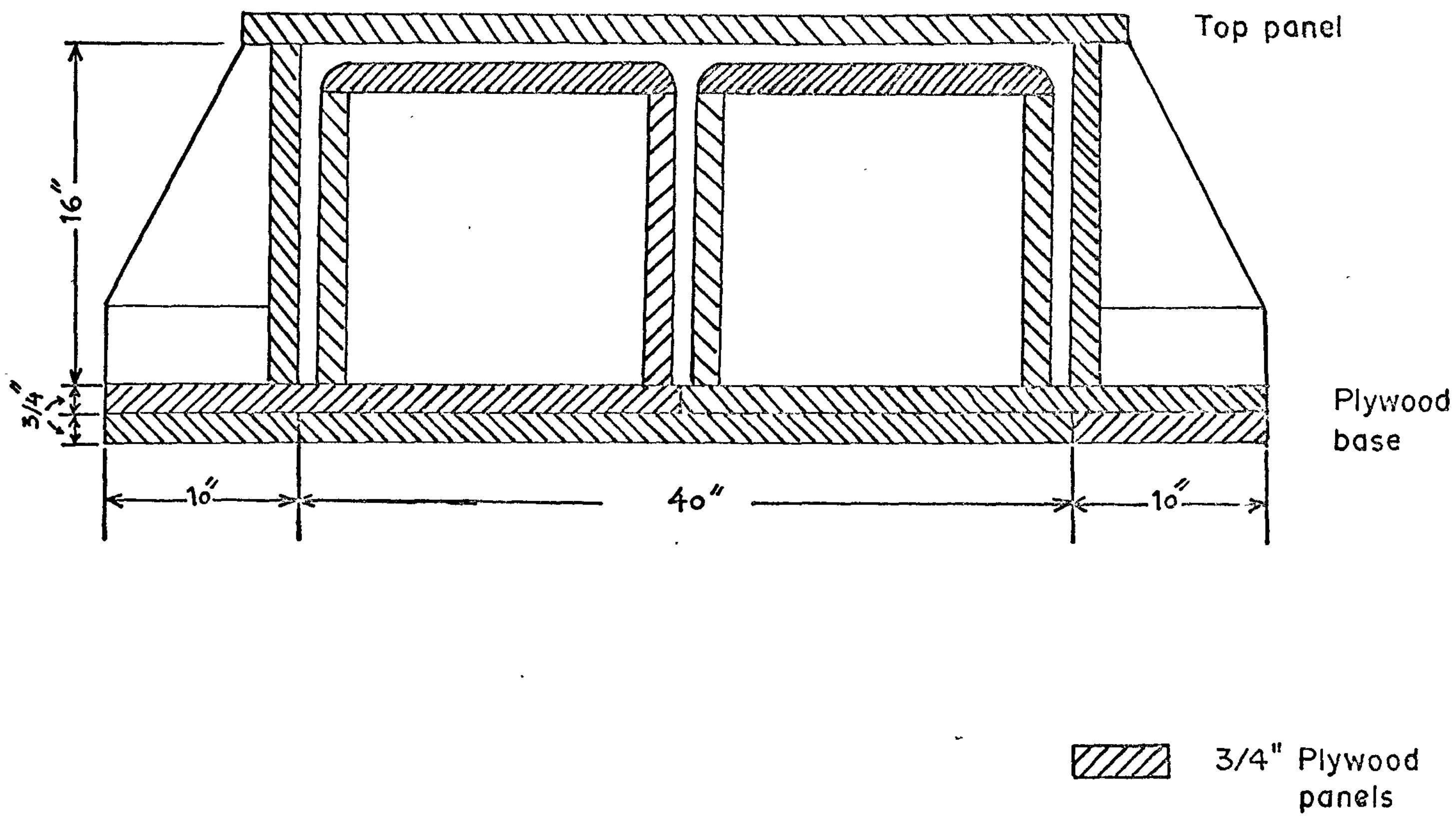

FIG.10_CROSS SECTION OF THE ASSEMBLED FORM-WORK.

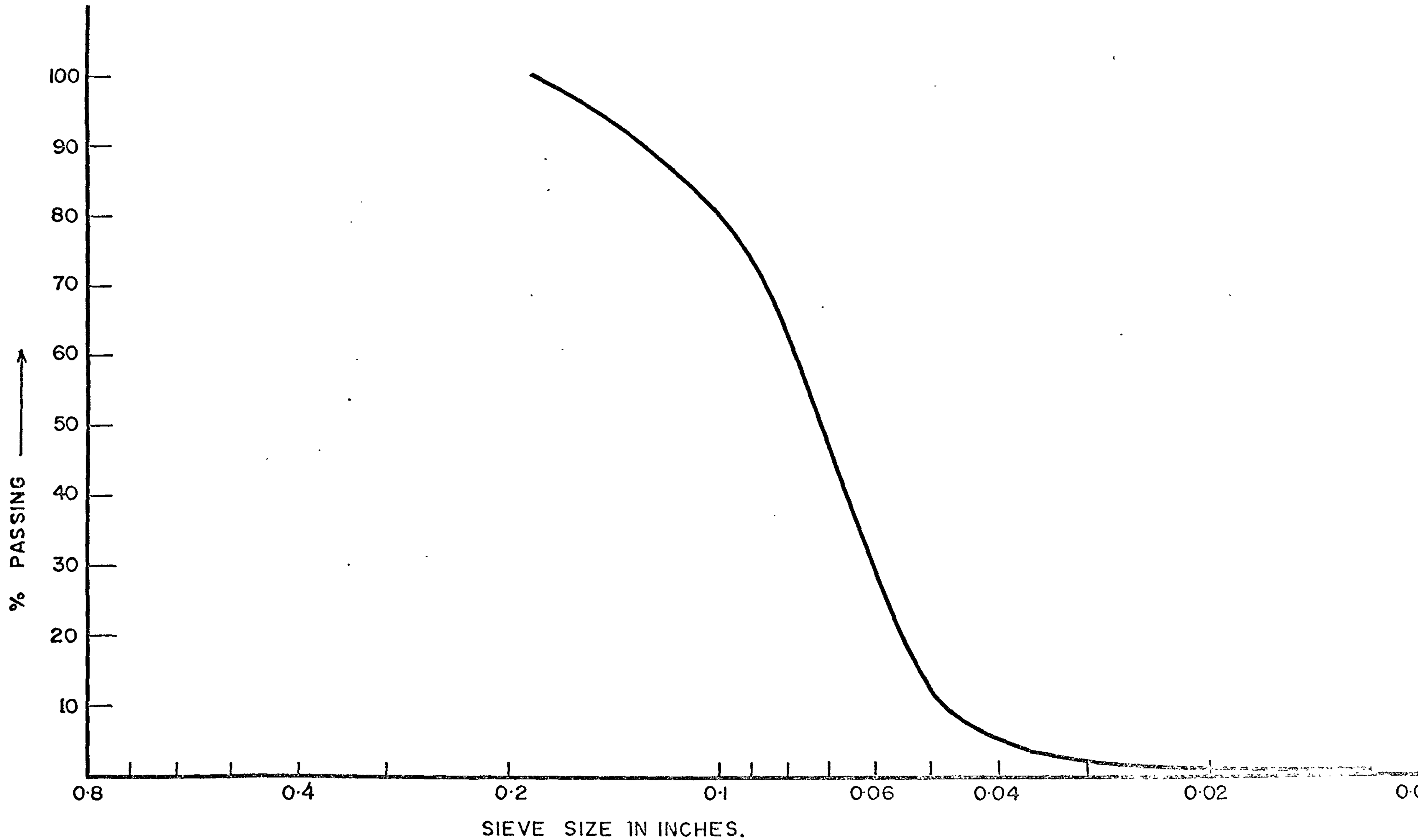

FIG. 11_ GRADING CURVE-DOLOMITE LIMESTONE.

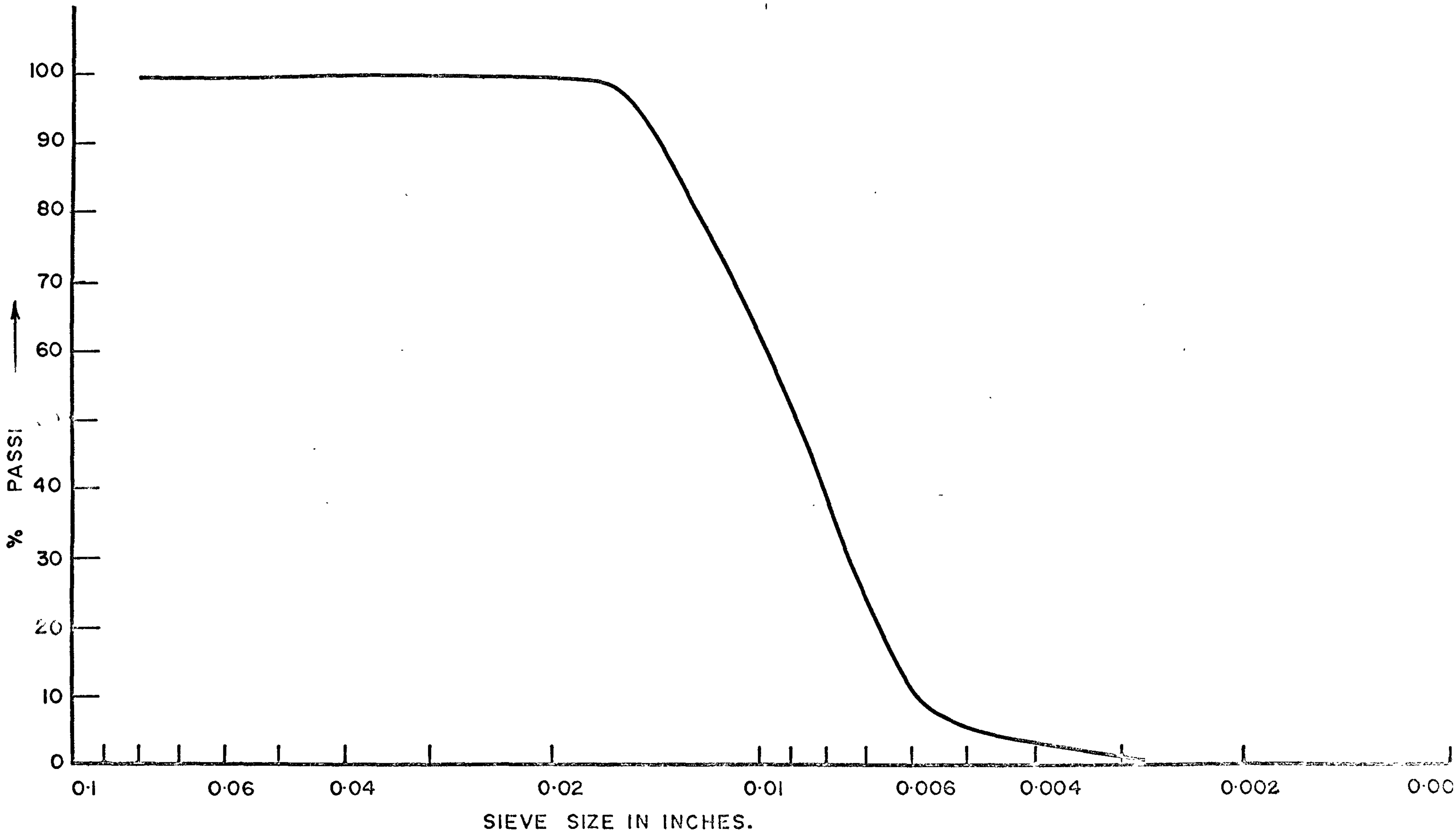

FIG. 12 _ GRADING CURVE - SILICA SAND.

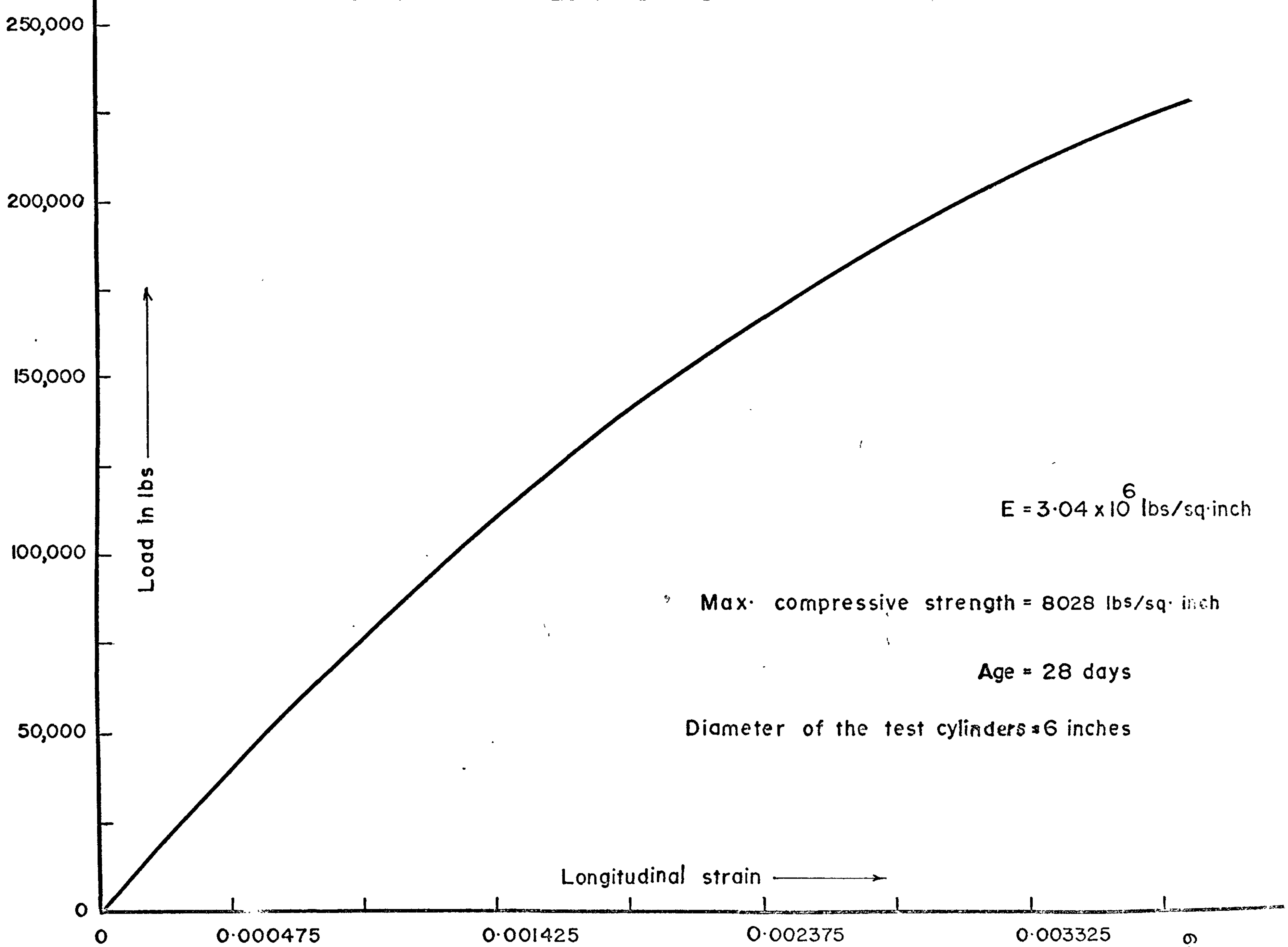

STRESS STRAIN CURVE– MODEL MIX

FIG. 13.

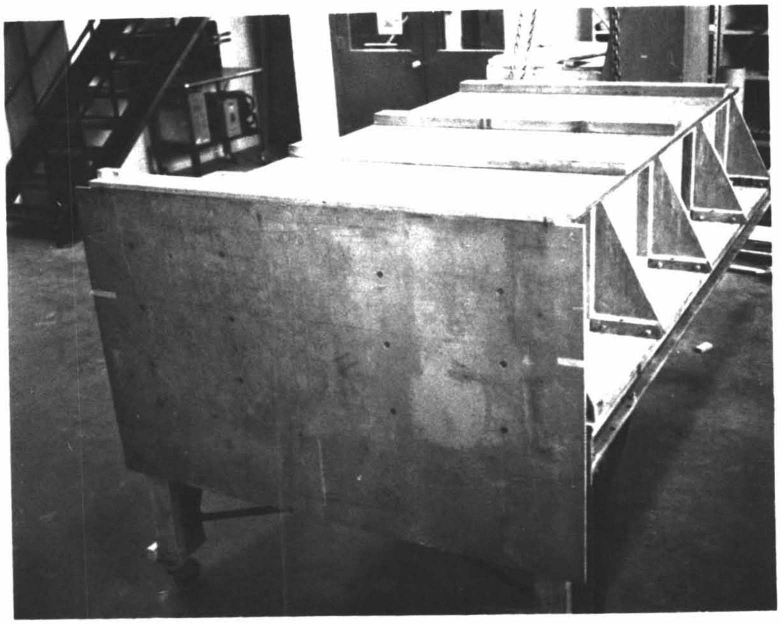

(a)

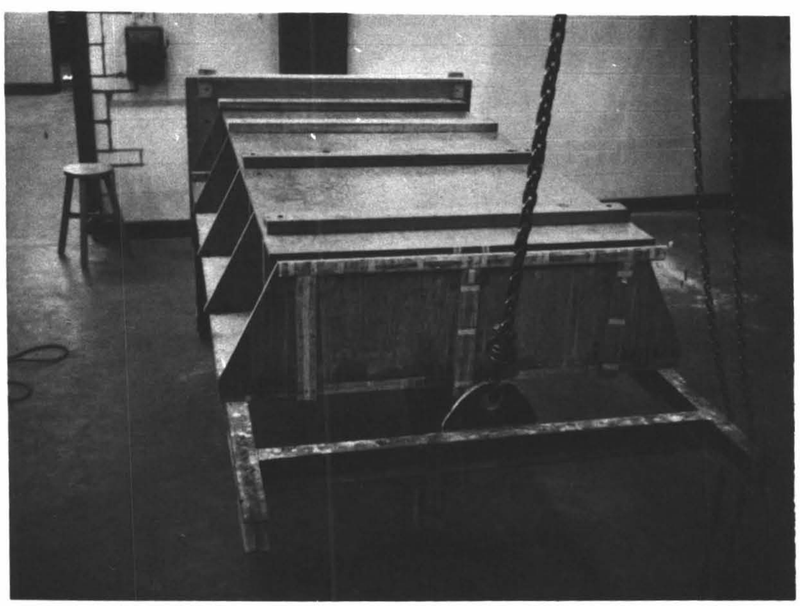

(b)

Fig. 14. Photographs showing a freshly poured model covered on top.

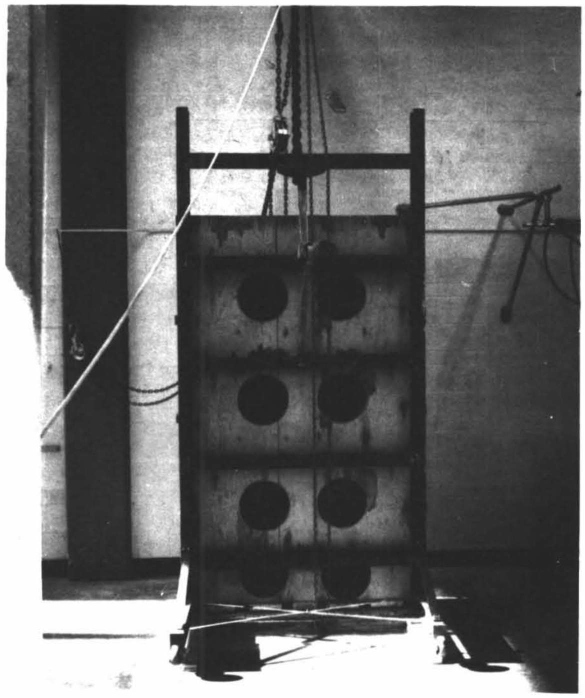

Fig. 15. Photograph showing the whole assembly erected in position.

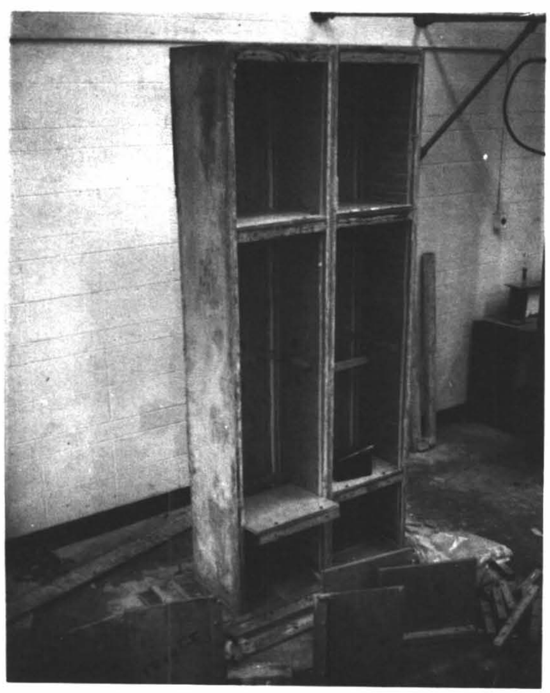

Fig. 16a. Removal of the form-work; base and the outer panels taken apart.

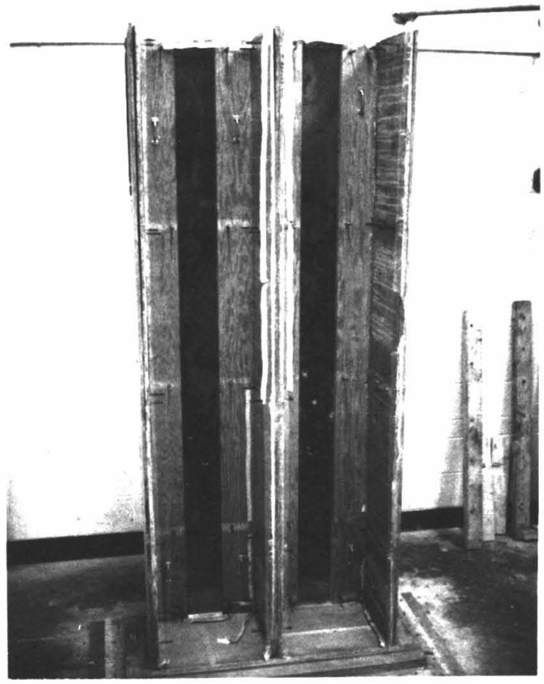

Fig. 16b. Removal of the form-work; wedge shaped central panels removed.

Fig. 16c. Removal of the form-work; inside panels removed.

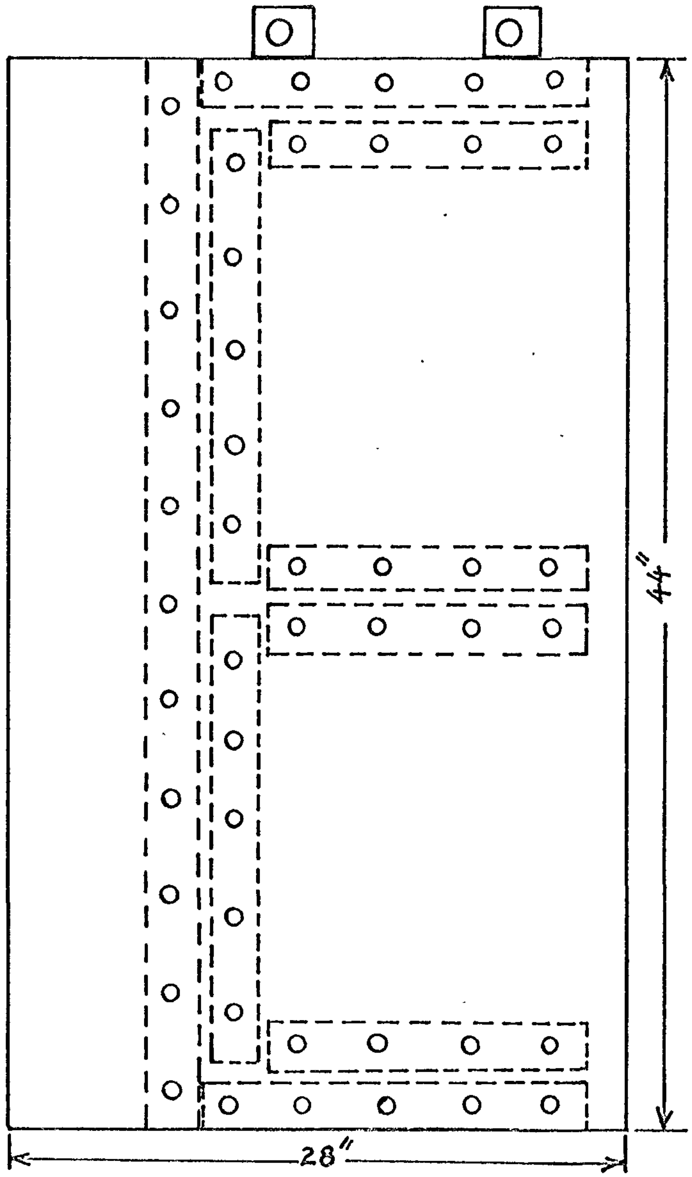

TOP VIEW

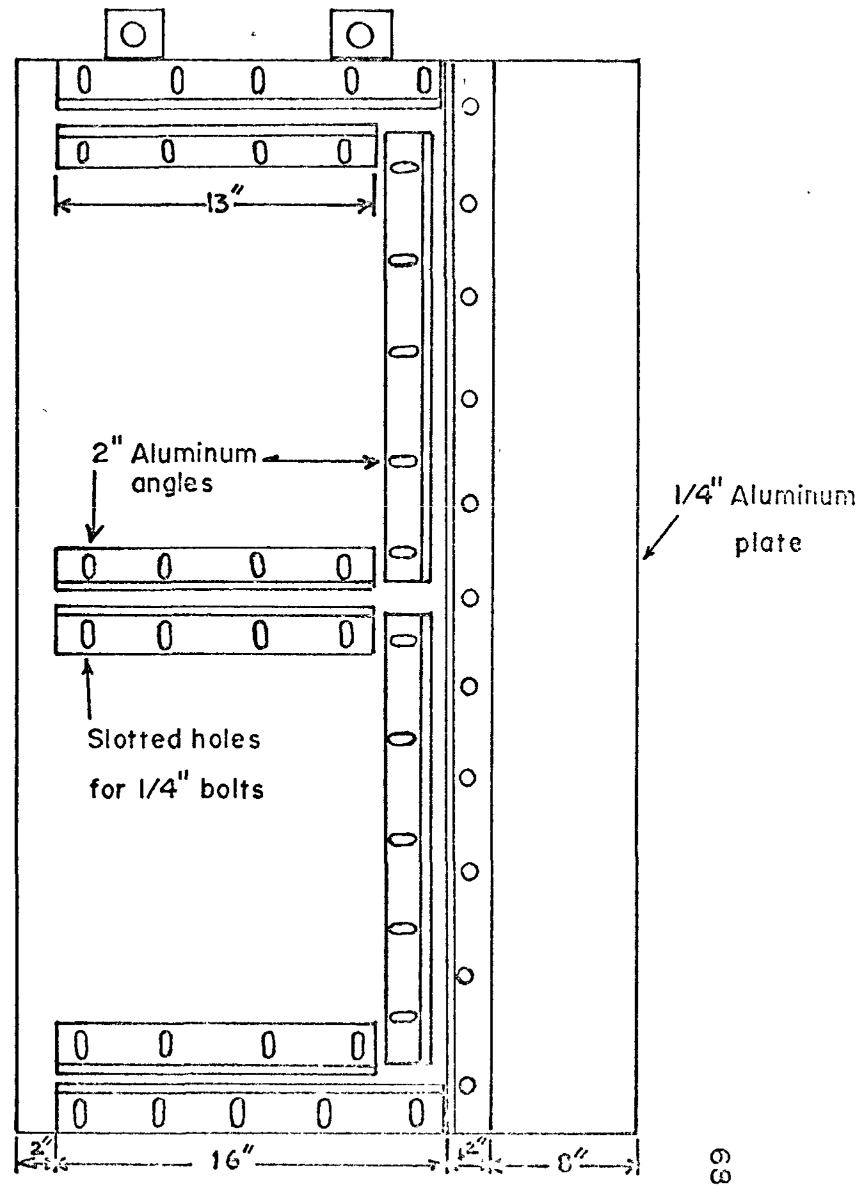

BOTTOM VIEW

FIG. 17- LOADING CAP

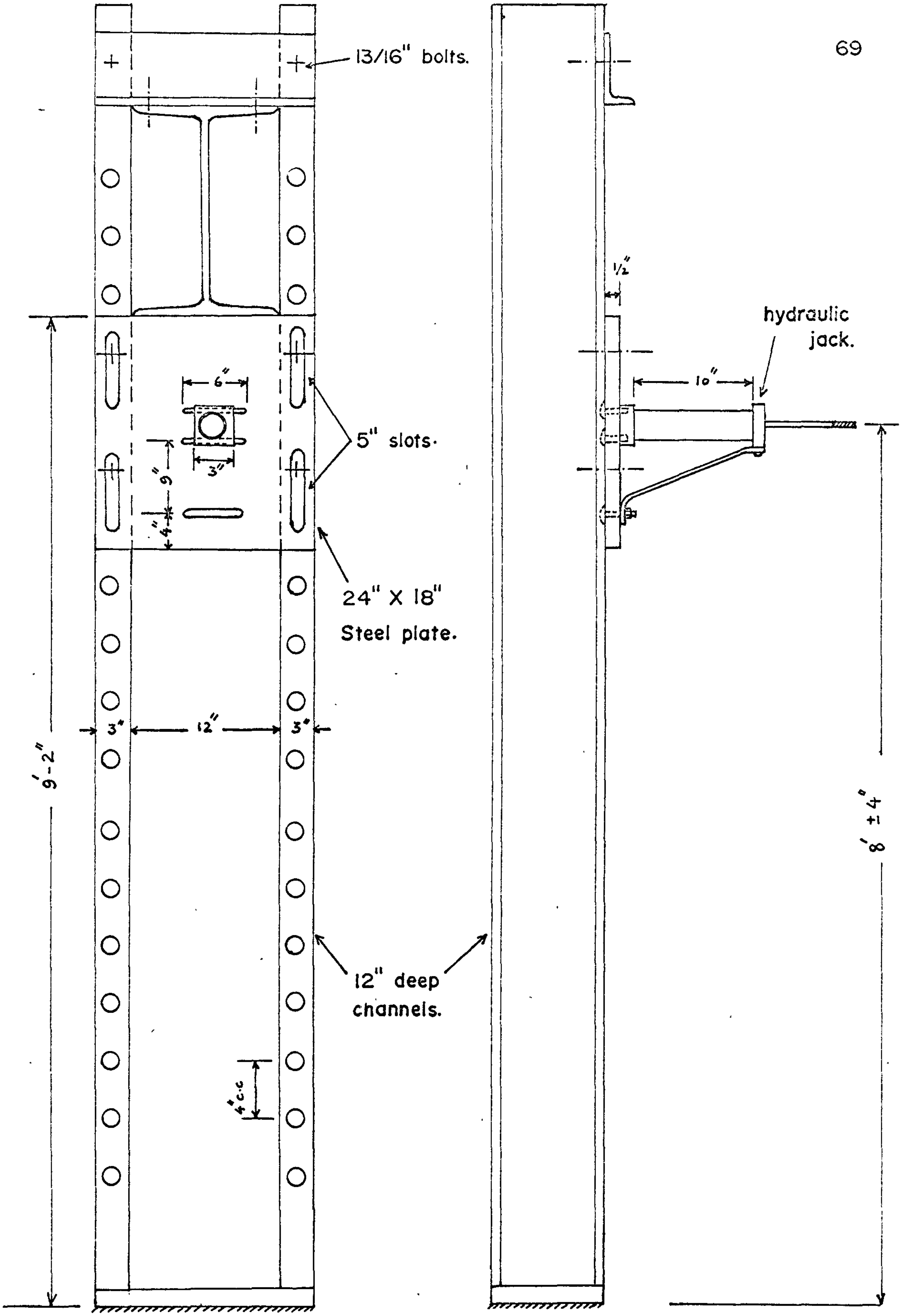

FIG. 18 _ SUPPORT FOR HYDRAULIC-JACK.

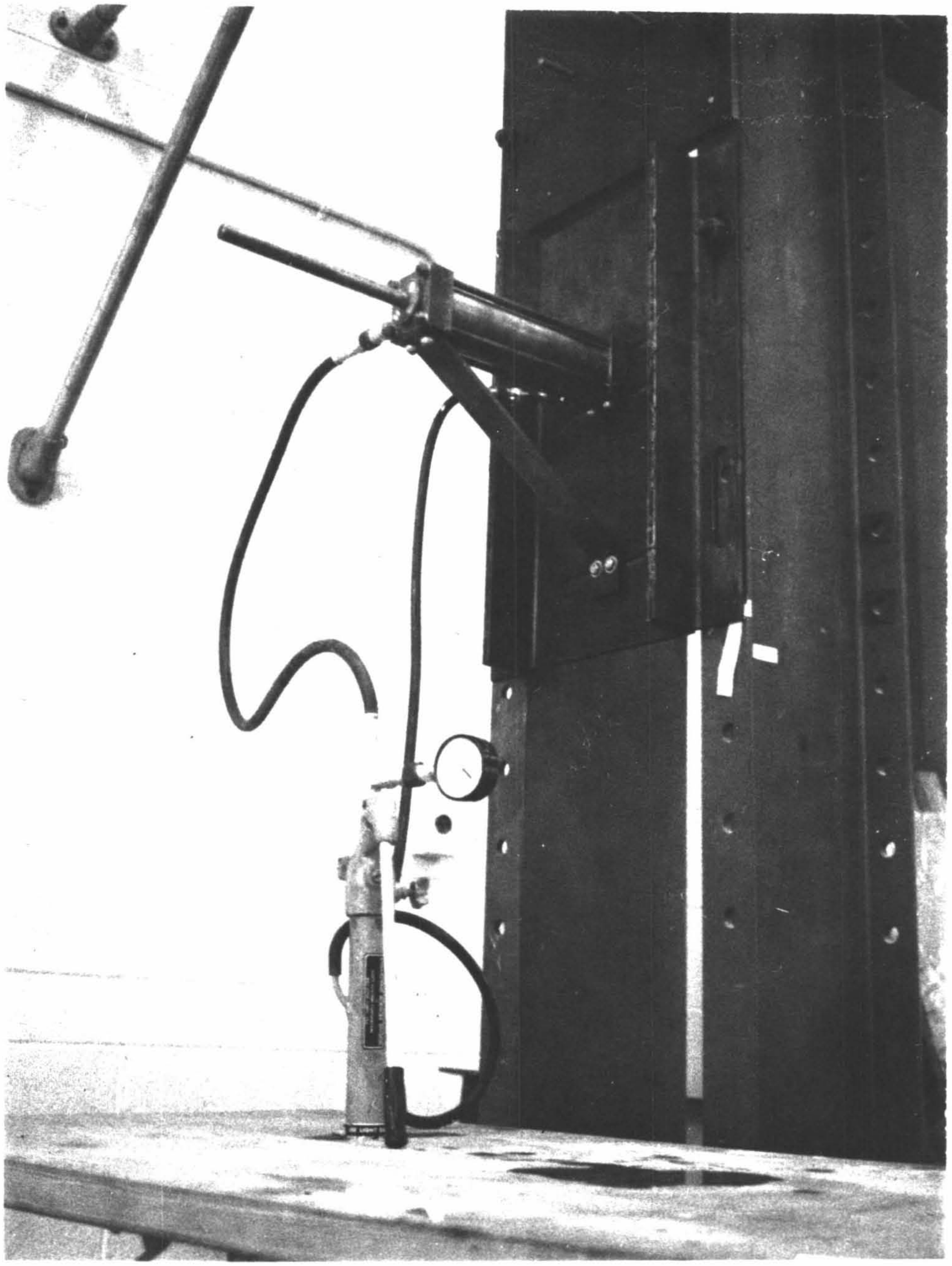

Fig. 19. Photograph showing the loading equipment and the column support.

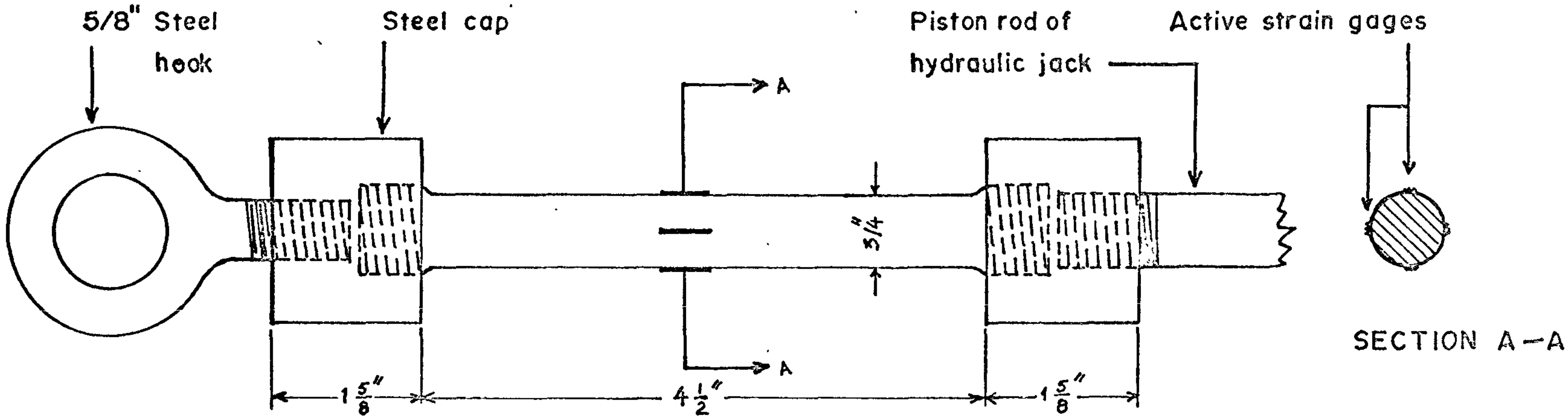

FIG. 20- DIMENSIONAL SKETCH OF LOAD-CELL.

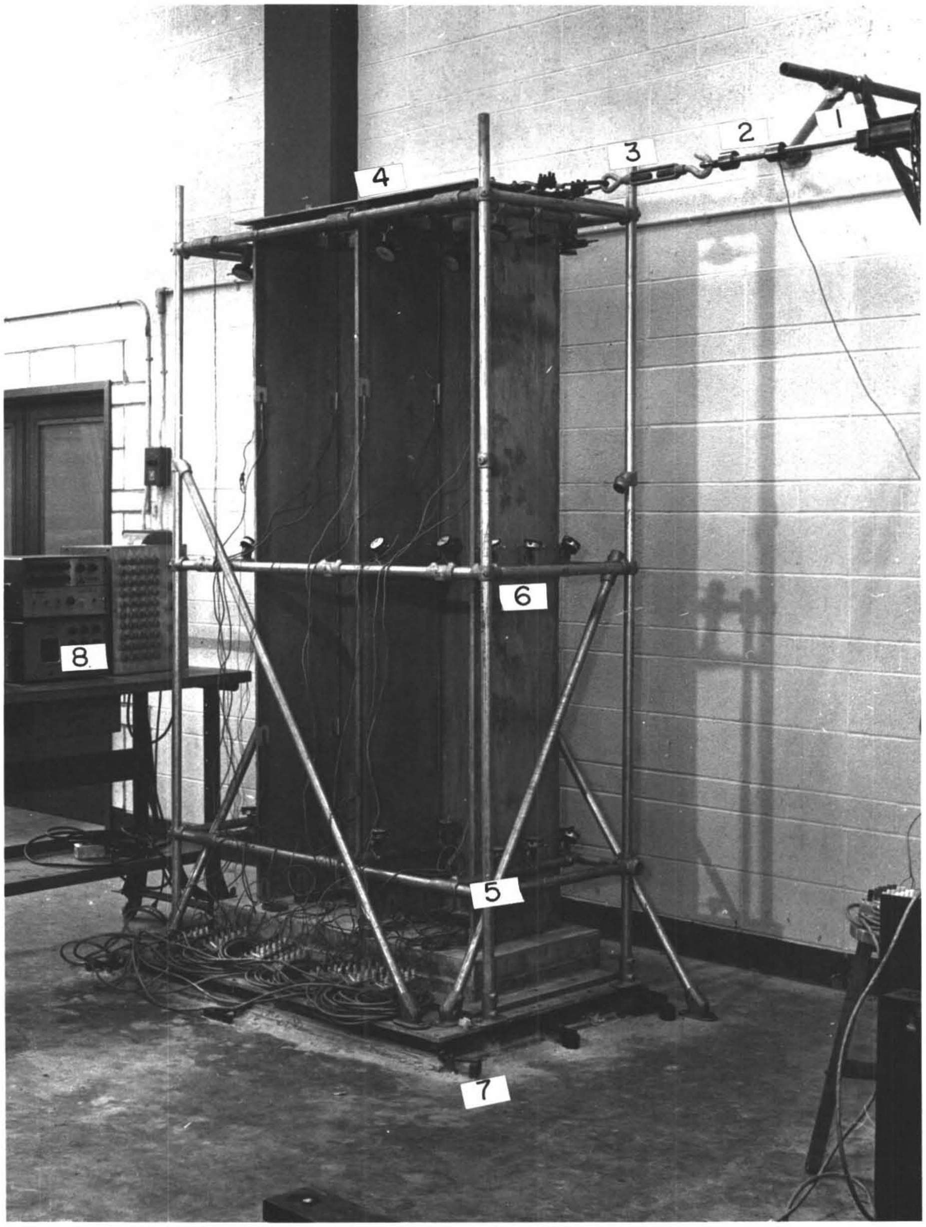

1. Hydraulic jack 2. Load cell 3. Connecting arrangement
4. Loading-cap 5. Cast-iron pipe frame
6. Model proper 7. Anchors 8. Strain indicator

Fig. 21. Photograph showing the experimental set-up.

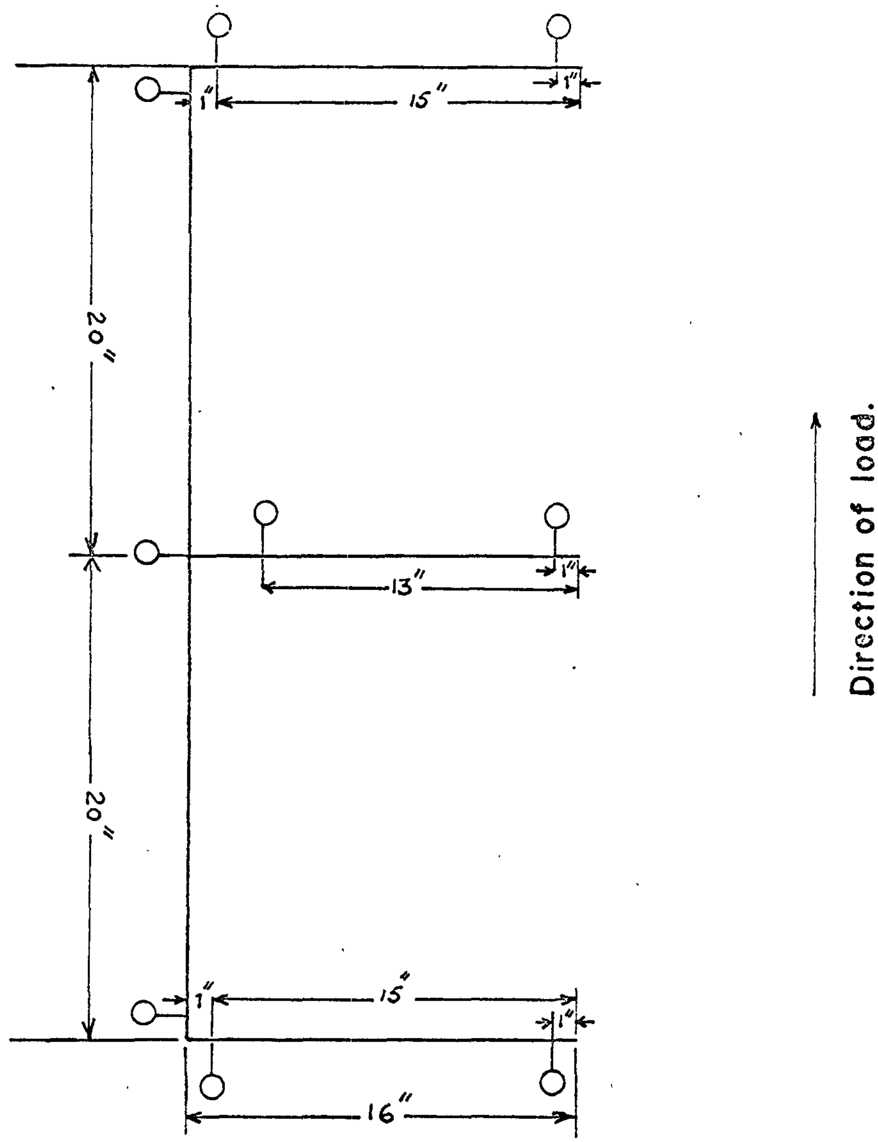

Z = 12", 48", & 85."

FIG. 22a_LOCATION OF DEFLECTION-GAGES.

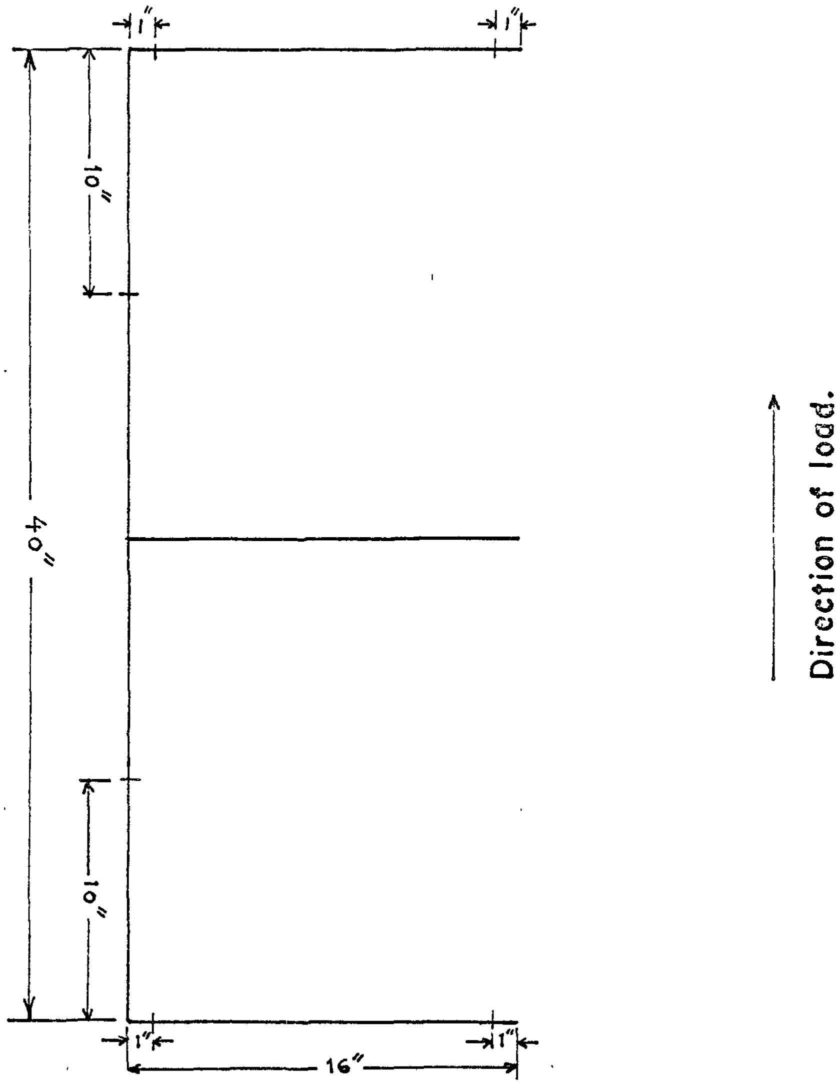

Z = 2", 22·75", & 68·25."

FIG.22b_LOCATION OF STRAIN-GAGES.

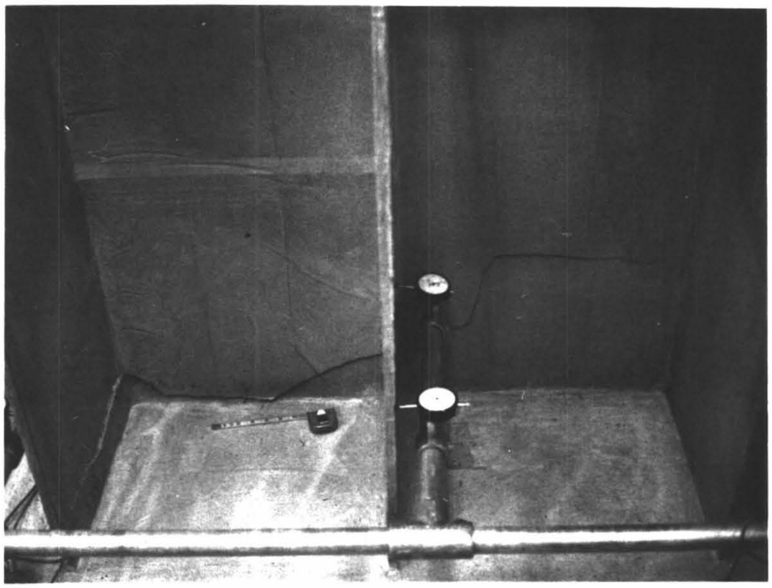

(a)

(b)

Fig. 23. Photographs showing the crack pattern (Model No.2)

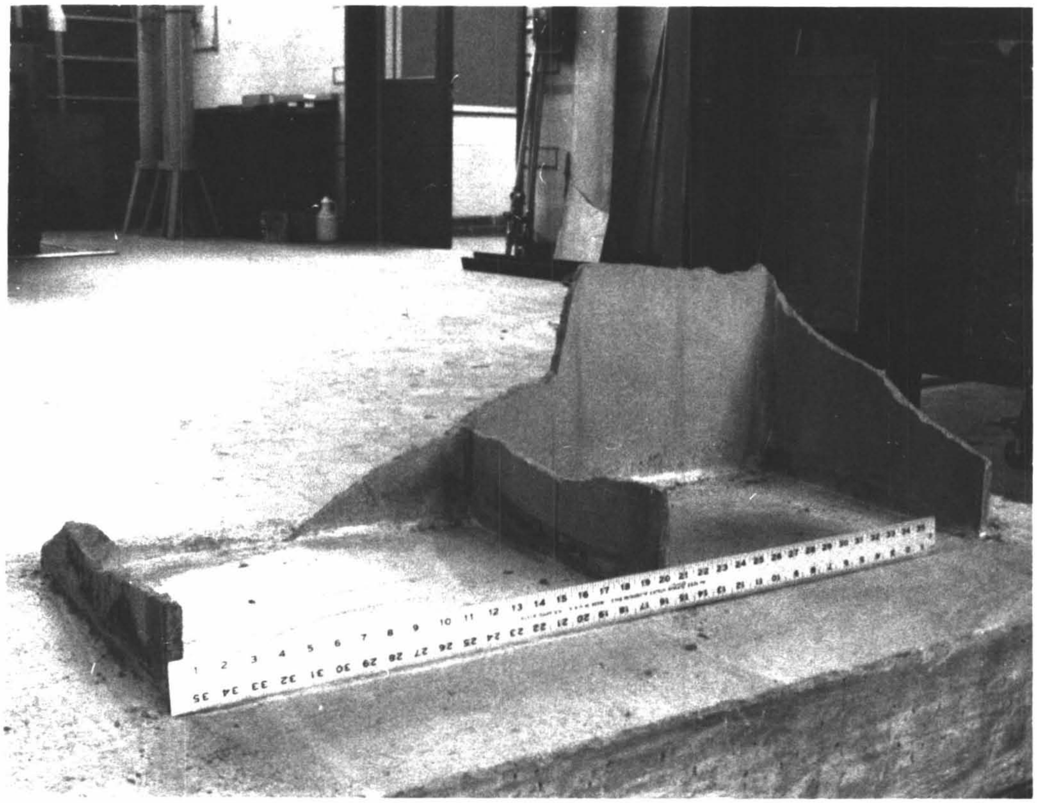

Fig. 23c. Photograph showing the crack pattern (Model No.2)

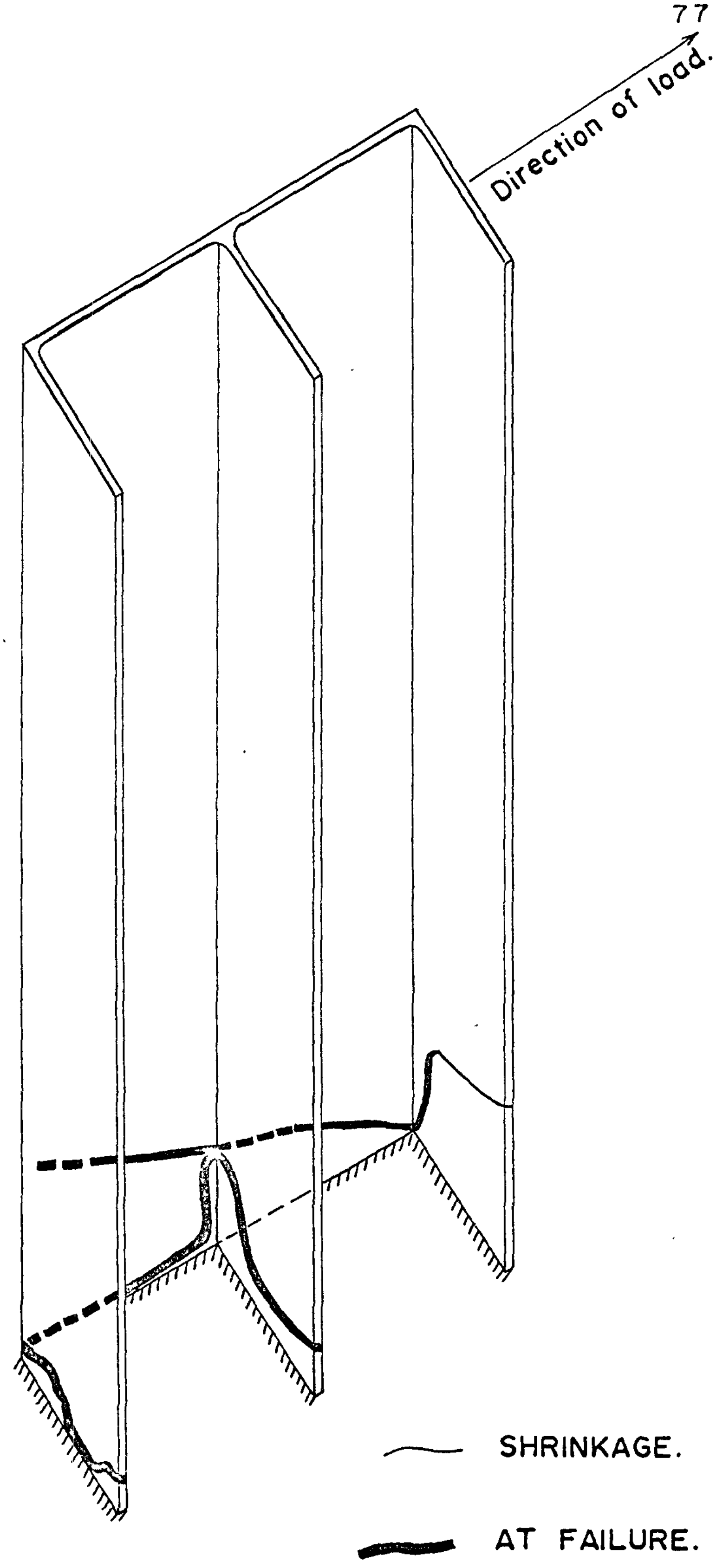

Scale: 1" = 16"

FIG. 24 — CRACK LOCATION - MODEL NO. 3.

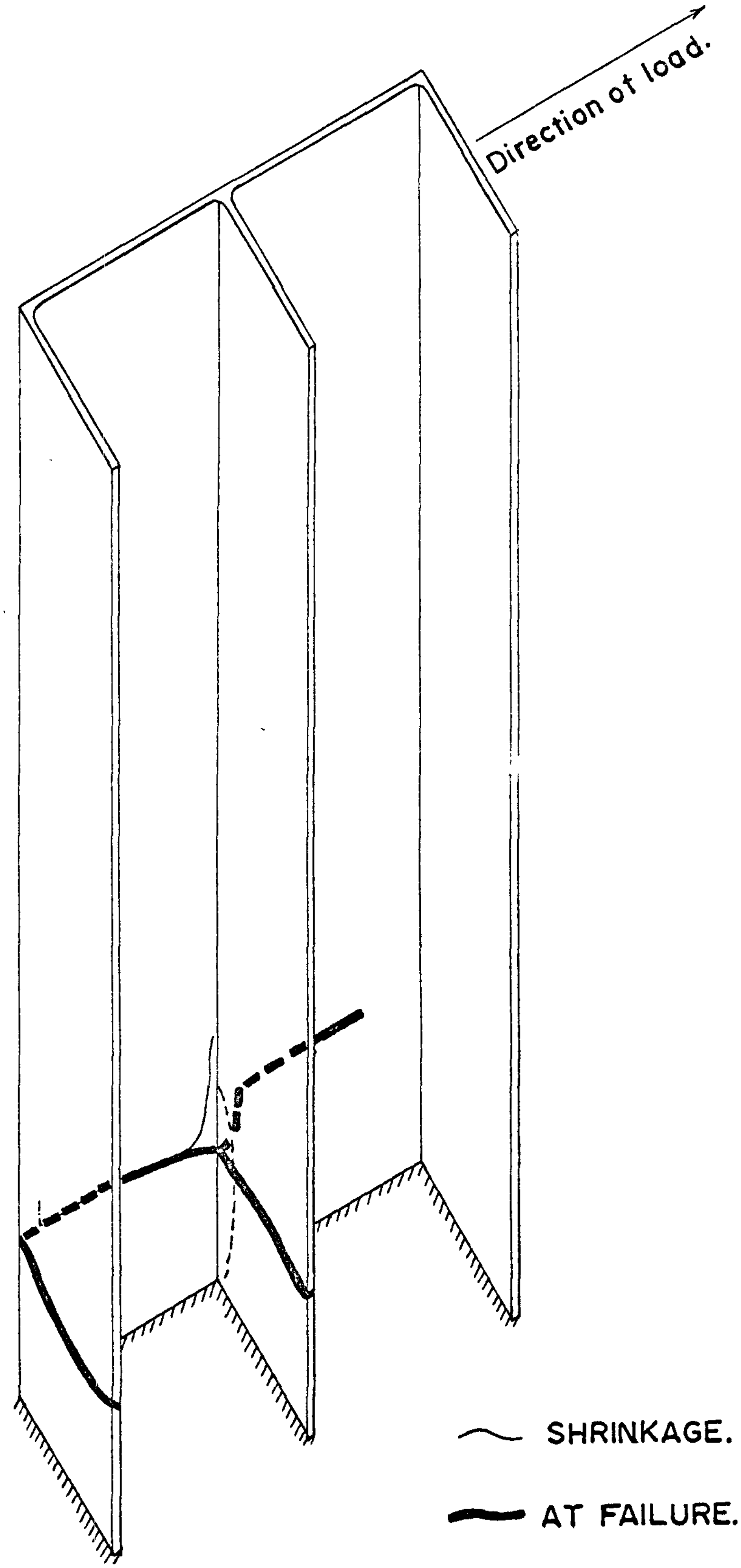

Scale: 1" = 16"

FIG. 25_CRACK LOCATION-MODEL NO. 4.

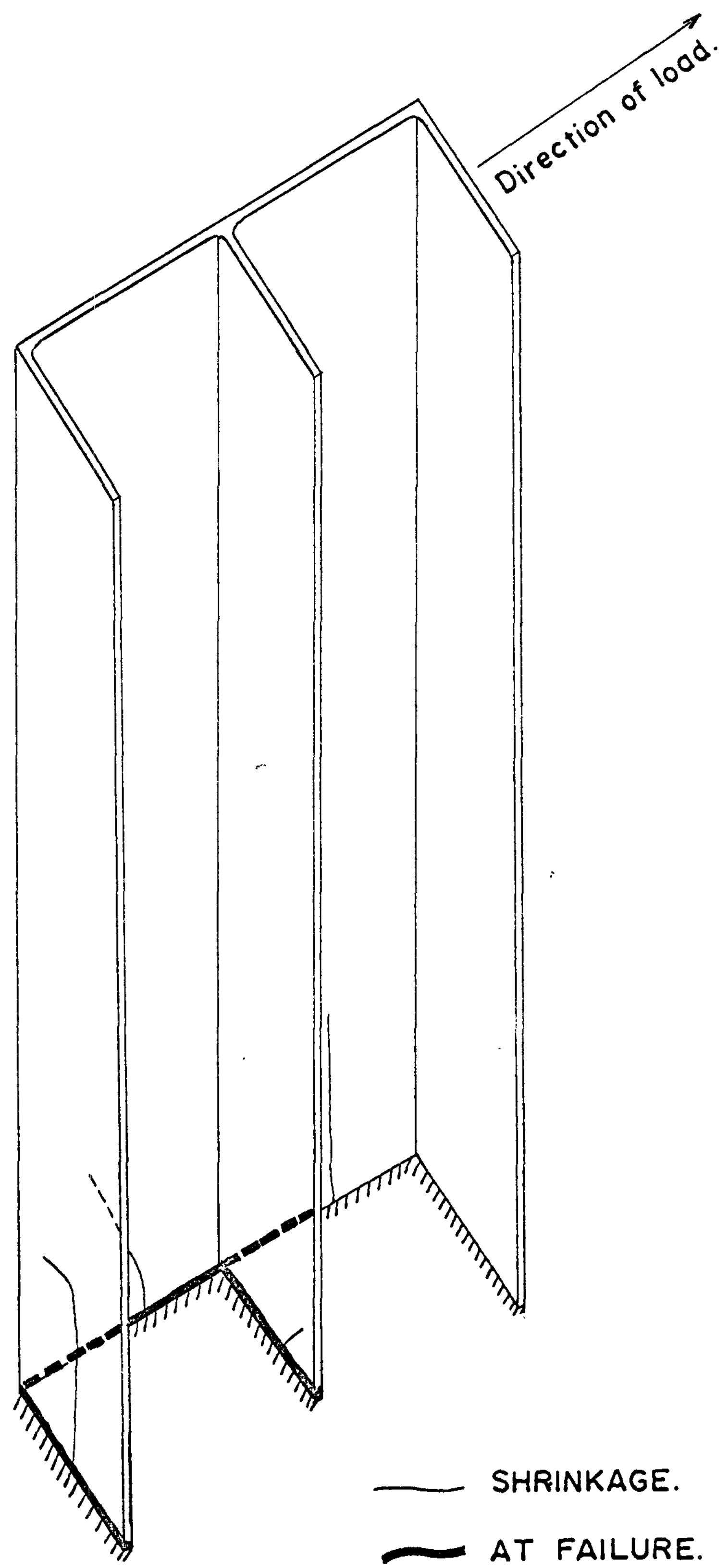

Scale · 1" = 16"

FIG. 26_CRACK LOCATION - MODEL NO.5.

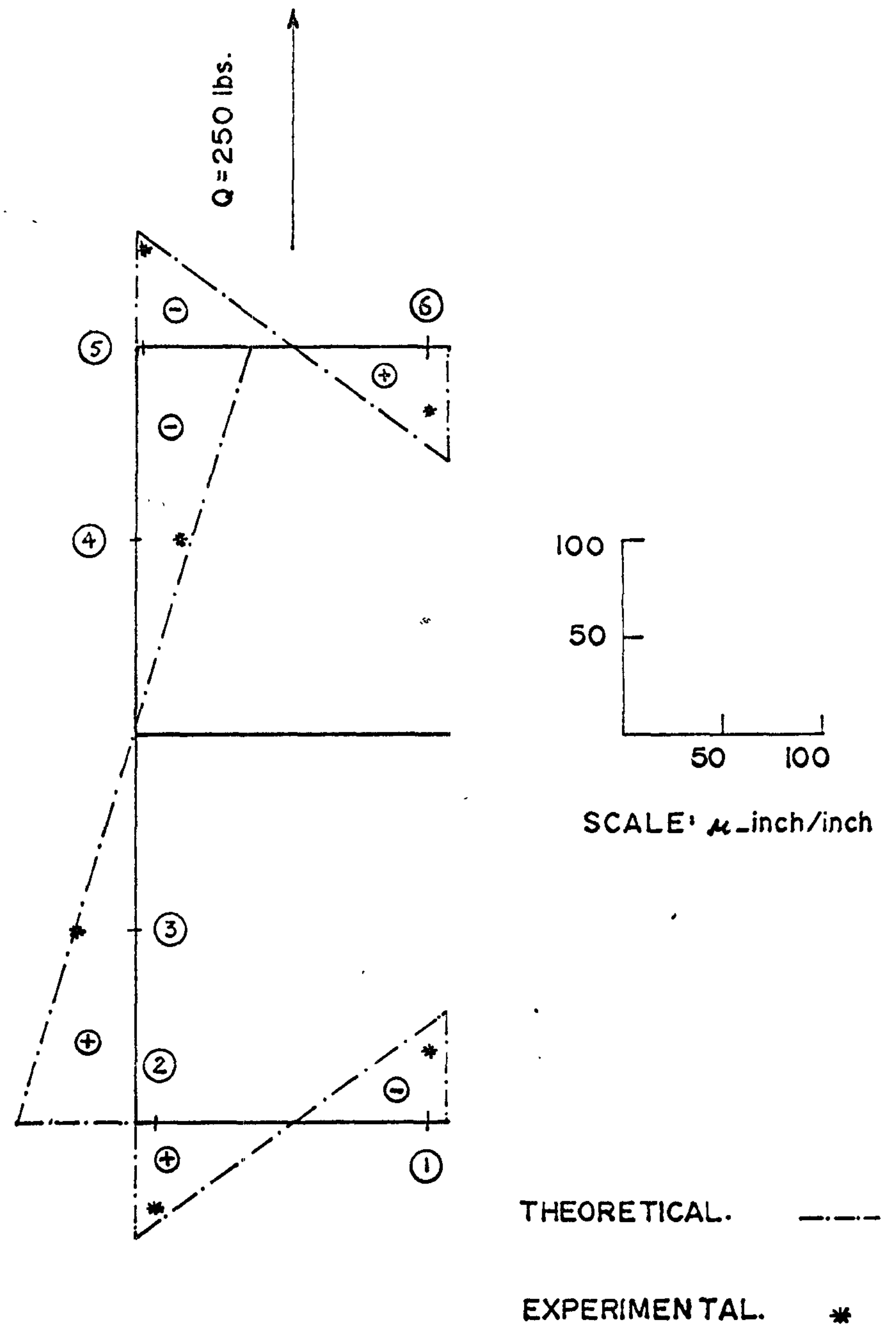

Points 1 to 6 refer to locations shown on page 97.

Z = 2"

FIG. 27—COMPARISON OF STRAIN DISTRIBUTION.
(MODEL NO. 2)

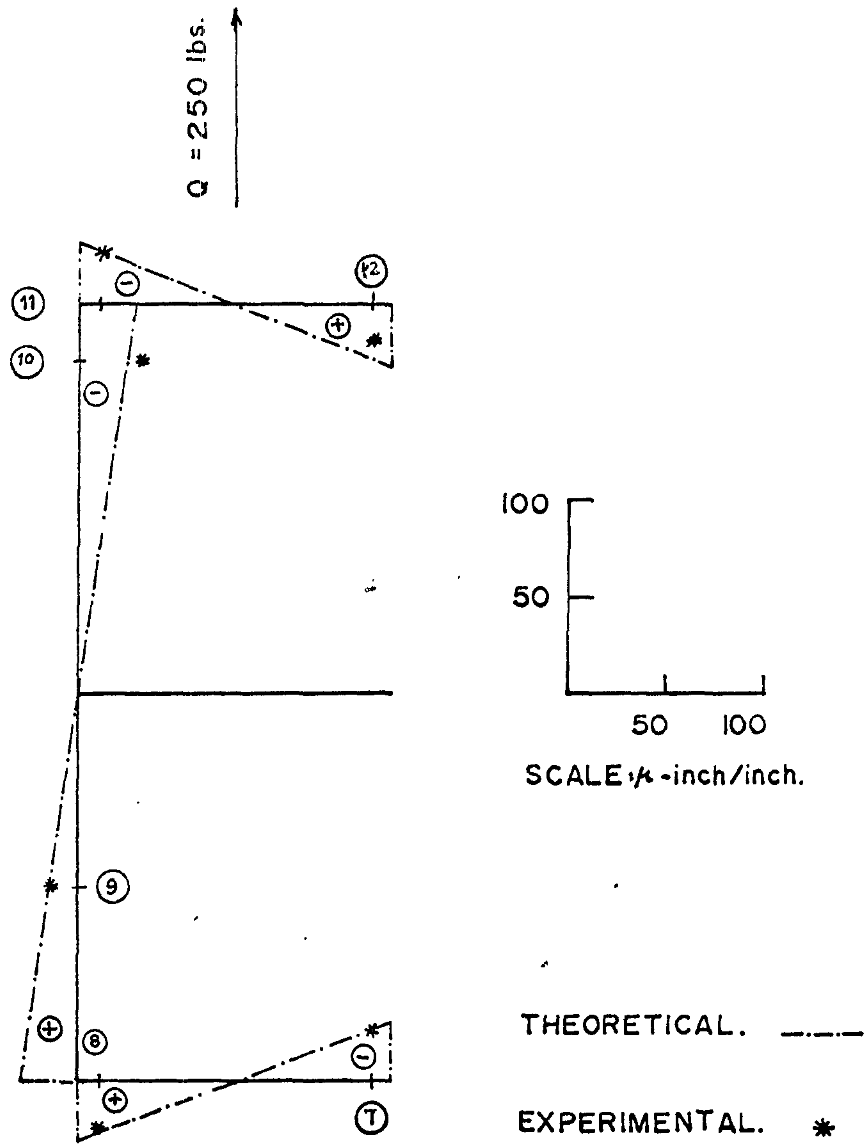

Points 7 to 12 refer to locations shown on page 97.

Z = 45."

FIG. 28_COMPARISION OF STRAIN DISTRIBUTION.

(MODEL NO. 2)

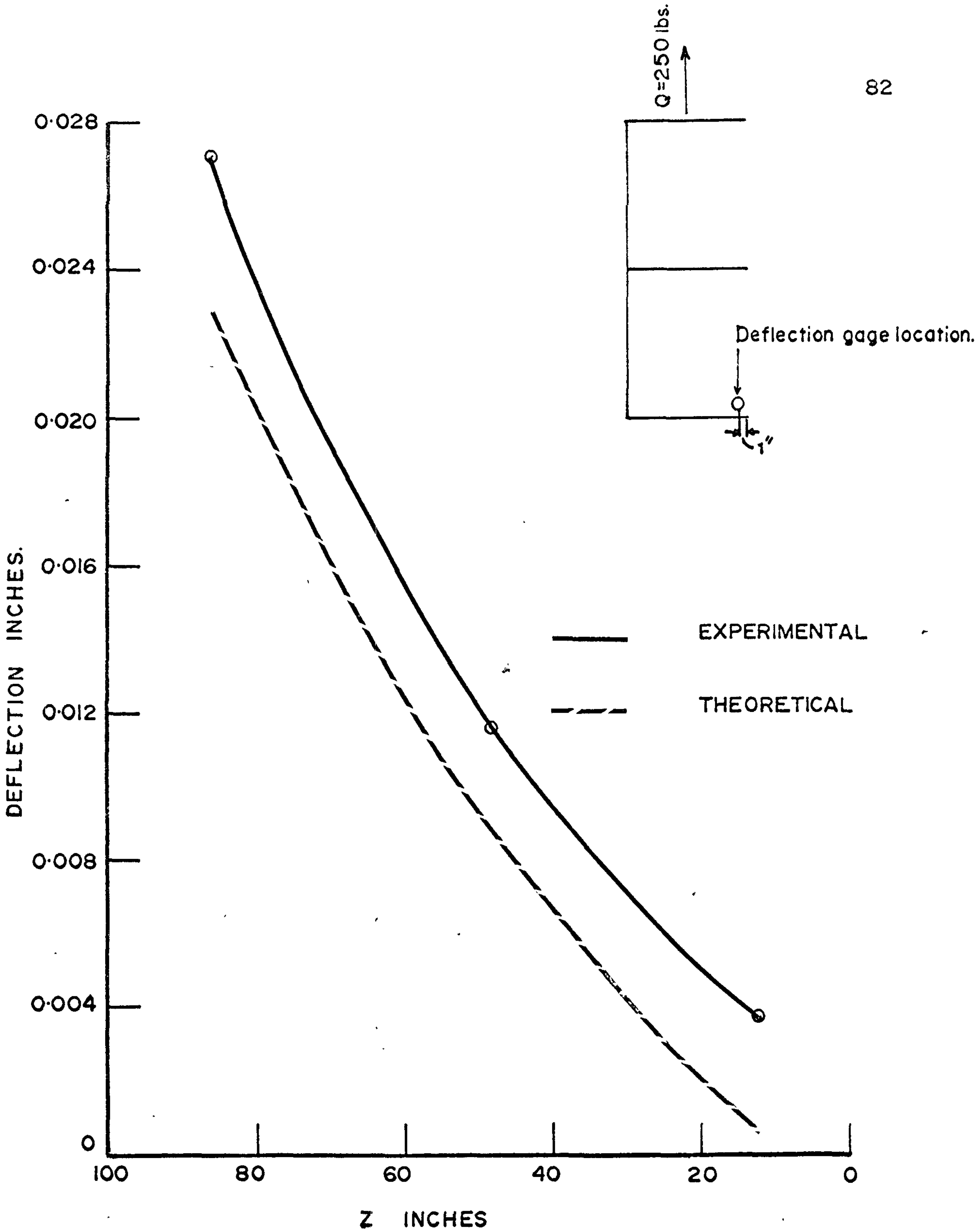

FIG. 29_COMPARISON OF DEFLECTIONS.
(MODEL NO. 2)

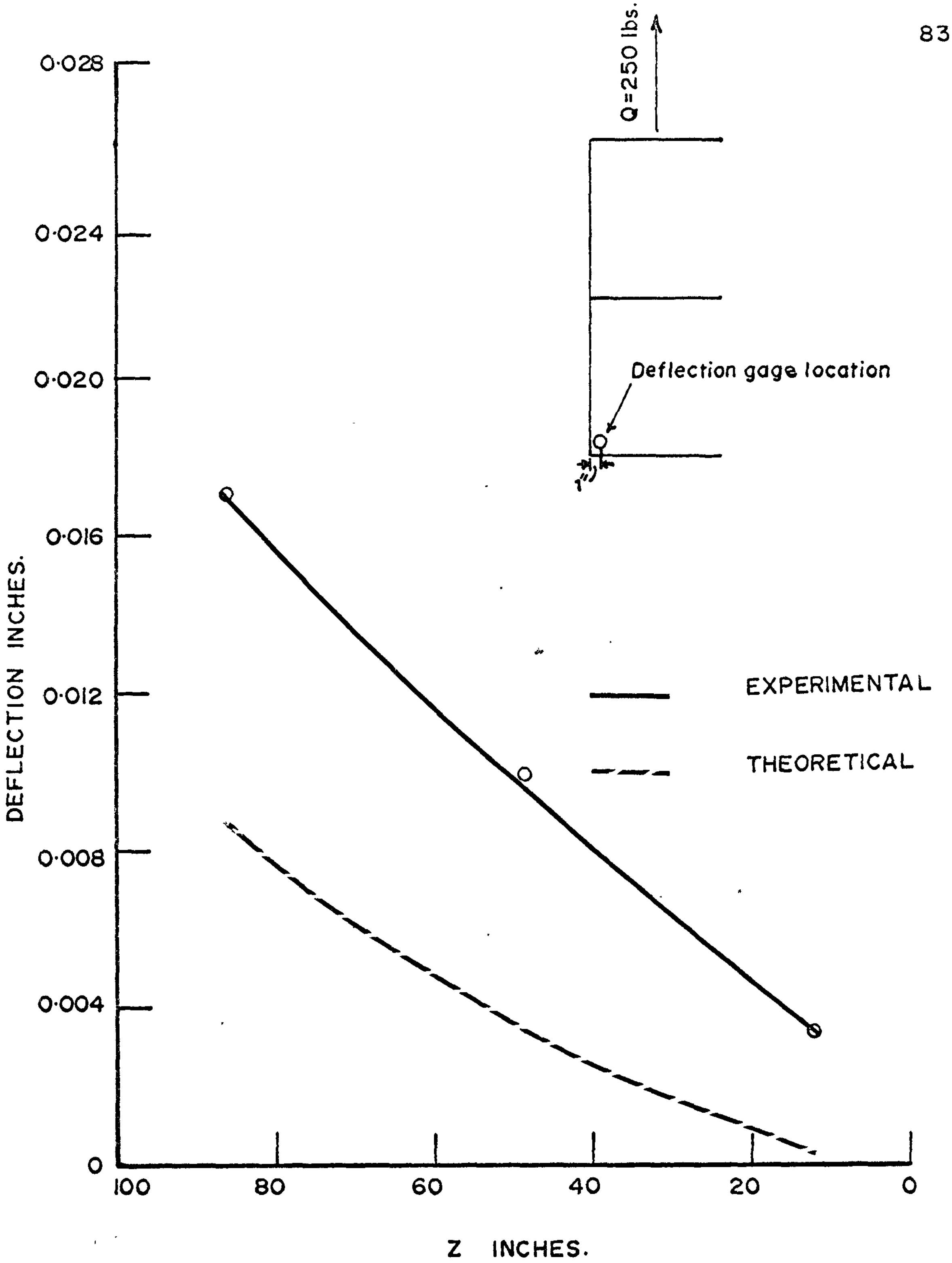

FIG. 30_COMPARISON OF DEFLECTIONS.
(MODEL NO. 2)

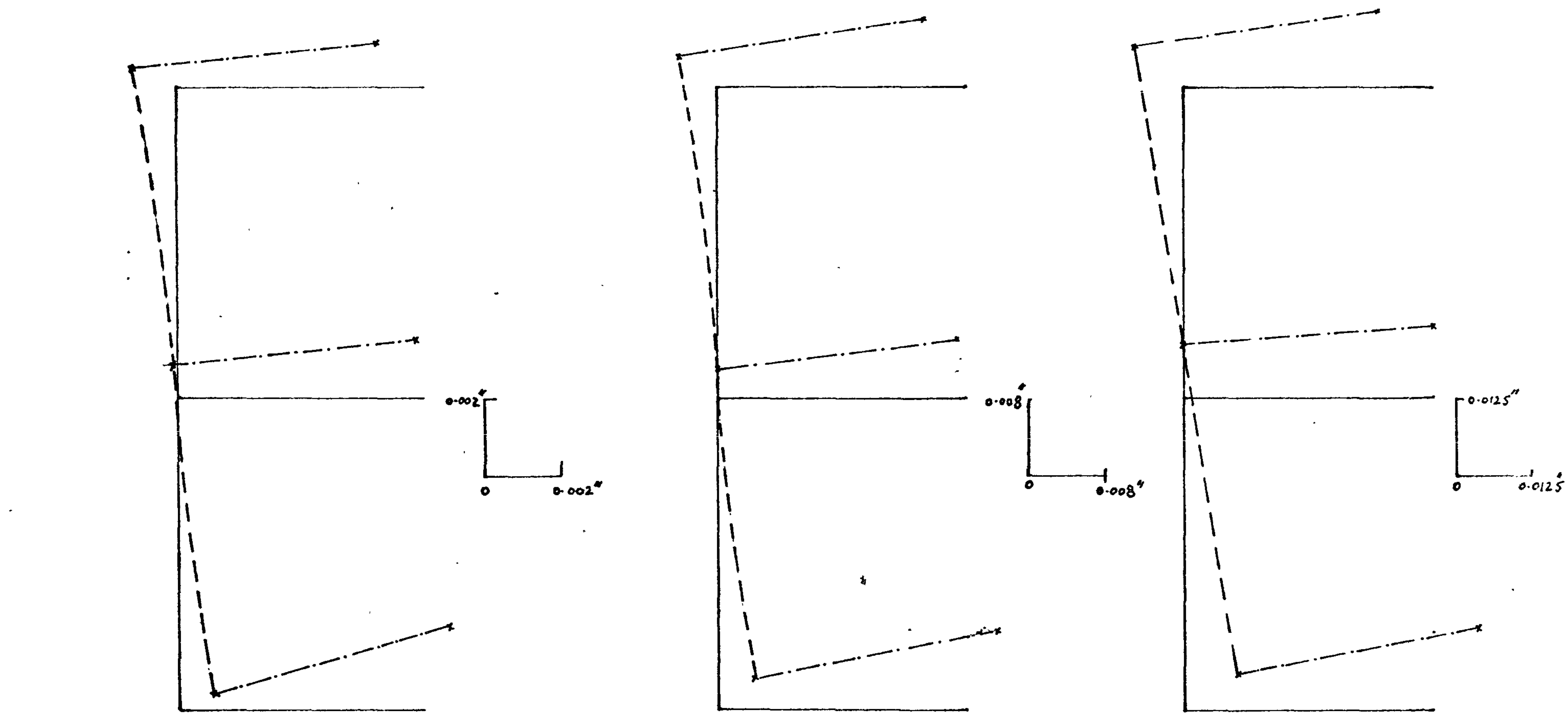

Z = 12" Z = 48" Z = 85"

FIG. 31 _ DEFLECTED SHAPE OF THE SECTIONS – Q = 40 lbs.
(MODEL NO. 5)

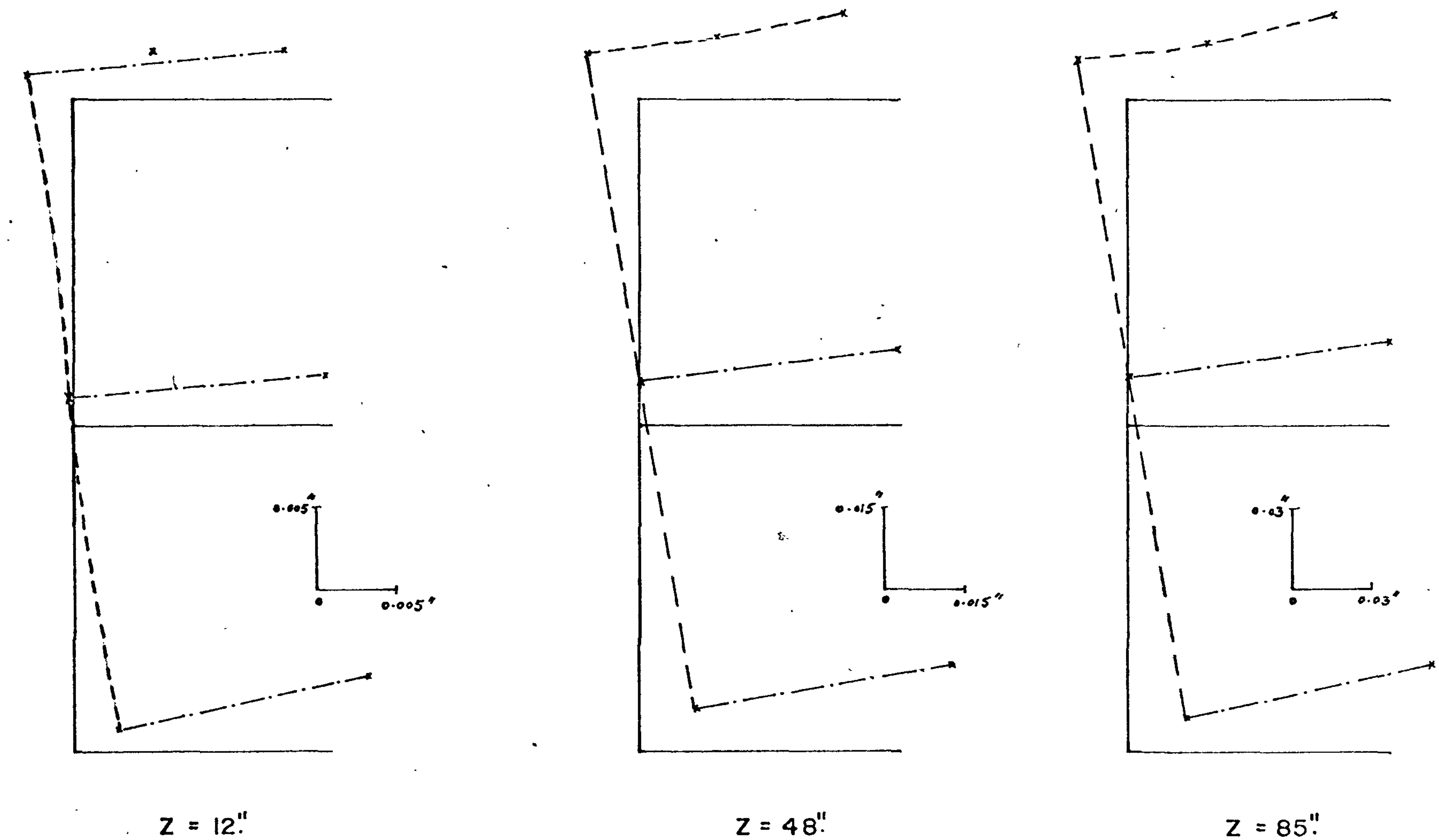

FIG.32_DEFLECTED SHAPE OF THE SECTIONS– Q=100 lbs.
(MODEL NO. 5)

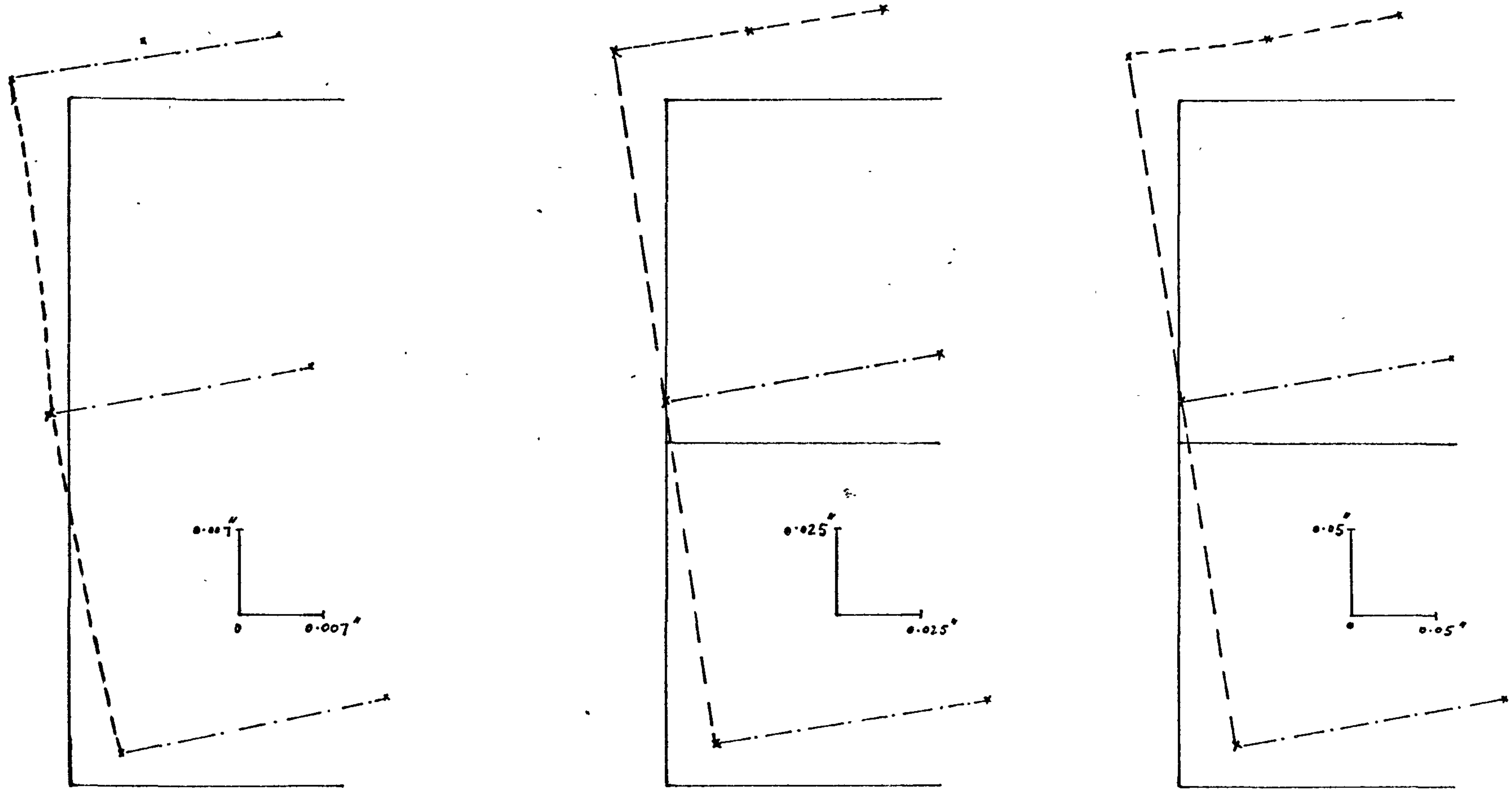

Z = 12"   Z = 48"   Z = 85"

FIG. 33 — DEFLECTED SHAPE OF THE SECTIONS — Q = 180 lbs.
(MODEL NO. 5)

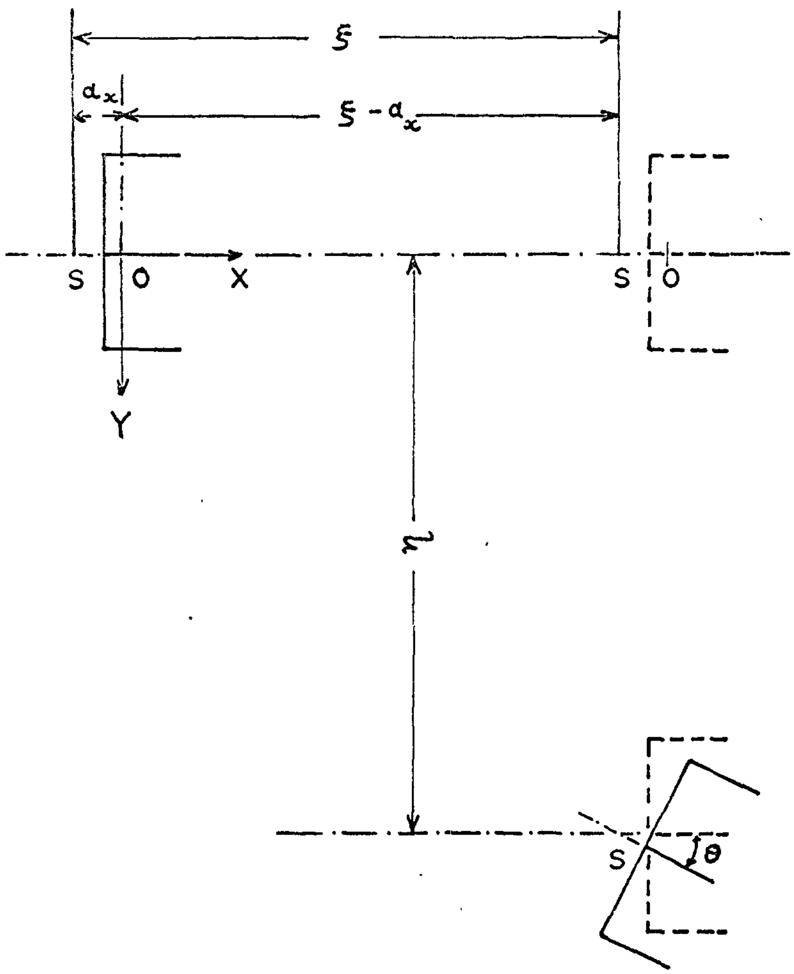

O — Centroid of the section.

S — Shear centre.

FIG.34 — DISPLACEMENT OF SECTION UNDER FLEXURAL–TORSIONAL LOADING.

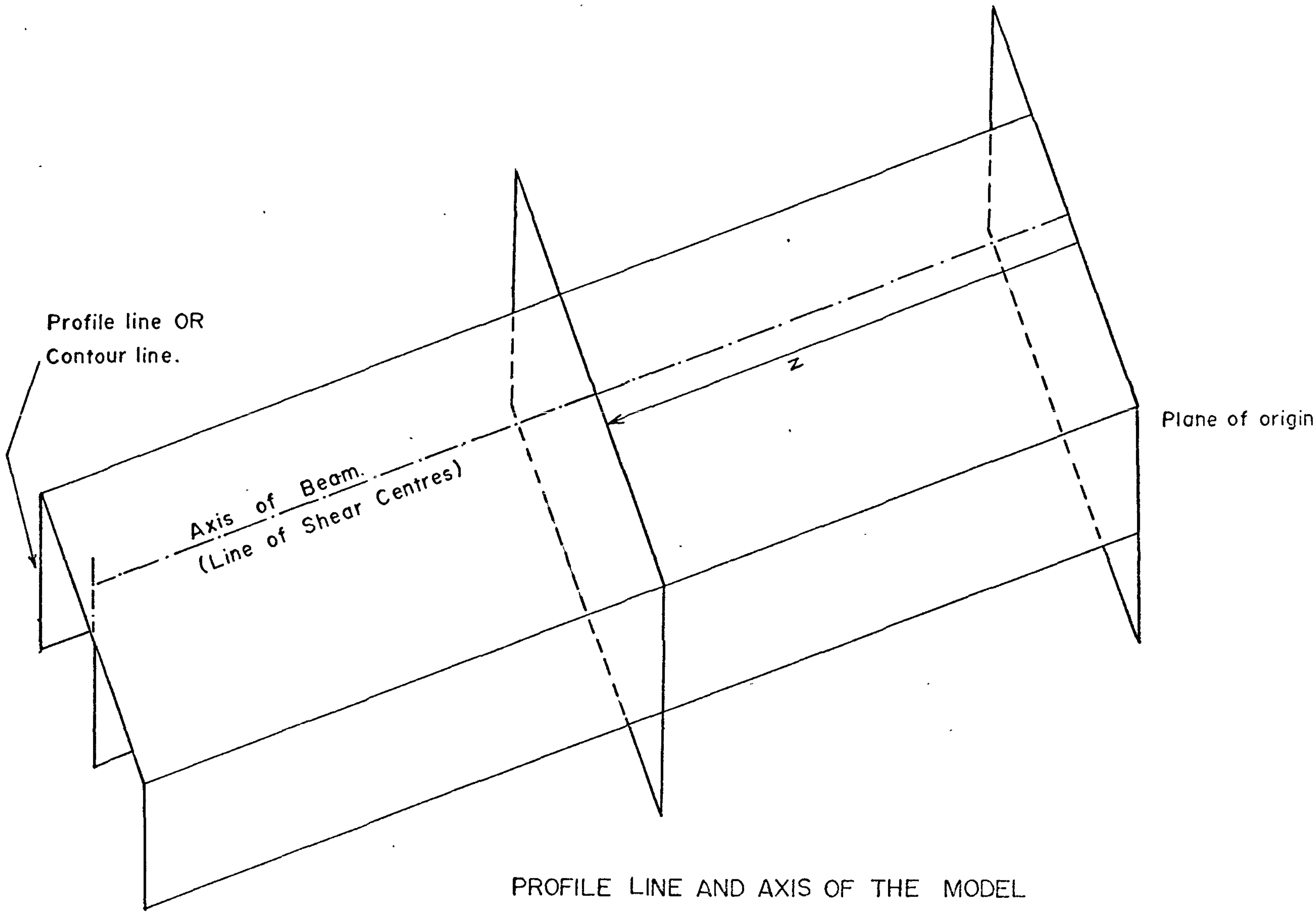

PROFILE LINE AND AXIS OF THE MODEL

FIG. 35

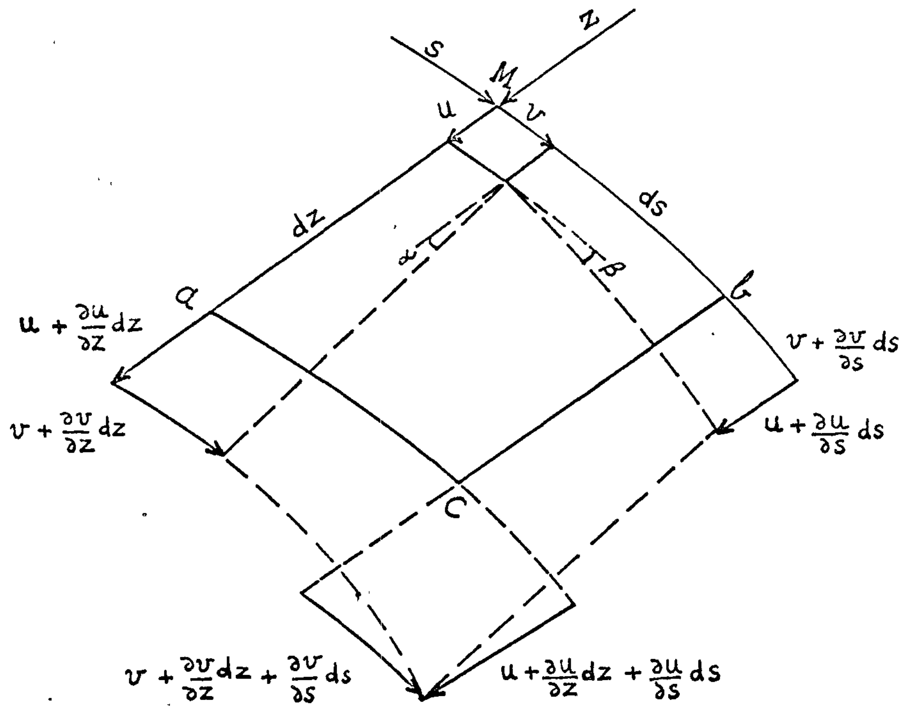

(a)

DISPLACEMENTS IN THE LONGITUDINAL PLANE.

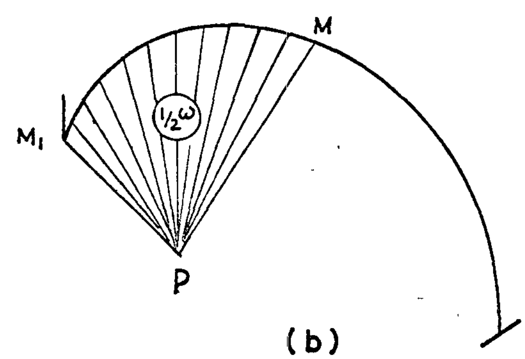

(b)

SECTORIAL AREA

FIG. 36

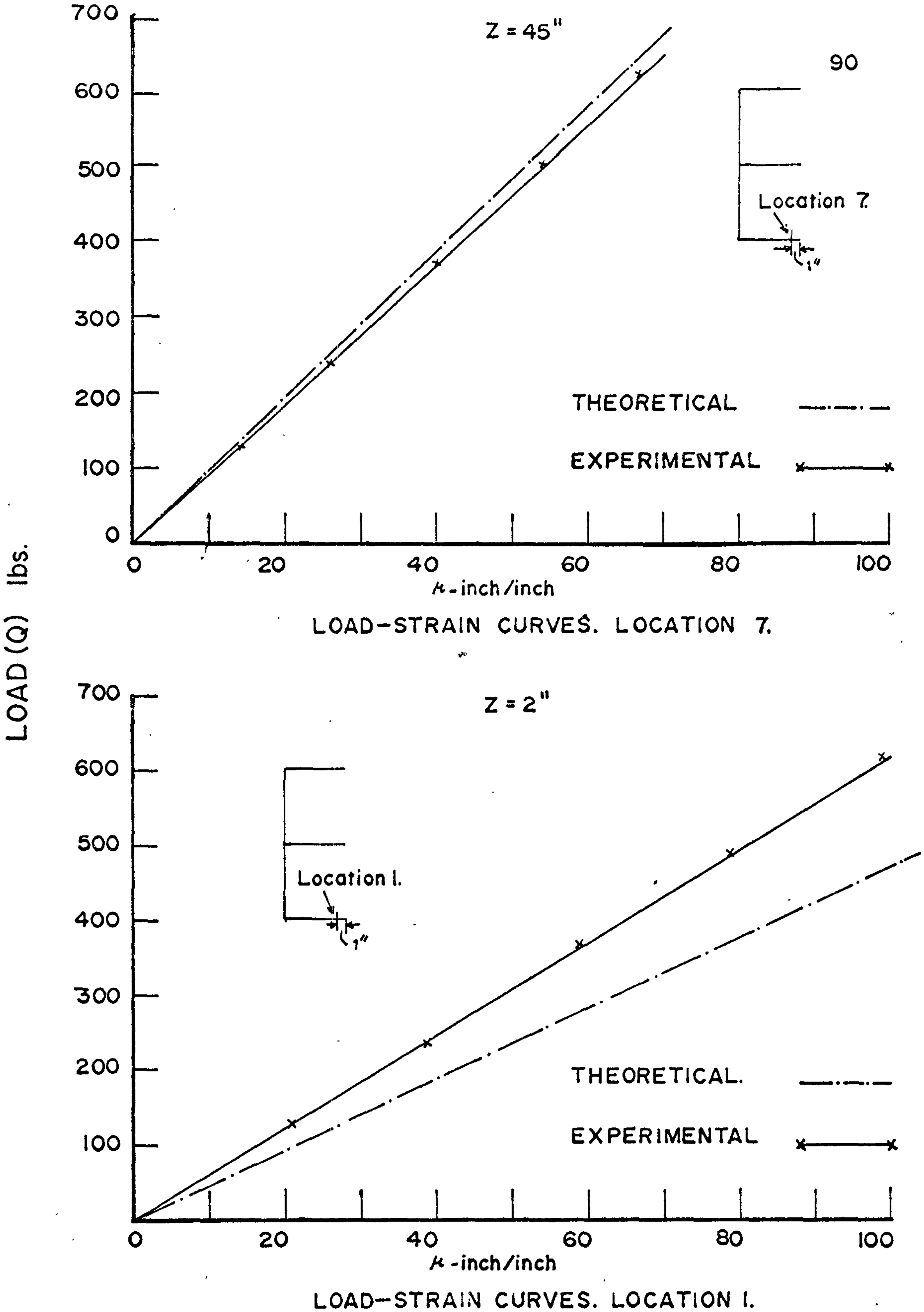

FIG. 37—LOAD-STRAIN CURVES.
(MODEL NO. 2)

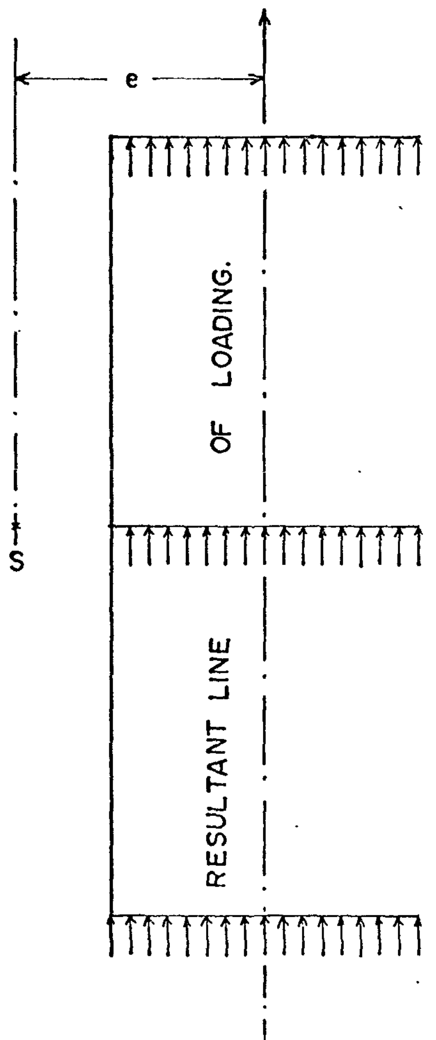

ASSUMED DISTRIBUTION OF LOAD

FIG. 38

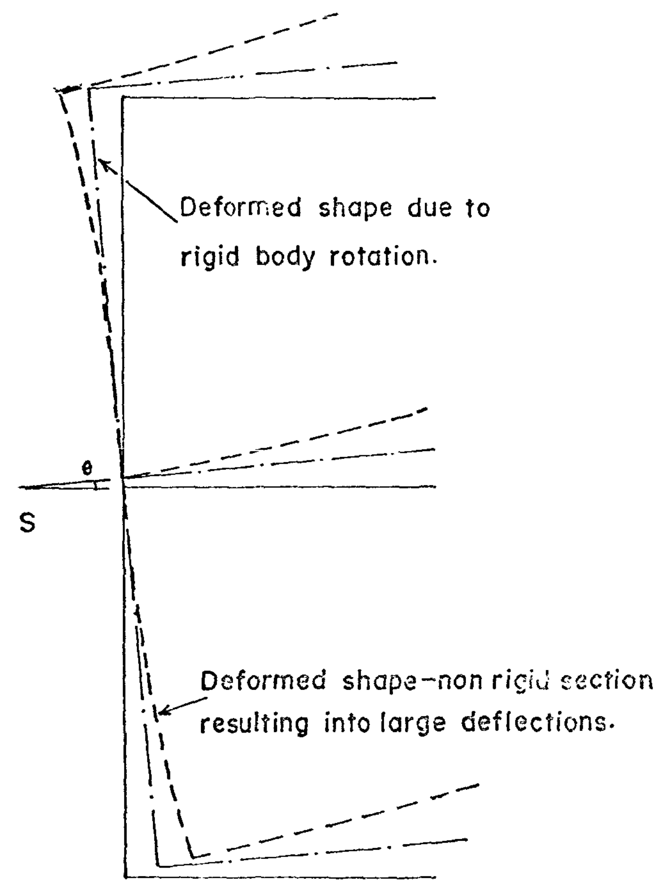

FIG.39

APPENDIX A

TABLES FOR EXPERIMENTAL DATA
FOR A REPRESENTATIVE MODEL
(MODEL NO. 2)

TABLE A-1

DEFLECTIONS IN INCHES FOR VARIOUS LOAD VALUES

1st Cycle of Loading

Dial Gage	Loading (lbs.)					Unloading (lbs.)			
No.*	125	238	362	475	600	475	362	238	Load Off
1	0.0009	0.0028	0.0055	0.0074	0.0096	0.0090	0.0081	0.0060	0.0017
2	0.0006	0.0009	0.0044	0.0059	0.0076	0.0076	0.0070	0.0053	0.0017
3	0.0035	0.0090	0.0175	0.0245	0.0340	0.0290	0.0245	0.0165	0.0045
4	0	0	0.0021	0.0057	0.0100	0.0072	0.0043	0.0002	0
5	0.008	0.019	0.027	0.043	0.062	0.053	0.041	0.025	0
6	0.004	0.011	0.021	0.029	0.038	0.033	0.027	0.018	0.003
7	0.008	0.0023	0.0047	0.0062	0.0081	0.0072	0.0065	0.0046	0.0008
8	0.0006	0.0020	0.0046	0.0060	0.0077	0.0073	0.0065	0.0045	0.0008
9	0.0054	0.0121	0.0216	0.0291	0.0381	0.0332	0.0282	0.0201	0.0045
10	0.0030	0.0074	0.0141	0.1880	0.0247	0.2120	0.0181	0.0129	0.0018
11	0.006	0.018	0.038	0.054	0.073	0.063	0.052	0.036	0.008
12	0.002	0.007	0.020	0.031	0.042	0.035	0.029	0.019	0.001
13	0	0	0.0017	0.0031	0.0054	0.0050	0.0050	0.0019	0.0004
14	0.0004	0.0020	0.0043	0.0058	0.0073	0.0061	0.0040	0.0007	0
15	0.0045	0.0120	0.0205	0.0265	0.0345	0.025	0.018	0.005	0.004
16	0.003	0.0075	0.0155	0.0200	0.0255	0.0200	0.0135	0.0025	0.0015
17	0.007	0.019	0.039	0.055	0.074	0.053	0.038	0.011	0.008
18	0.003	0.010	0.021	0.030	0.040	0.029	0.019	0.002	0.001
19									

* Numbers refer to locations as shown under Table A-2

TABLE A-2

DEFLECTIONS IN INCHES FOR VARIOUS LOAD VALUES

2nd Cycle of Loading

Dial Gage No.	Loading (lbs.) 138	238	362	487	600	Unloading (lbs.) 475	362	225	150	Load Off
1	0.0008	0.0036	0.0059	0.0075	0.0091	0.0086	0.0075	0.0051	0.0040	0.0003
2	0.0008	0.0032	0.0050	0.0061	0.0073	0.0074	0.0066	0.0049	0.0033	0.0007
3	0.0020	0.0115	0.0200	0.0265	0.0330	0.0290	0.0240	0.0155	0.0100	0.0020
4	0.0030	0.0095	0.0154	0.0190	0.0227	0.0207	0.0176	0.0115	0.0076	0.0001
5	0.009	0.027	0.045	0.059	0.073	0.064	0.053	0.034	0.024	0.001
6	0.006	0.016	0.026	0.034	0.040	0.035	0.030	0.020	0.014	0.001
7	0.0013	0.0038	0.0059	0.0072	0.0084	0.0079	0.0069	0.0048	0.0034	0.0005
8	0.0008	0.0035	0.0055	0.0068	0.0076	0.0074	0.0067	0.0046	0.0031	0.0002
9	0.0066	0.0159	0.0252	0.0318	0.0384	0.0346	0.0292	0.0200	0.0146	0.0029
10	0.0038	0.0109	0.0172	0.0212	0.0250	0.0227	0.0192	0.0128	0.0089	0.0015
11	0.011	0.030	0.048	0.062	0.076	0.067	0.056	0.038	0.028	0.004
12	0.005	0.019	0.031	0.040	0.048	0.043	0.036	0.025	0.017	0.001
13	0.0003	0.0023	0.0043	0.0056	0.0068	0.0068	0.0068	0.0068	0.0055	0.0027
14	0.0008	0.0034	0.0053	0.0065	0.0075	0.0073	0.0063	0.0042	0.0028	0
15	0.0065	0.016	0.023	0.029	0.036	0.031	0.026	0.0175	0.0130	0.0025
16	0.0045	0.0120	0.0170	0.0220	0.0255	0.0230	0.0200	0.0140	0.0095	0.0015
17	0.012	0.030	0.048	0.062	0.077	0.067	0.056	0.038	0.028	0.005
18	0.006	0.018	0.029	0.037	0.044	0.039	0.033	0.022	0.015	0.001

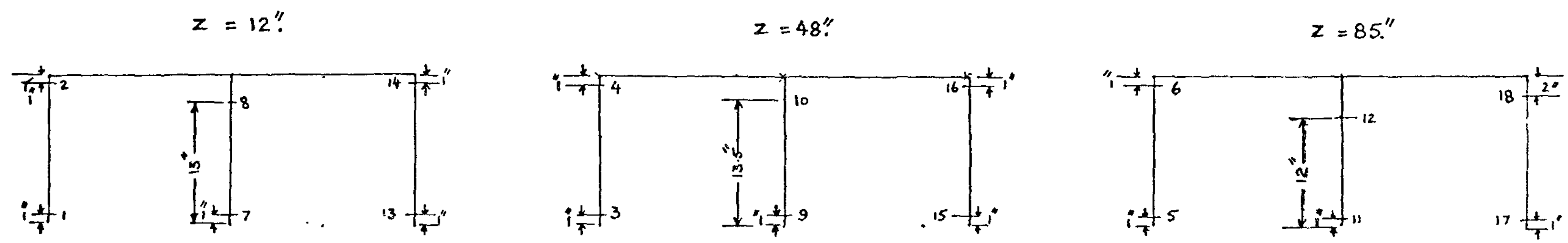

TABLE A-3

DEFLECTIONS IN INCHES FOR VARIOUS VALUES OF LOAD

3rd Cycle of Loading

Dial Gage	Loading (lbs.)					Unloading (lbs.)		
No.	125	250	362	487	600	487	250	Load Off
1	0.0011	0.0037	0.0057	0.0074	0.0087	0.0081	0.0051	0.0002
2	0.0004	0.0029	0.0045	0.0057	0.0067	0.0067	0.0042	0.0005
3	0.006	0.015	0.022	0.029	0.035	0.030	0.012	0.001
4	0.003	0.010	0.015	0.019	0.022	0.020	0.012	0
5	0.011	0.028	0.043	0.058	0.070	0.060	0.034	0.001
6	0.006	0.016	0.024	0.032	0.038	0.032	0.019	0.001
7	0.0011	0.0034	0.0051	0.0066	0.0077	0.0070	0.0044	0.0005
8	0.0005	0.0032	0.0050	0.0044	0.0073	0.0070	0.0044	0.0002
9	0.006	0.015	0.023	0.030	0.036	0.031	0.018	0.001
10	0.004	0.010	0.016	0.021	0.024	0.021	0.012	0
11	0.012	0.029	0.044	0.059	0.071	0.061	0.036	0.003
12	0.006	0.017	0.027	0.037	0.044	0.039	0.022	0
13	0.0008	0.0032	0.0050	0.0064	0.0074	0.0070	0.0047	0.0005
14	0.001	0.003	0.005	0.006	0.007	0.007	0.005	0.001
15	0.006	0.014	0.021	0.027	0.032	0.023	0.016	0.002
16	0.003	0.009	0.015	0.019	0.022	0.020	0.012	0
17	0.012	0.029	0.044	0.059	0.071	0.061	0.035	0.002
18	0.006	0.017	0.026	0.035	0.041	0.036	0.021	0

TABLE A-4

DEFLECTIONS IN INCHES FOR VARIOUS VALUES OF LOAD

Final Loading - Up To Failure

Dial Gage No.	Loading (lbs.) 338	487	712
1	0.0054	0.0074	0.0116
2	0.0046	0.0060	0.0082
3	0.019	0.028	0.048
4	0.014	0.019	0.026
5	0.039	0.057	0.098
6	0.022	0.031	0.044
7	0.0049	0.0066	0.0088
8	0.0049	0.0064	0.0084
9	0.021	0.030	0.044
10	0.015	0.020	0.029
11	0.040	0.057	0.097
12	0.026	0.037	0.057
13	0.0049	0.0064	0.0079
14	0.005	0.0064	0.009
15	0.019	0.026	0.030
16	0.013	0.018	0.025
17	0.040	0.058	0.088
18	0.024	0.034	0.048

Load at Failure = 800 lbs.

TABLE A-5

LONGITUDINAL STRAINS μ-INCH/INCH FOR VARIOUS LOAD VALUES

2nd Cycle of Loading

Strain Gage	Loading (lbs.)					Unloading (lbs.)				
No.**	138	238	362	487	600	475	362	225	150	Load Off
1	-21	-39	-60	- 80	- 99	- 84	-69	-49	-39	-12
2	+20	+41	+62	+ 83	+103	+ 86	+69	+45	+33	0
3	+12	+27	+43	+ 60	+ 76	+ 62	+47	+28	+20	0
4	-14	-26	-38	- 49	- 58	- 51	-41	-28	-23	- 8
5	-25	-51	-82	-109	-138	-115	-92	-64	-48	-16
6	+16	+33	+51	+ 68	+ 86	+ 69	+55	+36	+26	+ 2
7	-17	-29	-43	- 57	- 70	- 60	-49	-35	-28	-10
8	+11	+25	+41	+ 56	+ 70	+ 58	+46	+29	+21	+ 1
9	+ 5	+13	+23	+ 32	+ 40	+ 31	+24	+15	+11	- 2
10	-20	-36	-53	- 68	- 86	- 75	-58	-41	-34	-11
11	-15	-28	-44	- 57	- 72	- 60	-49	-36	-30	-12
12	+10	+18	+29	+ 39	+ 49	+ 39	+31	+19	+13	- 1

** Numbers refer to strain gage locations as shown under Table A-6

TABLE A-6

LONGITUDINAL STRAINS μ-INCH/INCH FOR VARIOUS LOAD VALUES

3rd Cycle of Loading

Strain Gage	Loading (lbs.)					Unloading (lbs.)		
No.	125	250	362	487	600	487	250	Load Off
1	-20	-37	-54	-72	- 90	- 75	-44	-7
2	+20	+41	+60	+79	+ 99	+ 79	+47	+3
3	+15	+30	+43	+61	+ 75	+ 61	+32	+2
4	- 9	-19	-30	-41	- 48	- 40	-21	0
5	-25	-48	-71	-98	-124	-100	-54	-8
6	+17	+33	+47	+66	+ 81	+ 66	+37	+4
7	-12	-23	-36	-48	- 60	- 50	-28	-4
8	+12	+26	+38	+54	+ 65	+ 54	+29	+1
9	+11	+19	+25	+36	+ 43	+ 36	+22	+4
10	-13	-27	-39	-56	- 72	- 57	-31	0
11	-11	-24	-35	-47	- 58	- 48	-26	0
12	+11	+19	+29	+39	+ 48	+ 39	+21	0

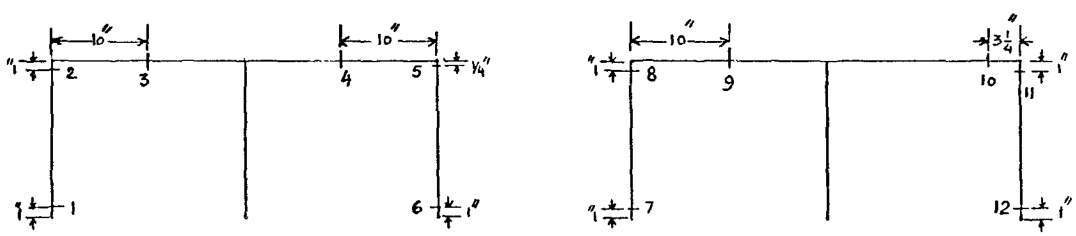

z = 2"   z = 45"

TABLE A-7

LONGITUDINAL STRAINS μ-INCH/INCH FOR VARIOUS LOAD VALUES

Final Loading - Up To Failure

Strain Gage No.	Loading (lbs.)		
	338	487	712
1	-40	-63	-117
2	+58	+84	+128
3	+45	+68	+ 94
4	-26	-37	- 54
5	-57	-88	-128
6	+45	+70	+ 79
7	-24	-35	- 75
8	+41	+61	+ 89
9	+28	+41	+ 56
10	-29	-45	- 71
11	-27	-39	- 60
12	+28	+42	+ 44

Load at Failure = 800 lbs.

APPENDIX B

CALCULATIONS OF THE GEOMETRIC PROPERTIES OF THE MODEL SECTION

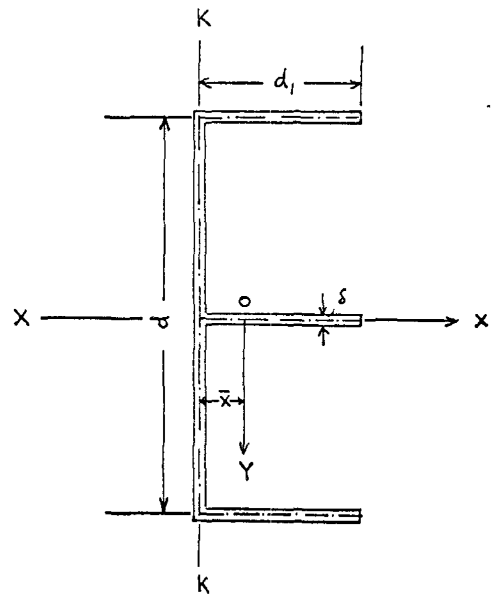

1. Centroid of the section: Let d_1, d and δ denote, respectively, the width of the flanges, web and thickness of the section along the middle surface. X-X is the axis of symmetry. The overall dimensions of the section are 40" x 16".

Area of the section = (40 x 1/2)+(3 x 15.5 x 1/2)= 43.25 $in.^2$

Taking moments about K-K.

$$\frac{3 \times 15.5 \times 8}{2} = \overline{X}A$$

$$\overline{X} = \frac{12 \times 15.5}{43.25} = 4.30 \text{ inches.}$$

2. (a) Moment of inertia about OX, $I_x = \int_A y^2 \, dA$

$$(1/12 \times 1/2 \times 40^3) + 3 \times 15.5 \times (1/2)^3 \times 1/12$$

$$+ 2 \times 15.5 \times 1/2 \times (19.75)^2$$

$$= \frac{64000}{24} + \underbrace{\left(\frac{3 \times 15.5}{8 \times 12}\right)}_{\text{negligible}} + (15.5 \times 390.06)$$

$$2666 + 6046 = 8712 \text{ in.}^4 = I_x$$

(b) Moment of inertia about OY, $I_y = \int_A x^2 dA$

$$\underbrace{[40 \times (1/2)^3 \times 1/2]}_{\text{negligible}} + [40 \times 1/2 \times (4.30)^2]$$

$$+ 3 \times \frac{(15.5)^3}{12} \times 1/2 + [3 \times 15.5 \times 1/2(8-4.30)^2]$$

$$= (20 \times 18.49) + \frac{3723.875}{8} + \frac{3 \times 15.5 \times (3.70)^2}{2}$$

$$= 369.8 + 465.49 + 318.29 = 1154 \text{ in.}^4 = I_y$$

3. Co-ordinates of the shear centre.

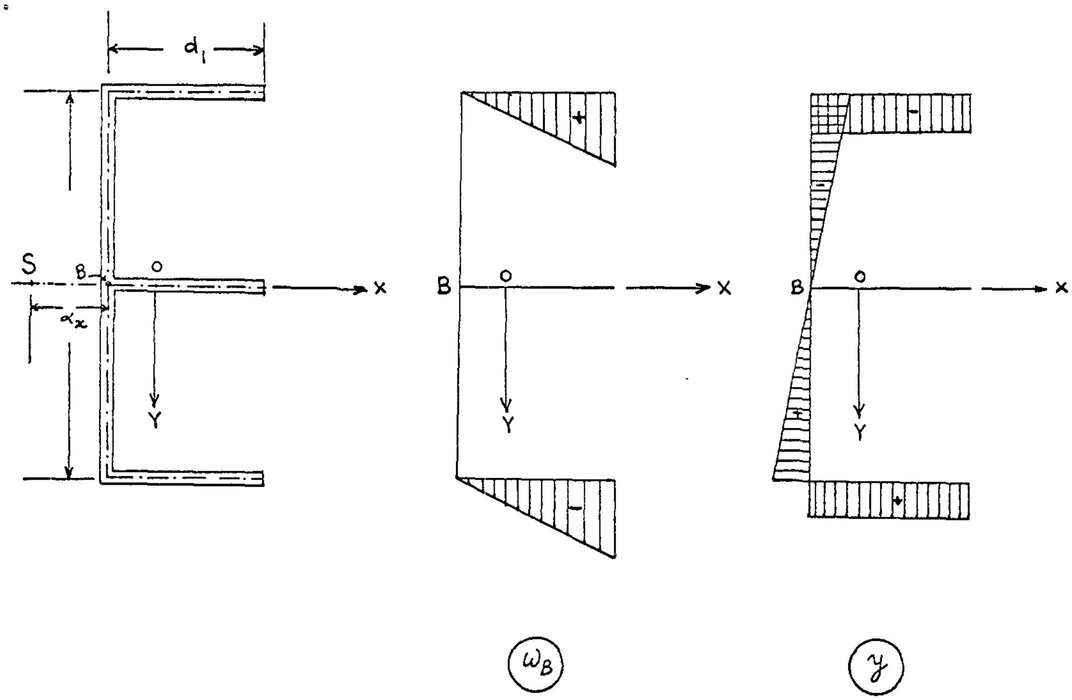

The shear centre S lies on the axis of symmetry OX. Point S is the pole for principal sectorial areas. The sectorial zero point is at the intersection of the axis of symmetry and the profile of the beam; which is also taken as the auxiliary pole. The diagrams of the sectorial area ω_B with respect to the auxiliary pole B and the ordinates y are shown. If a_x, a_y and b_x, b_y are the coordinates of points S and B respectively, then

$$\alpha_x = a_x - b_x = \frac{1}{I_x} \int_A \omega_B \, y \, dA$$

$$\alpha_y = a_y - b_y = -\frac{1}{I_y} \int_A \omega_B \, x \, dA$$

$$\alpha_x = \frac{1}{I_x} \int \omega_B \, y \, \delta \, ds$$

$$= -2\frac{1}{I_x} \, d/2 \; d/2 \; \delta \int_o^{d_1} x \, dx = - \frac{d^2\delta}{2I_x} \left| \frac{x^2}{2} \right|_o^{d_1} = - \frac{d^2\delta \, d_1^{\,2}}{4I_x}$$

substituting

$$\alpha_x = - \frac{(39.5)^2 x \; (15.75)^2}{8 \times 8712} = - \frac{1560.25 \times 15.75^2}{69696}$$

$$= - \frac{387039.5}{69696} = - 5.55''$$

$\alpha_x = - 5.55''$

$\alpha_y = o$, since both points S and B lie on x axis.

$\therefore \; a_x = \alpha_x + b_x = -5.55 - 4.30 = -9.85$ inches

$a_y = o$

4. Principal sectorial area ω.

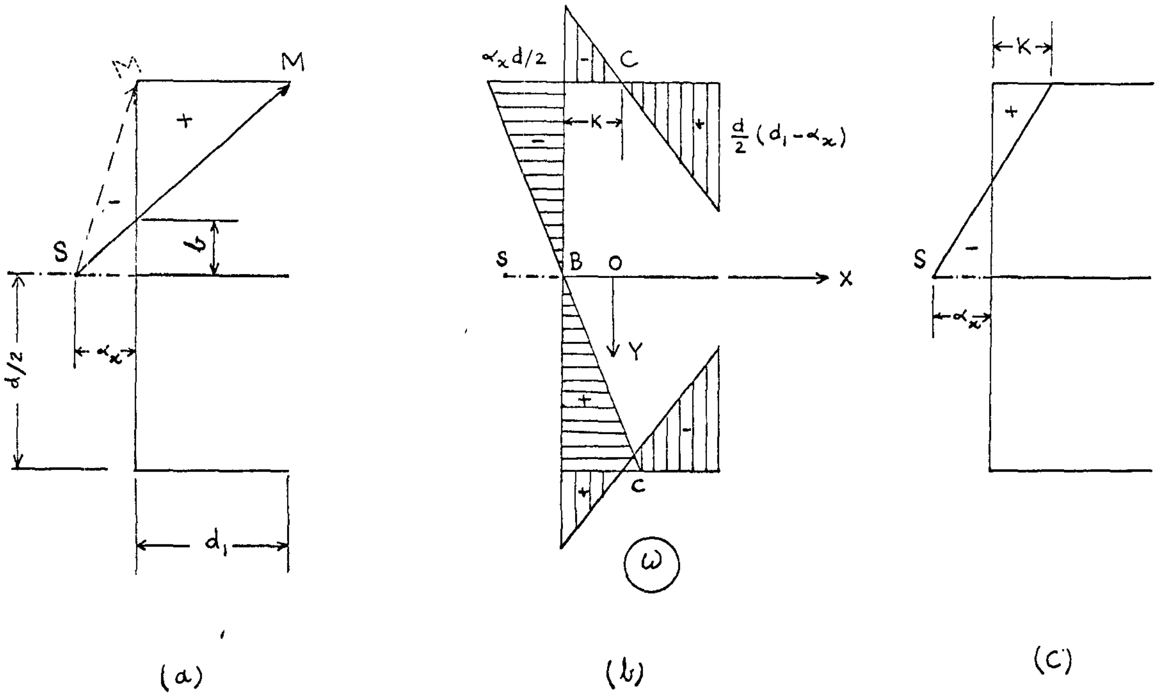

The diagram of the principal sectorial areas is skew symmetrical with respect to the axis OX. Point B lying on the axis serves as the origion of the areas. The sectorial areas for the points on the web below the axis OX, will be +ve, since these areas are swept in the clock-wise sense by the radius vector SM. The absolute values of the sectorial areas for end flanges decrease as we get further away from the web, until, at some point C removed from the web a distance K, the sectorial area vanishes.

Sectorial area ω_M at point M = $(d/2 - b)d_1 - \alpha_x b$

$$\text{Also}\quad \frac{b}{\alpha_x} = \frac{d/2 - b}{d_1}\ , \quad \therefore\ b = \frac{\alpha_x d}{2(d_1 + \alpha_x)}$$

$$\omega_M = \frac{dd_1}{2} - b(d_1 + \alpha_x)$$

$$= \frac{dd_1}{2} - \frac{\alpha_x d(d_1 + \alpha_x)}{2(d_1 + \alpha_x)} = \frac{dd_1}{2} - \frac{\alpha_x d}{2} = d/2(d_1 - \alpha_x)$$

From similar triangles Fig. (C), in order that the +ve and -ve areas are the same, $K = \alpha_x$. Also, sectorial area diagram vanishes for the middle flange.

5. Sectorial moment of inertia I_ω

$$I_\omega = \int_A \omega^2 \, dA.$$

$$I_\omega = 2\left[\int_0^{d/2} (\alpha_x y)^2 \delta \, dy + \int_0^{\alpha_x} \{d/2(\alpha_x - x)\}^2 \delta \, dx + \int_0^{d_1-\alpha_x} (d/2\ x)^2 \delta \, dx\right]$$

$$= 2\left[\alpha_x^2 \delta \frac{d^3}{24} + \delta \frac{d^2}{12} \alpha_x^3 + \delta \frac{d^2}{12} (d_1 - \alpha_x)^3\right]$$

$$= 2\left[\alpha_x^2 \delta \frac{d^3}{24} + \delta \frac{d^2}{12} \{\alpha_x^3 + d_1^3 - 3d_1^2\alpha_x + 3d_1\alpha_x^2 - \alpha_x^3\}\right]$$

$$= \alpha_x^2 \delta \frac{d^3}{12} + \delta \frac{d^2}{6} \left[d_1^3 - 3d_1^2\alpha_x + 3d_1\ \alpha_x^2\right]$$

$$= \alpha_x^2 \delta \left[\frac{d^3}{12} + \frac{d^2 d_1}{2}\right] + \frac{\delta d^2 d_1^2}{6}\left[d_1 - 3\alpha_x\right]$$

$$= \alpha_x^2 \left[\frac{d^3}{24} + \frac{d^2 d_1}{4}\right] + \frac{d^2 d_1^2}{12}\left[d_1 - 3\alpha_x\right]$$

$$= \alpha_x^2 \frac{d^2}{4}\left[\frac{d}{6} + d_1\right] + \frac{d^2 d_1^2}{12}\left[d_1 - 3\alpha_x\right]$$

$$= 1/4(5.55)^2(39.5)^2\left[\frac{39.5}{6} + 15.75\right]$$

$$+\left[\frac{(39.5)^2 x (15.75)^2}{12}\right][15.75-16.65]$$

$$= 268271 - 29028 = 239243 \text{ in.}^6 = I_\omega$$

6. Calculations for I_d

$$I_d = \frac{\alpha}{3}\,\Sigma\, d\delta^3$$

Taking $\alpha = 1$

$$I_d = \frac{1}{3}\,[\{3 \times 15.75 + 39.5\} \times (0.5)^3] = 3.62 \text{ in.}^4$$

APPENDIX C

Determination of functions $\eta(z)$ and $\theta(z)$ for the given boundary conditions:

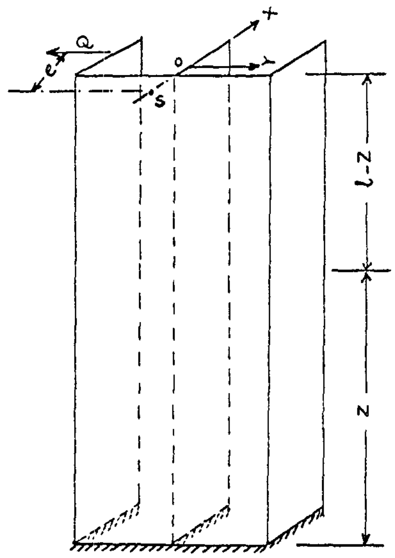

(a) Determination of function $\eta(z)$

$$EI_x\eta^{IV} = o \quad \text{(equation 7)}$$

$$EI_x\eta'' = Q(\ell-z)$$

$$EI_x\eta' = Q[\ell z - z^2/2] + C_1$$

$$EI_x\eta = Q[\ell z^2/2 - z^3/6] + C_1 z + C_2$$

The constants of integration C_1 and C_2 are both zero, since

$$\eta = \eta' = o \text{ at } z = o$$

$$\therefore \quad \eta(z) = \frac{Q}{6EI_x}(3\ell z^2 - z^3) \qquad \text{....(C-1)}$$
(equation 9)

$$\eta''(z) = \frac{Q}{EI_x}(\ell-z) \qquad \text{....(C-2)}$$
(equation 10)

(b) Determination of function $\theta(z)$

$$EI_{\omega}\theta^{IV} - GI_{d}\theta'' = o \qquad \text{(Equation 8)}$$

Dividing by EI_{ω} and denoting $\sqrt{\left(\frac{GI_d}{EI}\right)}/\ell$ by dimensionless quantity k

$$\theta^{IV} - \frac{k^2}{\ell^2}\,\theta'' = o$$

Let $\theta = e^{rz}$ be the solution

upon substitution

$$r^4\, e^{rz} - \frac{k^2}{\ell^2}\, r^2\, e^{rz} = o$$

and dropping the common factor e^{rz}

$$r^2\,(r^2 - \frac{k^2}{\ell^2}) = o \qquad \text{....(C-3)}$$

Equation (C-3) has four roots

$$r_1 = r_2 = o \text{ (a double root)}$$

$$r_3 = k/\ell,\; r_4 = -\,k/\ell$$

$$\therefore \quad \theta = C_1 + C_2 z + \overline{C}_3\, e^{k/\ell\; z} + \overline{C}_4\, e^{-k/\ell\; z}$$

Passing from exponential functions to hyperbolic functions through the formulae

$$e^{k/\ell\; z} = \cosh k/\ell\; z + \sinh k/\ell\; z,$$

$$e^{-k/\ell\; z} = \cosh k/\ell\; z - \sinh k/\ell\; z$$

and writing new constants $C_3 = \overline{C}_3 - \overline{C}_4$ and $C_4 = \overline{C}_3 + \overline{C}_4$, we get

$$= C_1 + C_2 z + C_3 \sinh k/\ell\; z + C_4 \cosh k/\ell\; z$$

$$\text{....(C-4)}$$

Boundary conditions:

$\theta = \theta' = o$, for $z = o$

$B = o$, $H = M$, for $z = \ell$ (free end)

where B = Bimoment, and H = resisting torsional moment.

$M = Qe =$ Applied torsional moment which is constant.

substituting $\theta = \theta' = o$ in (C-4),

$$o = C_1 + C_4 \qquad \text{....(C-5)}$$

$$o = C_2 + C_3\, k/\ell \qquad \text{....(C-6)}$$

$$B(z) = -EI_\omega \theta''$$

$$= -EI_\omega\, k^2/\ell^2\, [C_3 \sinh k/\ell\, z + C_4 \cosh k/\ell\, z]$$

$$= -GI_d\, [C_3 \sinh k/\ell\, z + C_4 \cosh k/\ell\, z]$$

$$B(\ell) = o = -GI_d\, [C_3 \sinh k + C_4 \cosh k]$$

$$\therefore C_4 = -C_3 \tanh k \qquad \text{....(C-7)}$$

$$H(z) = -EI_\omega \theta''' + GI_d \theta'$$

substituting the values for θ''' and θ'

$$H(z) = GI_d\, C_2$$

$$H(o) = H(\ell) = GI_d C_2 = Qe$$

$$\therefore C_2 = \frac{Qe}{GI_d} \qquad \text{....(C-8)}$$

and from (C-6) and (C-7)

$$C_3 = -\ell/k\, \frac{Qe}{GI_d} \qquad \text{....(C-9)}$$

$$C_4 = \ell/k \tanh k\, \frac{Qe}{GI_d} \qquad \text{....(C-10)}$$

and finally from (C-5)

$$C_1 = -\ell/k \tanh k\, \frac{Qe}{GI_d} \qquad \text{....(C-11)}$$

$$\therefore \quad \theta(z) = \frac{Qe}{GI_d} \; [z - \ell/k \; \{\tanh k \; (1-\cosh k/\ell \; z)$$

$$+ \sinh k/\ell \; z\}] \qquad \text{....(C-12)}$$

(equation 11)

and differentiating twice,

$$\theta''(z) = \frac{Qe}{GI_d} \; k/\ell \; [\tanh k \cosh k/\ell \; z - \sinh k/\ell \; z]$$

....(C-13)
(equation 12)

BIBLIOGRAPHY

1. Frischmann, W. W.; Multistorey Frames and Interconnected Shear Walls Subjected to Lateral Loads, Concrete and Constructional Engineering, Vol. 58, p. 227 and 283, 1963.

2. Pippard, A. J. S. and Francis, W. E.; The Stresses in a Wire Wheel with Non-Radial Spokes Under Loads Applied to the Rim, Phil. Mag. XI, pp. 233-85, February 1931.

3. Chitty, L.; On the Cantilever Composed of a Number of Parallel Beams Interconnected by Cross-bars, Phil. Mag. Series 7, Vol. 38, pp. 685-99, 1947.

4. Rosman, R.; Approximate Analysis of Shear Walls Subjected to Lateral Loads, Journal A.C.I., Vol. 61, pp. 717-32, 1964.

5. Barnard, P. R. and Schwaighofer, J.; The Interaction of Shear Walls Connected Solely Through Slab, Symposium on tall buildings, University of Southampton, April 1966, Pergamon Press London.

6a. McHenry, D.; A Lattice Anology for the Solution of Stress Problems, Journal The Institution of Civil Engineers, pp. 59-83, December 1943.

6b. Hrennikoff, A.; Solution of Problems of Elasticity by the Frame-work Method, Journal of Applied Mechanics, pp. A169-A175, December 1941.

7. MacLeod, I. A.; Lateral Stiffness of Shear Walls with Openings, Symposium on tall buildings, University of Southampton, April 1966, Pergamon Press London.

8. McCormick, C. W.; Plane Stress Analysis, Journal of the Structural Division, ASCE 89, p. 37, 1963.

9. Grinter, L. E.; Statistical State of Stress Studied by Grid Analysis, Numerical Methods of Analysis in Engineering, Macmillan, 1949.

10. Kazimi, S. M. A.; An Investigation into the Linear Elastic Behaviour of Shear Wall Structures, Ph.D. Thesis, University of Southampton, 1964.

11. Argyris, J. H., Kelsey, S. and Kamel, H.; Matrix Methods of Structural Analysis, Pergamon, 1964.

12. Whitney, C. S., Anderson, B. G. and Cohen, E.; Design of Blast Resistant Construction for Atomic Explosions, Journal A.C.I., Vol. 51, pp. 655-73, 1955.

13. Benjamin, J. R. and Williams, H. A.; The Behaviour of One-Storey Reinforced Concrete Shear Walls, Proc. A.S.C.E., Vol. 83, No. S.T.5, Paper No. 1254, 1957.

14. Benjamin, J. R. and Williams, H. A.; Behaviour of One-Storey Reinforced Concrete Shear Walls Containing Openings, Journal A.C.I., Vol. 30, pp. 605-18, 1958.

15. Benjamin, J. R. and Williams, H. A.; The Behaviour of One-Storey Brick Shear Walls, Proc. A.S.C.E., Vol. 84, No. S.T.4, Paper No. 1728, 1958.

16. Benjamin, J. R. and Williams, H. A.; Reinforced Concrete Shear Wall Assemblies, Proc. A.S.C.E., Vol. 86, No. S.T.8, Paper No. 2566, pp. 1-32, 1960.

17. Jenkins, W. M. and Harrison, T.; Analysis of Tall Buildings with Shear Walls under Bending and Torsion, Symposium on tall buildings, April 1966, Pergamon Press London.

18. Vlasov, V. Z.; Thin-Walled Elastic Beams, Israel programme for scientific translations, Jerusalem, Israel, 1961.

19. White, R. N.; Small-Scale Models of Concrete Structures, A.S.C.E., Str. Eng., 1964.